Feasibility of ocean energy and offshore wind hybrid solutions

T. van Riet

TU Delft

Feasibility of ocean energy and offshore wind hybrid solutions

By

T. van Riet

in partial fulfilment of the requirements for the degree of

Master of Science

in Sustainable Energy Technology

at the Delft University of Technology,

to be defended publicly on day January 30, 2017 at 02:30 PM.

Supervisor:	Prof. dr. A. V. Metrikine	
Thesis committee:	Prof. dr. A. V. Metrikine,	TU Delft
	Dr. Ir. E. Lourens,	TU Delft
	Dr. ir. A. Viré,	TU Delft
	Ir. A. Jarquin Laguna,	TU Delft

This thesis is confidential and cannot be made public until month 02, 2017.

TU Delft Delft University of Technology

Abstract

In order to meet future energy demand, a more sustainable energy society is essential because fossil fuel reserves are depleting while the total energy consumption worldwide increases. One type of renewable energy which can play a role is ocean energy having the theoretical potential to exceed both current and future human energy needs. This study researches the feasibility of a hybrid system using two sources of ocean energy, namely offshore wind and wave energy. It is concluded that a single horizontal floating wind turbine sharing a foundation with a wave energy converter is most interesting to research. The main reason for this is that offshore wind energy is still limited to relative shallow depths and thus only limited locations are suitable. At further depths, floating foundations become more important. By sharing the mooring system, electrical infrastructure and other structure components with a wave energy converter, costs can be reduced while increasing energy yield in comparison to two separate systems.

A classification of existing concepts within the same category is made. By comparing these different concepts based on platform motions and energy production, it is chosen to look into the combination of a WindFloat with a buoy point absorber. Motivation for this combination is the technical stage at which the WindFloat currently is. In addition, it has good overall stability and minimal heave motions which were found through numerical simulations in the time domain when comparing different floating wind turbines under similar wind and wave conditions using state of art software. Furthermore, a point absorber is used since minimal changes would be necessary to the WindFloat platform. In addition, the power take off system can be placed outside the water making contingent operation and maintenance easier to fulfill.

The point absorber is modeled as a mass spring damper system with a power take off system relative to both a fixed and a floating platform. For both cases it is concluded that the relative heave oscillation between the WEC and platform should be maximized and thus the natural frequency of the system should match the peak frequency of the sea state. The steady state behavior of the hybrid system is investigated in eight sea states, which is modeled using the JONSWAP wave spectrum. Different buoy shapes are investigated which eventually leads to an optimal conical shaped buoy with a diameter of 5 meter. Hydrodynamic parameters of this buoy are found in literature and validated using state of art software. The power production of the WindFloat is found by introducing aerodynamic theory coupled to a wind wave relationship based on the Sverdrup-Munk-Bretschneider nomogram.

Now that both response and power production of both subsystems are known they are coupled to see its effect. The wave energy converter will have no effect on the WindFloat motions due to the relatively low forces interacting between the power take off system and the platform. It can be concluded that the coupling results in a very low impact of wave energy on the total increase in energy production. Absorbed wave energy is between 0.75 and 73.07 [kW] which is in terms of contribution is respectively 0.07 and 1.44 [%]. Increasing the buoy size up to 25 meter shows the potential of wave energy contribution which can go up to 10.7 [%] for strong wave environment.

Keywords: wave energy, offshore wind energy, wind wave hybrid system

Contents

List of Figures

List of Tables

Nomenclature

Acronyms

BEM	Boundary Element Method
CAPEX	Capital Expenditures
COG	Center of Gravity
DFT	Discrete Fourier Transformation
EU	European Union
FFT	Fast Fourier Transformation
FWT	Floating Wind Turbine
FOWT	Floating Offshore Wind Turbine
HWT	Horizontal Wind Turbine
JONSWAP	Joint North Sea Wind Project
LCOE	Levelized Cost of Energy
MIT	Massachusetts Institute of Technology
O&M	Operations and Maintenance
OPEX	Operating Expenditures
OVF	Oscillating Vertical Flaps
OWC	Oscillating Water Column
OWSC	Oscillating Water Surge Converter
PA	Point Absorber
PTO	Power Take Off
RAO	Response Amplitude Operator
SFC	TLP with Rotating Flap Combination
SPD	Submerged Pressure Differential
STC	Spar Torus Concept
SWEC	Spherical Wave Energy Device
TLP	Tension Leg Platform
VWT	Vertical Wind Turbine
WEC	Wave Energy Converter
WWHS	Wind Wave Hybrid Systems
2D	2 dimensional
3D	3 dimensional

Symbol list

Symbol		Unit
a	Axial induction factor	[-]
A_1	Initial condition constant	[-]
A_2	Initial condition constant	[-]
α_s	JONSWAP parameter	[-]
A_w	Water line area	[m^2]
A_T	Wind turbine area	[m^2]
b_d	Damping coefficient	[kgs^{-1}]
b_{hyd}	Hydrodynamic damping coefficient	[kgs^{-1}]
b_c	Critical damping coefficient	[kgs^{-1}]
β_f	Phase angle force	[rad]
β_{mot}	Phase angle motion	[rad]
β_{pl}	Phase angle platform	[rad]
β_s	Phase angle	[rad]
c	Wave speed	[ms^{-1}]
C_1	Integration constant 1	[-]
C_2	Integration constant 2	[-]
c_p	Power coefficient	[-]
C_x	JONSWAP parameter	[-]
D	Depth	[m]
d_{buoy}	Diameter buoy	[m]
d_r	Draft buoy	[m]
D_f	Depth function	[-]
η_{abs}	Absorption efficiency	[-]
η_d	Damping ratio	[-]
f	Frequency	[s^{-1}]
F	Force	[$kgms^{-2}$]
F_a	Force amplitude	[$kgms^{-2}$]
$F_{a,sign}$	Significant force amplitude	[$kgms^{-2}$]
F_{buoy}	Buoyancy force	[$kgms^{-2}$]
$F_{bex,sign}$	Significant hydrodynamic damping force	[$kgms^{-2}$]
F_{damp}	Damping force	[$kgms^{-2}$]
F_{ex}	External force	[$kgms^{-2}$]
F_g	Gravity force	[$kgms^{-2}$]
$F_{msup,sign}$	Significant supplementary mass force	[$kgms^{-2}$]
F_{rad}	Radiation force	[$kgms^{-2}$]
F_{res}	Hydro restoring force	[$kgms^{-2}$]
$F_{t,sign}$	Significant total force	[$kgms^{-2}$]
F_{tun}	Tuning force	[$kgms^{-2}$]
g	Gravity constant	[ms^{-2}]
γ	Peak enhancement factor	[-]
h	Wave height function	[m]
h_c	Cone height	[m]

Symbol		Unit
h_{ref}	Reference height	[m]
H_s	Significant wave height	[m]
H_w	Wave height	[m]
$\mathbf{i}$	Imaginary number	[-]
k	Spring coefficient	[kgs^{-2}]
k_w	Wave number	[m]
L	Length	[m]
λ_p	Absorption length	[m]
λ_w	Wave length	[m]
m	Mass	[kg]
m_{added}	Added mass coefficient	[kg]
m_{buoy}	Mass buoy	[kg]
m_{sup}	Supplementary mass	[kg]
μ	Phase shift	[rad]
ω_n	Natural frequency	[$rads^{-1}$]
ω_d	Damped natural frequency	[$rads^{-1}$]
ω_p	Peak frequency	[$rads^{-1}$]
P	Power	[kgm^2s^{-3}]
p	Pressure	[$kgm^{-1}s^{-2}$]
p_0	Atmospheric pressure	[$kgm^{-1}s^{-2}$]
P_a	Air pressure	[$kgm^{-1}s^{-2}$]
P_{abs}	Wind power	[kgm^2s^{-3}]
P_w	Absorbed power	[kgm^2s^{-3}]
$\boldsymbol{\pi}$	Pi constant	[-]
PR_w	Power ratio	[-]
q	Ordinary differential equation constant	[-]
R_{air}	Gas constant air	[$m^2s^{-2}K^{-1}$]
RAO_{heave}	Response amplitude in heave mode	[m]
RAO_{pitch}	Response amplitude in pitch mode	[rad]
R_d	Universal gas constant	[$m^2s^{-2}K^{-1}$]
ρ	Mass density	[kgm^{-3}]
r_x	Numerical stability factor x domain	[-]
r_y	Numerical stability factor y domain	[-]
S	JONSWAP wave spectrum	[m^2s]
S_{bex}	Hydrodynamic damping spectrum	[kg^2s^{-1}]
S_{fa}	Force spectrum	[$kg^2m^2s^{-3}$]
σ	Spectral width parameter	[$rads^{-1}$]
S_{msup}	Supplementary mass spectrum	[kg^2s]
t	Time	[s]
T	Temperature	[K]
T_0	Reference temperature	[K]
Θ	Power law wind constant	[-]
T_p	Wave period	[s]
U_w	Wind velocity	[ms^{-1}]
v	Velocity	[ms^{-1}]
v_a	Velocity amplitude	[ms^{-1}]
x	Displacement in x axis	[m]
x_h	Homogenous solution	[m]
x_p	Particular solution	[m]

Symbol		Unit
x_t	Total solution	[m]
ξ_a	Wave amplitude	[m]
y	Displacement in y axis	[m]
z	Displacement in z axis	[m]
z_a	Steady state motion	[m]
z_{af}	Amplitude of the free oscillation	[m]
z_{as}	Significant amplitude of motion	[m]
z_{forced}	Forced oscillation motion	[m]
z_{free}	Free oscillation motion	[m]
z_{pl}	Platform heave motion	[m]

1. Introduction

This research is done for the Offshore Engineering department at the Technical University of Delft. This master thesis project will explore the technical feasibility of a hybrid system which combines an offshore wind turbine with an ocean energy device. This chapter will introduce the background of this topic in subsection 1.1. Then the thesis objectives are stated in subsection 1.2, the thesis approach is discussed in subsection 1.3 and finally the structure of the report is listed in subsection 1.4.

1.1 Background

The increase in population in combination with the worldwide energy increase per capita leads to an exponential increase of the overall energy consumption worldwide (United Nations, 2013) (Mackay, 2008). This exponential increase is expected to result in a total increase of 53% in 2035 compared to the quantity of 2011 (IEA, 2011). This significant increase in energy consumption is mostly because of rapid economic development, industrialization and population growth and will negatively influence the environment and the availability of limited fossil fuels reserves which are essential for energy production (Khayyat, 2015).

Nowadays, many countries recognize and support the need for renewable energy and are adopting policies which encourage investment in the development of such technologies (Edenhofer et al, 2011). Renewable energy has become more attractive in today's energy-based economy because it will increase the energy security by ending the fossil fuel resource dependency while reducing the greenhouse gas emissions. Furthermore, the potential is enormous and its production could potentially exceed the world's energy demand. Therefore, it is expected that the global electricity generation from renewable energy resources to grow with 270% between 2010 and 2035 (Ellaban et al, 2014).

One type of renewable energy which can play a role is ocean energy. The renewable ocean energy comes from six distinct sources: waves, tidal range, tidal currents, ocean currents, ocean thermal energy conversion and salinity gradients, each with different origins and requiring different technologies for conversion. The theoretical potential for ocean energy technologies has been estimated at 7400 EJ per year (Bigerna et al, 2015). This is confirmed by the prediction of (Lewis et al, 2011), which states that the theoretical potential of only ocean energy could meet human energy requirements. Advantages of ocean energy are apart from its abundant availability, limited waste production during operation and high power density (P. Lynn, 2013) (Falnes, 2007). All ocean energy technologies, except tidal barrages, are currently undergoing research and development, or are still in the pre-commercial prototype and demonstration stage and thus are still relatively expensive in comparison to fossil fuels (Bigerna et al, 2015). However, costs in the long-term are expected to decrease from the first commercial project level as experience is gained with deployment (OES, 2015). Among the different ocean energy technologies, tidal and wave conversion systems are expected to contribute the most to the European energy system in the short to medium term (2025–2030), due to both local availabilities of the resources and advanced technological status (JRC, 2014). As the technology continues to develop, there is potential for ocean energy. Not only to contribute towards a sustainable energy future but also to create jobs and economic growth in countries with suitable resources (European Commission, 2012). Eight EU countries have already included ocean energy in their National Renewable Energy Action Plans (SWD, 2014). In 2014, the European Commission strengthened the support to the development of ocean energy through a dedicated policy framework and its involvement in both the blue growth agenda and the 2050 energy agenda (COM, 2012) (COM, 2014).

In the future, the use of arrays of wave energy converters or hybrid concepts based on wave, current and wind energy could result in cost-effective designs which could make offshore energy cost competitive with fossil fuels. The capital, operation and maintenance costs must be decreased to realize significant cost reduction. These costs are indirectly correlated with design choices, emphasizing the importance of the existence of optimized design based on verified concepts, which are unfortunately lacking in number due to the current stage of development of ocean energy technologies (Karimirad, 2014). However, there is potential in combining wind and wave energy devices to reduce system costs through shared infrastructure, load reduction and increase the system energy yield.

Furthermore, since wind and wave conditions are environmentally related (Barth and Eecen, 2006), the idea of merging the technology is becoming more attractive due to the limit available space for arrays of such devices (Borg, 2013). Also both technologies benefit from high wind speeds which results in a higher wave height environment. Combining wind and wave energy converters into one hybrid system is an attractive solution to increase the energy density on the specific offshore site locations (Barth and Eecen, 2006). Commercial wind farms are expected to occupy large areas; due to the fact that offshore wind turbines need to be placed at several blade diameters away from each other to reduce wake effects (Frandsen et al, 2005). According to Carballo and Iglesias (2013) the energy extraction of wave energy converters creates wake effects by reducing the mean wave heights and thus influences the local wave climate. Therefore, in order to increase power production in the farm several wave energy devices can be placed in between the wind turbines (Muliawan, 2012). This is possible in various ways; it might be ideal to combine these devices into certain farm configurations. For example, the wave energy converters can be placed on specific sites to reduce wave loads on wind turbines (Marquis, 2012). Other examples are to combine both technologies into one platform or by integrating wave energy converters into wind turbines to increase power production due to the coupling effects of both wind and wave motions (Gao et al, 2016).

While offshore wind energy is maturing, it is still limited to relative shallow depths and thus only specific locations are suitable. At further depths, fixed bottom foundations are not cost competitive and other solutions such as floating foundations become more important. Wave energy itself is also still in pre-demonstration phase, especially due to the high costs of the technology. By combining wind and wave energy, the mooring system, electrical infrastructure and other structure components can be shared (Ding et al, 2015). Especially the electric grid infrastructure represents one of the most important costs for an offshore project, which can go up to 30% of the entire project (Musial and Ram, 2010). Therefore, the combined production of electricity using a shared grid infrastructure would become an important factor in reducing energy costs. Costs for licensing can also be reduced since it will contain one combined project instead of two separate projects (Karimirad, 2014). Moreover, the absorption of waves can result in calm water areas which can be used as artificial harbor, providing safer and easier transfer for operation and maintenance activities, resulting in a minimized downtime and thus also directly positively affect the leveled cost of electricity (Thomas et al, 2015). Ocean energy projects also require the use of specific marine tools such as harbor space and installation vessels which can also be shared (Casale et al., 2012).

Furthermore, the proposed hybrid concept improves the probability of continuous power supply due to the minimized interruptions and power fluctuations (Lakkoju, 1996). This has several reasons, from which first of all the delay effect between wind and wave relationship is the result. Namely, when the wind speed decreases, the waves still continue to roll up to 9 hours afterwards (Marquis, 2012). The wave resources are also more predictable and less variable than the wind resources (Veigas et al., 2014a). Abrupt changes in wind power from minimum to a maximum are faster than similar changes in wave power. Power curves from the Wave star project show that the wind power increase from 30% to maximum power in 8 hours while that was 11 hours for wave power only concept. In other words, in the hybrid systems the fast changes in wind lead to lower or reduced variation in power (Marquis, 2012). This results in a reduction of the balancing costs which is related for the cost of the integration of non-fully predictable renewable energy. The balancing costs cover the

difference between the bid to the day-ahead electricity market and the actual power produced. It is showed that when wave converters are combined the balancing costs stay low, 45 % lower than for wind turbines. Finally, a united scenario of wind and wave technologies brings balancing costs 35–45 % down compared to the wind only scenario (Chozas et al, 2012). This also reduces the leveled cost of energy which considers all the cost required during development and operation on a site (Thomas et al, 2015).

However, it should be noticed that the hybrid system also has possible disadvantages (Pérez and Iglesias 2012; Pérez-Collazo et al. 2013). Since wave energy converters are not technically mature when compared to offshore wind turbines the longer time for development has a negative effect on the project costs. Insurance cost is consequently higher due to the lack of experience and knowledge of the wind wave hybrid concept. The concept itself is still in pre-development phase and therefore there is lack of real data supporting the reliability. Combining wave energy converters directly to offshore wind turbines could result in extra loading on the support structure which then has to be analyzed for strengthening reasons. The costs for strengthening should be compared with the extra power produced over the life time of the concept in order to find out the overall feasibility (Karimirad, 2014). Although as mentioned before as an advantage, locations with both ideal wind and wave conditions might be considerable lower than for both stand-alone options. All these disadvantages should be taken into account and minimized if possible, when choosing a suitable wind wave hybrid system.

One of the difficult uncertainties of ocean energy technologies is its unidentified environmental impact, both in short- as long term (Abanades et al, 2014). Research into the environmental impacts associated with marine renewable energy is still in its infancy (Boehlert and Gill 2010) (Wilhelmsson et al. 2011). The environmental impacts from a single device or a small number of devices are likely to be of little concern, but unclear is the impact associated with the establishment of arrays (Shield, 2014). Still, the hybrid system presents an important advantage in environmental terms since it is likely to have a reduced impact relative to independent installations. This again will lead to a better usage of the natural resources. At last, this could also result in a transfer of knowledge on the environmental impacts from one sector to another (Perez-Collazo et al, 2013).

1.2 Thesis objective

The thesis objective is to study the feasibility of a hybrid concept based on the combination of both ocean energy as offshore wind energy.

In order to accomplish this objective, several sub objectives should be fulfilled. First the understanding for the need for sustainable energy should be understood. From this, comprehensive overviews should be made for both wave and offshore wind energy. From this, hybrid concepts containing both sources of ocean energy should be investigated and a general classification should be made. After comparing the different concepts, the optimal concept for research is chosen. In order to improve the understanding of both subsystems, numerical simulations should be done so that the responses and power production is known. Then, the wave energy converter is modeled as a mass spring damper system relative to a fixed and floating reference in the frequency domain. Optimization for the wave energy converter is done for buoy size and shape. Furthermore, characteristics values for the power take of system should be chosen such that power production is maximized while taking some restrictions into account. Eventually, a comparison can be made between the subsystems and the coupled system. Furthermore, the effect of sizing up the wave energy converter is looked into to see its effect on the contribution of the power production of the hybrid system. At last, the potential of wave energy contribution by scaling up the buoy size will be looked into.

1.3 Thesis approach

In order to strengthen the motivation for a hybrid concept based on sustainable energy technologies, a literature study is done in order to find the importance of a shift from a fossil fuel based energy market to a more sustainable future. To see how both wave and offshore wind energy, separately and together, can contribute to this shift, a study of literature is done. From this literature study, a comprehensive overview of the current status and eventual potential of both technologies will be made. When the potential of both sources of sustainable energy is found, combinations of different hybrid concepts of both ocean and offshore wind is looked into. These concepts are compared based on power production, platform loads and motions. From this comparison a certain wind wave hybrid design is proposed. The irregular behavior of the ocean will be looked into by solving the wave equation and using the JONSWAP wave spectrum for eight sea states. In order to improve the understanding of the response of different floating wind turbine types, numerical simulations in the time domain will be done by subjecting the turbines to similar environmental conditions using state of art software. Numerical simulations for the wave energy converter will also be done in order to see what influences its response and power production. Then, the behavior of the wave energy converter in frequency domain will be modelled as a mass spring damper system with both fixed and floating reference. The power take off system will be included and the buoy will be optimized in size and shape for maximal power production. Furthermore, both subsystems will be coupled and its effect on the corresponding responses and power production are compared to the separate subsystems. At last, the effect of sizing up the buoy and its corresponding hydrodynamic parameters and mass is done, in order to see the potential of wave energy contribution.

1.4 The scope of the thesis

The comprehensive overview of both wave and wind energy is done in terms of the explanation of its environmental behavior, listing of (dis) advantages, market status and its eventual potential. Comparison between different wind wave hybrid concepts will only be made in the specific chosen category; single horizontal wind turbine sharing a foundation with a single wave energy converter. The concepts are only compared based on platform movement and power production. Numerical simulations in the time domain for the wave energy converter are only done by varying the hydrodynamic damping coefficient, wave height and wave period using state of art software. The modeling of the wave energy converter as mass spring damper system is done in the frequency domain to find the steady state solution, thus neglecting free oscillations. Optimization of this wave energy converter is done in order to maximize power production whilst taking certain restrictions into account. Furthermore, optimal buoy shape, draft and size are taken into account. At last, phase control is also incorporated. For the calculation of absorbed power of the wave energy converter in regular and irregular waves, mechanical friction, viscous losses and neither turbine nor generator losses in the conversion system are taken into account. In order to find the power production and responses in six degrees of freedom in the time domain for four different types of floating wind turbines, simulations are performed subjecting similar wind and wave conditions. In addition, the comparison between the hybrid system and separate subsystems is done based on platform movement, necessary infrastructure and power production. The comparison will not be made in economic terms and is therefore not a part of the scope of the research. At last, in order to increase the wave energy contribution for the hybrid system, the buoy size is increased from 5 to 25 meter. The technical and economic feasibility of such a buoy size is not in the scope of this project and will also be difficult to find out since current wave energy projects are based on small scale applications.

1.5 Report structure

The first chapter gives insight into the motivation for wind wave hybrid systems, starting from the point of view that while the energy demand increases, fossil fuel reserves are depleting. Then a hybrid concept based on wind and wave energy is proposed and it is stated how this type of hybrid system could play as a part of the eventual solution. The second chapter gives respectively a comprehensive overview of wave and wind energy. Then the third chapter gives a detailed description of several possibilities of these hybrid concepts from which one is chosen to be investigated further. In order to describe its behavior, the modelling of ocean waves is explained in the fourth chapter using both the wave equation as a standard wave spectrum. The fifth and sixth chapter describes the modeling of the wave energy converter and the offshore wind turbine. The coupling of both subsystems is done in the seventh chapter, in which the combined platform motions and energy production will be investigated. These results are then compared to that of both subsystems and from these results a conclusion is given about the coupling of the two sustainable energy technologies, followed by several recommendations for further research.

2. Comprehensive overview ocean energy

In this chapter a comprehensive overview of two sources of ocean energy will be given. Subsection 2.1 will discuss wave energy while subsection 2.2 will discuss offshore wind energy.

2.1 Wave energy

In this subsection an introduction in wave energy is given. First the environmental occurrence of waves is explained, followed by the best wave conditions for wave energy production and the advantages and disadvantages of this type of renewable energy. Then the current market status and its eventual potential are described. At last, the drivers and drawbacks of the development of wave energy are given.

Wave energy is a concentrated form of solar energy. Since the distance of the sun is different across the globe, the heating of the surface is unevenly distributed causing temperature differences on different locations. The temperature differences create high and low pressure fields which causes winds to blow over the ocean surface. The wind creates swells on the ocean surface which then can travel huge distances with almost no loss of energy. When the deep-water waves, meaning greater water depth than 40 meter, reach the shore and the water depth is less than half a wave length it starts to slow down, decreasing its wavelength which causes vertical growth and eventually wave breaking (Cruz, 2008). The idea is then to transform the energy of the waves into electricity. This can be done in several ways but is not in the scope of this research.

Advantages of wave energy are its abundancy, that its pollution free during energy production and leads to reduction of fossil fuel dependency and that it presents no barrier for fish and aquatic animals (Wavestar, 2016). Furthermore, wave energy has the added advantages of being 23% more predictable than wind power one day in advance. Further to this, the resource is higher in winter, when electricity demands are larger (Thomas et al, 2015). However, disadvantages of wave energy are: visual impact of wave energy converters along the shoreline, location dependent placement since significant wave height is necessary for sufficient energy production, intermittent power generation because waves come in intervals and do not generate power during calm periods, high power distribution costs in order to send the generator power from offshore to land, must be able to withstand forces resulting in high capital, construction and maintenance costs (Smith and Barber, 2007).

The best wave conditions for exploitation are in medium-high latitudes and deep water since wave energy is found to reach power densities of 60-70 [kWm^{-1}] in those locations (IRENA, 2014). Derivation of the power density is described in subsection 6.4.1. As mentioned in the introduction, the potential of wave energy is estimated around 2 [TW] which would exceed the current human energy demand. As can be seen in Figure 1, these medium-high latitudes are indeed the location where most wave energy developers' headquarters are located.

The potential market of wave energy has attracted researchers since early 19^{th} century. However, until 1970 no substantial efforts have been done in the research and development of feasible and reliable wave energy converters. Since 2009 more than 100 projects have been announced in Europe alone, for a total installed capacity of 1200 MW. However, projects with a total of 770 MW have already been put off, for the most part due to economic uncertainties and the early stage of technology development (JRC, 2014). In economic terms, the current levelized of electricity of wave energy based on first-commercial-scale projects is predicted between 120 and 470 dollars per MWh. Wave energy has a high availability percentage which is between 95-98% and the capacity factor of wave energy is estimated around 35-40% (OES, 2015).

Mainly because of this relative high Levelized Cost of Energy (LCOE), Bloomberg New Energy Finance (2004) has reduced the expected global installed capacity of wave energy to 21 MW by 2020, a drop of 72 % compared to 2013 forecasts.

Figure 1 Wave energy network as it was in 2014 (JRC, 2014)[1]

As mentioned before, there are different ways of converting wave energy in electricity. This lack of technological convergence in terms of design of wave energy converters has been highlighted as one of the main barriers currently hindering the development of the sector (MacGillivray et al. 2013). More barriers have been proposed by different wave energy developers of small-scale devices which offer a range of potential benefits (Renew Economy, 2014):

- Increased survivability: low-rated devices do not need to operate in the most powerful resources to generate electricity.
- Smoother learning process: building small-scale devices allows developers to reduce their risk in deployment at sea, and offers them the possibility to try and to test their devices before upscaling to higher power ratings.
- Maintenance: small-scale devices are associated with reduced maintenance, since they are designed to operate in farms and a defect to one unit may not affect the overall array performance, hence reducing the time necessary for maintenance.

Summarized, the progress of wave energy converters depends on several crucial factors, including efficient technical performance; economic manufacture, installation and operation; high reliability and survivability in extreme conditions; and acceptable environmental impact (Lynn, 2013). In other words, the wave energy industry is dedicating increased effort to improving current technologies, to identify and ensure long-term reliability and survivability of devices, and therefore to close the gap with other renewable energy technologies (JRC, 2014).

2.2 Offshore wind energy

In this subsection an introduction in wind energy is given**.** First, the environmental occurrence of wind is briefly explained followed by the advantages and disadvantages of wind energy. Then the current market status and its eventual potential are described. Finally, the drivers and drawbacks of the development of wind energy are given.

[1] *Developers' headquarters are marked blue while test and demonstration sites are marked red.*

Wind is the airflow that consist the movement of the gases in the atmosphere, caused by uneven heating of the atmosphere, rotation of the earth and irregularities on the ground surface (Khaligh and Onar, 2010). Generating electricity from the wind requires that the kinetic energy of moving air be converted to mechanical and then electrical energy. The Rankine–Froude theory shows the relation between the wind speed and power production, a 10 % increase in the relative wind velocity results in a 33 % increase in produced power (Hansen, 2015), as can also be seen in Figure 2. Therefore, a location with high wind speed is essential.

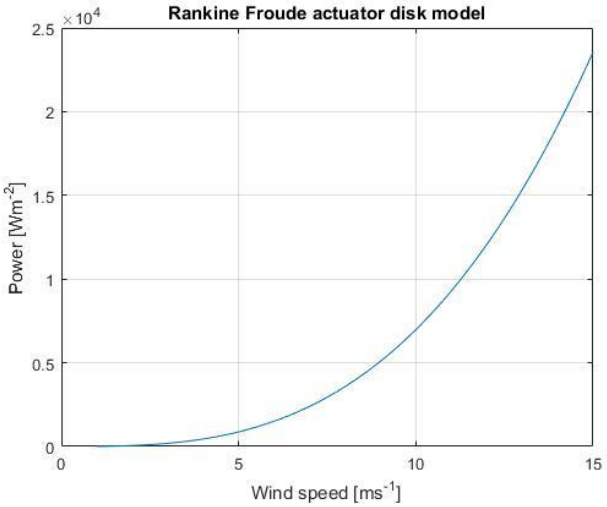

Figure 2 Rankine Froude actuator disk model

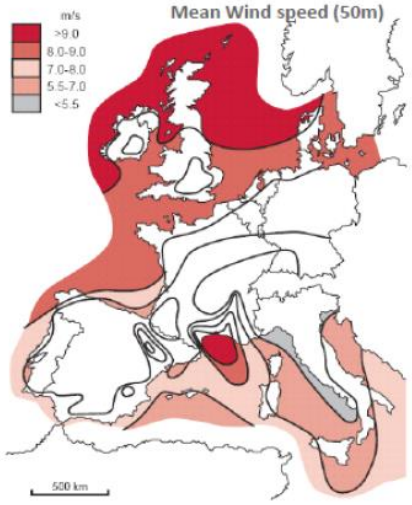

Figure 3 Mean wind speed around Europe (EDP Renovaveis, 2012)

Wind energy has several advantages: its abundant availability, it produces no water or air pollution during operation, relative inexpensive renewable energy compared to other technologies, lands around wind farms can also have other uses. The potential of wind power as a global source of electricity is assessed by using winds derived through merging of data from a variety of meteorological sources. The analysis indicates that a network of land-based 2.5-megawatt [MW] turbines restricted to non-forested, ice-free, nonurban areas operating at as little as 20% of their rated capacity could supply more than 40 times current worldwide consumption of electricity which equal 5 times total global use of energy in all forms (Lu et al, 2009). The disadvantages of wind energy are: impact on both land as along the coast, requires strong wind environment and is thus limited to certain locations. In addition, it also has the following negative environmental impacts: noise production, landscape change, soil erosion and the potential of killing birds (Koller et al, 2006).

As mentioned before, a strong wind environment is essential for power production. Furthermore, the greatest barriers of onshore wind energy historically have been visual impact and noises. Offshore wind energy can deal with some part of these issues (EWEA, 2009). Offshore there is high resource of wind energy available, as can also be seen in Figure 3 and Figure A1, and therefore offshore wind technology has been rapidly developed in recent years. This led to large-scale commercial deployment of offshore wind farms with an average annual increase in installed capacity about 30% between 2010 - 2015 (Gao et al, 2016). However, while the costs of offshore wind technology are decreasing, it is still higher than land-based wind power (IEA, 2013).

Within the EU alone, plans for the development of offshore wind include nearly 40 GW of installed capacity by 2020 and the installation of another 100 GW between 2020 and 2030 (EWEA, 2011). The Global Wind Energy Council projected the possibility of a 17-fold increase in wind-powered generation of electricity globally by 2030 (GWEC, 2008). In 2006, the capacity factor of offshore wind energy was around 36% with 90% availability (Tavner, 2006). A series of great challenges are accompanied by the emerging status of the offshore wind industry, including development of new concepts, design criteria and specific standards, manufacturing,

installation, operation and maintenance, decommissioning, reliability and serviceability. All these challenges must be overcome in a cost-effective way to guarantee the affordability and the competitiveness of the offshore wind industry (Marin, 2014). As can be seen in Figure 4, the offshore wind installations are moving further away from shore into deeper waters. Advantages and disadvantages of floating wind energy have already been mentioned in the introduction of this report.

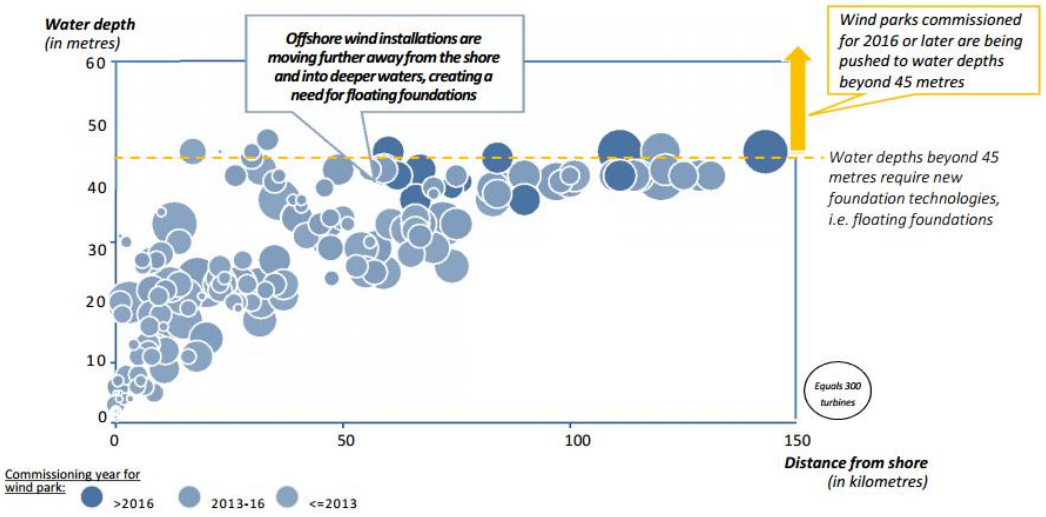

Figure 4 Offshore wind installations are moving further offshore (Bellow, 2014)

Even though wind turbines currently provide only 1% of the worldwide power supply, wind energy is one of the fastest growing renewable energy technologies all over the world. From 2000 to 2007, the global wind power generation increased to approximately five times of its previously recorded capacity (WWEA, 2008). Based on current market trends, it is expected that fixed-bottom offshore wind farms will continue to dominate up to 2030, but the next 5-10 years is an important development period for floating technology, with more prototype demonstrations and pilot arrays to prepare the technology for commercial projects from 2020-2025 (Carbon Trust, 2015).

3. Design selection for hybrid concept

In this chapter the hybrid concept is explained in more detail. First a classification of wind wave hybrid systems is given, followed by a detailed description of the possible design choices. From all these sub classifications the most interesting options are chosen. Then, all the known concepts with similar design choices are listed in order to improve the oversight of the current status of the concept. At last, several concepts which fall in the same category as discussed before are compared to each other and from that comparison a final design is chosen which then will be further investigated.

3.1 Hybrid Concept

As stated in the introduction, hybrid concepts based on wind and wave energy could result in cost-effective designs which could make offshore energy comparable with fossil fuels. In order to choose such an appropriate hybrid concept, several design choices have to be taken into consideration. For example, in order to limit the extra cost and deviation from original design of the offshore wind turbine, minimum changes of support structure should be applied (Karimirad, 2014). Other main points in the selection of a combined system for a specific site are feasibility, serviceability, constructability as well as the cost of produced energy (Karimirad, 2014). The cost of produced energy can be expressed as LCOE, which is mostly taken as measurement of the overall competiveness of different generating technologies. It represents the per-kWh cost of building and operating a generating plant over an assumed financial life and duty cycle. Key inputs to calculating LCOE include capital costs, fuel costs, fixed and variable operations and maintenance (O&M) costs, financing costs, and an assumed utilization rate (IEA, 2016). In other words, for the design to be cost competitive, the design should be maximized in energy production while minimizing the aforementioned costs. LCOE of offshore wind energy is composed by several key factors as can be seen in Figure 5 (The Crown Estate, 2011).

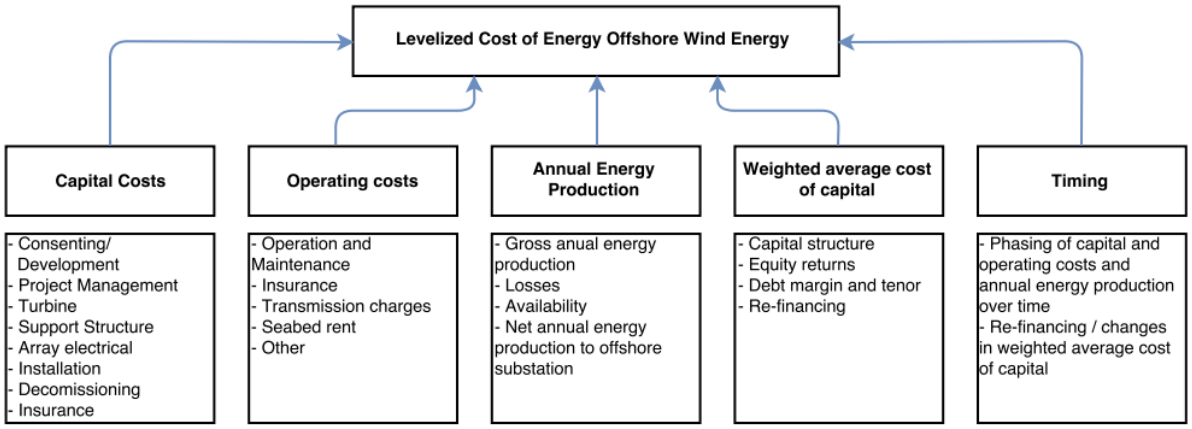

Figure 5 Levelized cost of energy offshore wind

The last couple of years several Wind Wave Hybrid Systems (WWHS) have been proposed by various companies. While all of them are based on the co-configuration of both wind and wave energy production, they can still be classified in different main categories and subtypes. In order to improve the insight in the different design options, the proposed classification has been made and is shown in Figure 6.

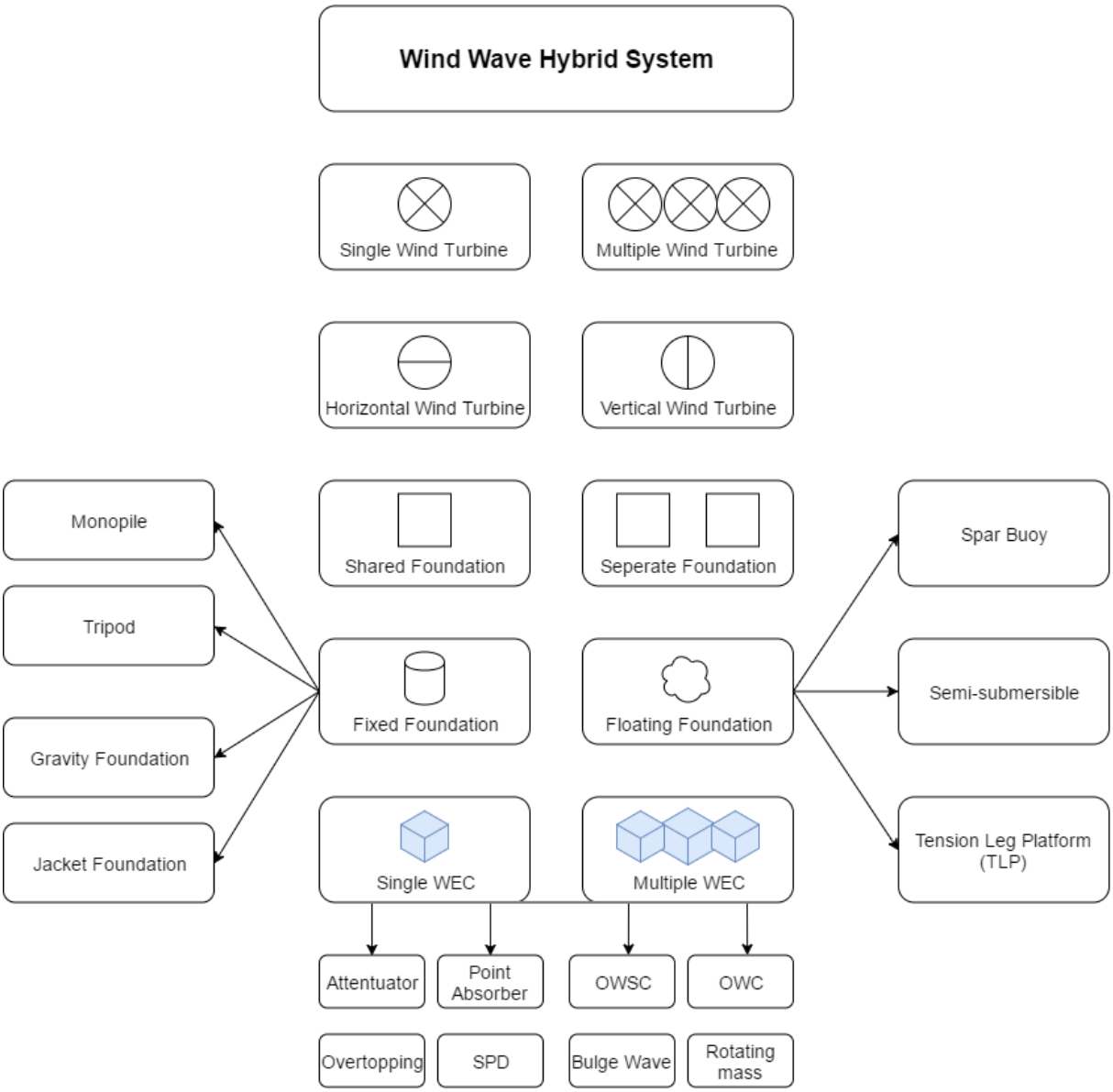

Figure 6 Classification wind wave hybrid systems[2]

Using the proposed classification as shown in Figure 6, known concepts can be listed which is done in chapter 3.2. First the different types and subtypes are briefly explained, all with their own pros and cons.

[2] The wave energy converter classification which is visualized at the bottom of Figure 6 has been taken from (EMEC, 2014b) (SI Ocean, 2013a). List of acronyms can be found on page vii.

3.1.1 Single versus Multiple Wind Turbines

The first option is the choice between a single and multiple wind turbine(s). The integration of a single turbine was proved to be the best option to minimize the LCOE, instead of multiple turbines (Floating Power Plant, 2016). The main reason for this is due to the wake effect. The wake effect reduces the energy production of nearby wind turbines because of disturbance of wind flow fields (Gonzalez, 2012). In order to minimize this effect, the wind turbines have to be placed several diameters apart and in parallel to the wind direction. This would therefore result in large and costly structures, which are also hard to build and transport, very capital intensive and very difficult to maintain during the expected time of the concept (Karimirad, 2014). On the other hands, having only a single wind turbine results in a relatively lower power output and power density per offshore area.

3.1.2 Horizontal versus Vertical Turbine

The second sub classification which is proposed is the difference between a horizontal (HWT) and a vertical wind turbine (VWT). While both types have their practical application, the following general characteristics can be named: horizontal wind turbines have a higher efficiency and power output compared to a similar sized vertical wind turbine (Manwell et al, 2009). Another property of horizontal wind turbines is that it produces well in turbulent wind fields and if wind dominates from one specific direction, while vertical wind turbines can be powered from wind from all directions. Furthermore, vertical wind turbines are mostly used in small wind applications (Manwell et al, 2009). The inherent difference in the interaction between the incident wind and a VAWT and a HAWT results in substantially different aerodynamic forces generated on the support structure. While the thrust force of a HAWT is relatively constant, the VAWT thrust force is highly oscillatory (Borg, 2015).

The impact of the mass and the center of gravity (COG) of the wind turbine on the static stability of the whole floating offshore wind turbine (FOWT) system is illustrated as follows: the potentially lower wind turbine mass and lower position of the COG of a VAWT was beneficial towards the static stability of the system, as it leads to a lower total FOWT COG position. Hence, the restoring contribution required from the second moment of the water plane area and the mooring system can be reduced (Borg, 2015). While the vertical turbine have good potential due to their lower COG, the horizontal wind turbine will be used for this research because so far limited research is done into floating vertical wind turbines and turbine manufactures are using state of the art technology.

3.1.3 Shared versus Separate Foundation

The following sub classification is that between shared and separate foundation of the wind and wave technology. This option already has been discussed in the introduction of this report but the key facts will now be summarized. Shared foundations often have higher loadings on the support structure in comparison to a stand-alone offshore wind turbine (Pérez and Iglesias, 2012). Shared foundation increases the complexity of the system and increase difficulty in operation and maintenance. However, when locating both the wind and wave energy converters close to each other would allow the sharing of common installations such as grid connection. Another option could be the placement of wave energy converters on the perimeter of a wind park as wave shield for wind turbines. Wave energy converters could also be deployed throughout the wind park in order to increase the energy yield of offshore locations (Balitsky et al, 2014). Unfortunately, the current status of wave energy converters is still yet mostly in demonstration phase and therefore in order to make this type of energy harvesting more attractive, sharing certain common costs with offshore wind applications could increase its potential. On the other hand, as until of today there is a lack of experience in co-located devices which makes it risky for developers (Karimirad, 2014). Second of all, the risk of accident or collision between a wave energy converter and a wind turbine should be taken into account, this consequently increases the insurance costs for global projects.

3.1.4 Fixed versus Floating Foundation

The next sub classification which can be made is that of a fixed versus floating foundation. Several known and well proven foundations are already known, which are also shown in Table 1. First general fixed versus floating considerations is mentioned; fixed foundations are superior to floating wind turbines as matter of costs for shallow water regions, up to around 30 meter (Jonkman, 2011). While technology develops, this depth will for sure increase but will eventually come to its limits due to massive and thus expensive underwater foundations. The range of optimal water depth for the different deep water floating wind turbine applications are shown in Figure 7 (Carbon Trust, 2015). While depths are 30 to 50 meter will now be threatened as transitional depth, from 50 meter depths floating wind turbines seem to be favorited in comparison to fixed foundations. However, according to (Maine International Consulting, 2015) actually only two different concepts are currently in (pre-) commercial phase, respectively WindFloat and Hywind, as also can be seen in Figure 8.

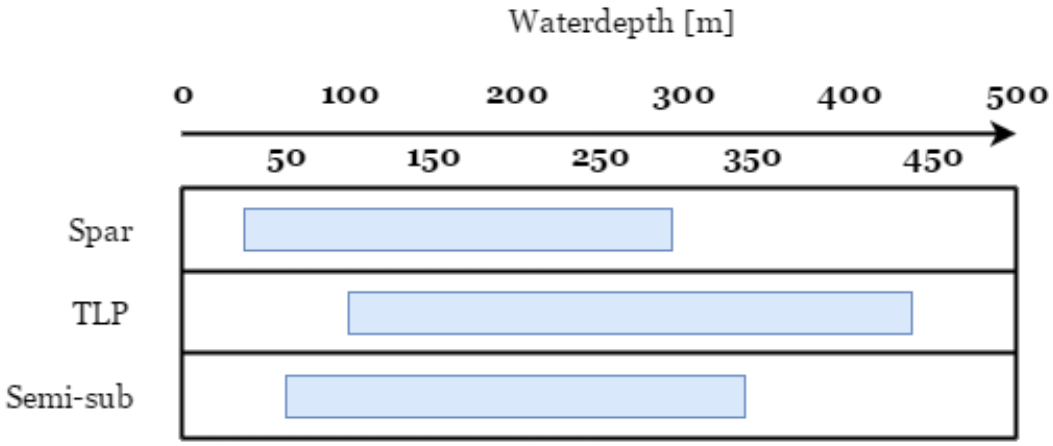

Figure 7 Optimal water depths of different floating wind turbine types

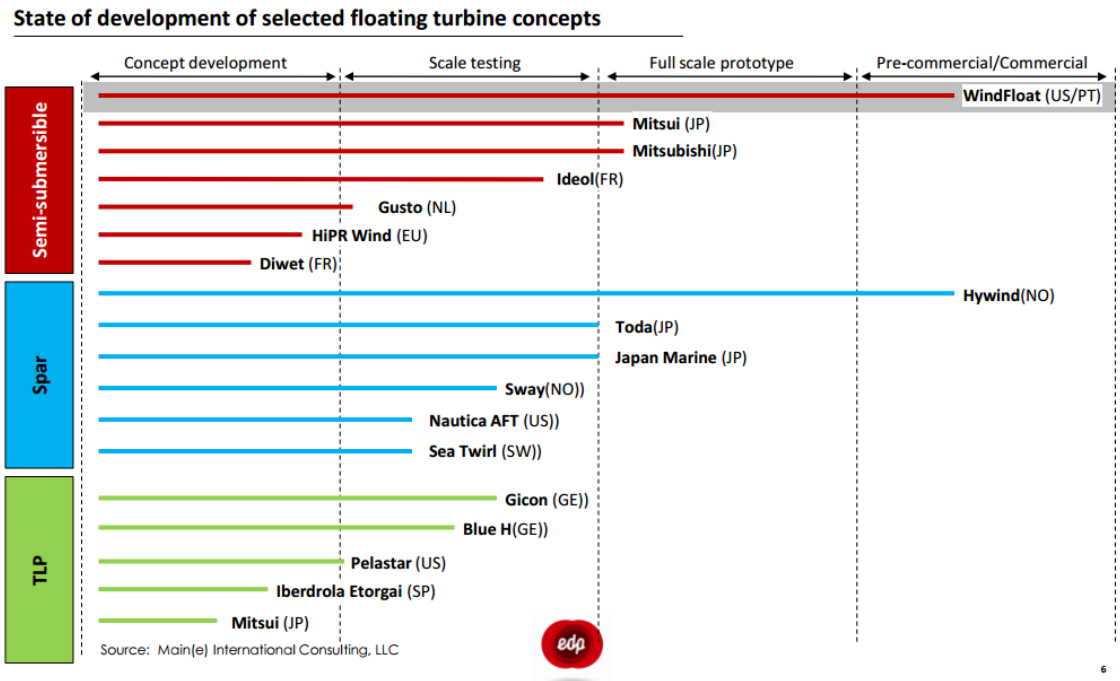

Figure 8 Stage of development of selected floating turbine concepts (Maine International Consulting, 2015)

Furthermore, floating wind turbines provide access to a significantly larger market than traditional offshore wind, which is limited to relatively modest water depths (Thomas et al, 2015). Europe's floating wind capacity potential is estimated around 4000 GW (Carbon Trust, 2015), and the European Union (EU) targets for offshore wind usage of 40 GW by 2020. It is expected that a usage of 150 GW is achievable by 2030, by using predominantly conventional fixed-bottom foundations in water depths of under 50 meter. However, by 2050, offshore wind capacity in Europe could reach 460 GW, which can only be achieved by accessing deep water sites greater than 50 meter using floating technology (EWEA, 2013).

Floating wind applications also allow development in areas further from land, and with increased wind resources, hereby reducing certain environmental and human impacts (Thomas et al, 2015). The absence of commercial floating wind farms makes it difficult to compare cost competitiveness, since existing prototypes have understandably high costs and are not a useful reference point for comparative analysis with operational fixed-bottom wind farms. However, studies by EWEA (2013) and DNV-GL (Legacy GL Hassan, 2012) using cost estimates from industry, suggest that floating designs could be competitive in terms of the LCOE with fixed-bottom foundations in water depths greater than 50 meter. Beyond 50 meter, the cost competitiveness of floating wind improves exponentially. According to extensive research, done by (Carbon Trust, 2015), floating wind turbines have lower operation expenditures (OPEX) compared to fixed offshore wind turbines, while having higher capital expenditures (CAPEX). An explanation follows in the next paragraph.

First of all, the balance of the system is expected to be higher for floating wind projects. This is largely due to the need for a floating substation and dynamic cables, which are both less established technologies that are more expensive than the equivalent transmission methods used for fixed-bottom projects. Though only a relatively small share of total CAPEX, floating wind can also offer benefits in decommissioning. While fixed-bottom foundations require specialized equipment and vessels to decommission (with budget reserved from the beginning of the project), the case is significantly less complicated for floating wind. Once the anchors are removed, or the moorings are cut, the full structure can be towed back to the shore at a significantly lower cost. Another key driver of cost savings of floating versus fixed-bottom projects is reduced operational expenditure. While the cost of minor repairs is expected to be similar for both fixed-bottom and floating projects, with analogous technician access by crew transfer vessel for each, there are expected cost savings for major repairs, such as gearbox replacement, which can represent 35-50[of total OPEX for offshore wind farms (DNV GL, 2012). Whereas major repairs for fixed-bottom turbines require expensive jack-up or dynamic positioning vessels, most floating wind structures are designed in such a way that they can be disconnected from their moorings and towed back to the shore to conduct repairs at port (Carbon Trust, 2015).

In order to drive down the costs of floating wind turbines, the platform size is highlighted as the most critical challenge. Another important aspect is the amount of installation procedures, particularly for TLP and spar-buoy concepts. Further CAPEX savings are expected from developing floating transformer stations, advanced control systems, and improved mooring & anchoring systems. Meanwhile, OPEX savings could be achieved by developing robust procedures for port-side major repairs, for which the technical feasibility and cost benefit are currently not well understood. It is also evident that while some challenges are more pressing in the short-term (e.g. advanced modelling tools), others become increasingly important as the technology advances to commercial scale (e.g. floating transformer stations, high voltage dynamic cables, wake effects) (Carbon Trust, 2015).

In order to compare the LCOE, and thus the cost competitiveness of floating wind with conventional fixed-bottom wind farms, a combination of the CAPEX and OPEX documented above must be considered, together with the expected energy output of the respective wind farms. While CAPEX has shown to be considered slightly higher for floating wind, OPEX is expected to be lower and the energy output is variable and site dependent. However, the greater flexibility of floating wind and ability to potentially access higher wind speeds at deep water locations, unsuitable for fixed-bottom foundations, could improve its cost competitiveness as visualized in Figure 9.

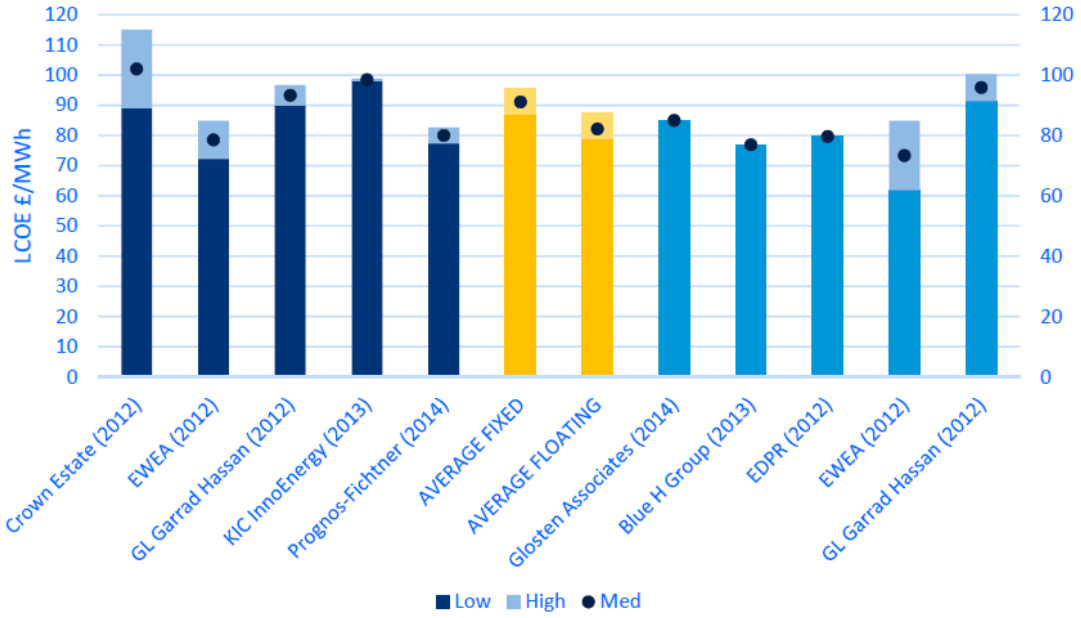

Figure 9 Expected LCOE of floating versus fixed wind turbines (Carbon Trust, 2015)

Early demonstrations indeed appear to confirm the potential for floating turbines to capture high energy yield, with Statoil's 2.3 MW Hywind demonstrator attaining capacity factors of around 50%, compared with a 40% average for fixed offshore turbines and 25-30% onshore (Statoil, 2014). However, yield will also be influenced by the level of wake effects in the wind farm, which has had little to no attention in the context of floating wind technology (Carbon Trust, 2015).

In order to get an overview of the different proposed floating wind turbines from the last years, a classification, including the name of the design with their relevant references, has been created as shown in Table 1. This classification is based on a similar classification proposed earlier in subsection 3.1.

Table 1 Floating wind turbine concepts

	Types	*Subtype*	*Design*	*Reference*
Water depth < 50m	Fixed	Tripod	-	(Karimirad, 2014)
		Mono pile	-	(Thomsen, 2012)
		Gravity based	-	(Karimirad, 2014)
		Jacket foundation	-	(Karimirad, 2014)
Water depth > 50m	Floating	**Spar-Buoy**		
		Single Horizontal Axis Turbine	Advanced Spar	(Fukushima, 2015)
			Hybrid Spar	(Castro-Santos, 2016)
			Hywind	(Statoil.com, 2009)
			Sway	(Sway, 2016)
			WindCrete	(WindCrete, 2016)
			Kabashima Island Spar	(Maine Int. Consulting, 2013)
			MIT Double Tout Leg	(Lee, 2005)
		Single Vertical Axis Turbine	Deepwind Spar	(DeepWind, 2016)
			SeaTwirl	(SeaTwirl, 2016)
		Semi-Submersible		
		Single Horizontal Axis Turbine	Compact Semi-Sub	(Fukushima, 2015)
			Fukushima	(Japanfs.jp, 2009)
			IDEOL	(IDEOL, 2016)
			Nautilus Semi-Sub	(Nautilus, 2016)
			Nezzy SCD	(SCD, 2016)
			SeaReed	(DCNS, 2015)
			TetraFloat	(TetraFloat, 2016)
			Trifloater	(GustoMSC, 2015)
			VolturnUs	(Viselli et al, 2015)
			V-Shape Semi-Sub	(Fukushima, 2015)
			WindFloat	(WindFloat, 2016)
			DeepCWind	(Robertson et al, 2012)
			Dutch TriFloater	(ECN, 2002)
		Multiple Horizontal Axis Turbine	Hexicon	(Hexicon, 2016)
			WindLens	(Maine Int. Consulting, 2013)
			WindSea	(WindSea, 2016)
		Single Vertical Axis Turbine	SpinFloat	(GustoMSC, 2015)
			VertiWind	(VertiWind, 2012)

		Tension Leg Platform *Single Horizontal Axis Turbine*	AFT Blue H TLP Eco TLP GICON-SOF PelaStar TLP Wind UMaine TLP	(Nautica, 2016) (Blue H Engineering, 2016) (DBD Systems LLC, 2016) (GICON-SOF, 2016) (Glosten, 2016) (IBERDROLA, 2016) (Stewart, 2012)
		Barge Platform *Single Horizontal Axis Turbine*	ITI Energy Barge	(Jonkman, 2010)

3.1.5 Single versus Multiple Wave Energy Converters

The last design choice which must be made is between a single or multiple wave energy converters and which type is most suited to combine with a floating offshore wind turbine. This choice is alike the first one since more wave energy converters lead to an increase in power production while the costs and complexity of the hybrid system increases. It should be noted that the presence of multiple wave energy converters in such a relatively small area will drastically influence each other's behavior. In addition, as mentioned in the introduction, the contribution of wave in comparison to that of wind is low and in the order of 1-10%. The reason for this is that wave energy is less mature and relatively more expensive in comparison to wind energy. This is something which could eventually change when wave energy matures, but for this research a configuration with low wave energy contribution is looked into.

The following trends can also be noted for wave energy converters in general (IRENA, 2014):

- 67% of the current wave energy converter concepts are floating
- IRENA has shown that 64 % of wave energy converters have been designed for offshore operation
- Over half (53%) of wave energy converter concepts developed are point absorbers while 33% are overtopping/terminator and 14% attenuators
- Of the current wave energy converter concepts developed 42% use hydraulic systems, 30% direct-drive systems, 11% hydraulic turbines, and 11% pneumatic systems.

The different types of wave energy converters, as listed in Figure 6, all have their practical application. The distinction between different wave energy converters is not in the scope of this project, more information can be found in (EMEC, 2014b) (SI Ocean, 2013a). The addition of a single point absorbed needs minimal changes to the floating wind turbine construction. In addition, the power take of system can be placed outside the water which improves durability and makes contingent operation and maintenance easier to fulfill.

When combining all the previously described types and subtypes, the following combination seems to be most interesting to further investigate; *Single Horizontal Wind Shared Floating Single WEC.* For this type, most of the different known concepts are listed in Table 2, to give an overview of ongoing projects.

3.2 Classification of hybrid systems

The different hybrid systems are listed in Table 2; this also gives an overview of the current ongoing projects in the field of wind wave hybrid designs. The attractive designs for this research are listed under *Floating combined hybrid - Single Horizontal Wind.* Hybrid concepts with separate wind and wave constructions have not been taken in this Table.

Table 2 Wind wave hybrid classification

	Types	Subtype	Design	Reference
Water depth <50m	Fixed Combined Hybrid	**Single Horizontal Turbine**		
		Monopile + Point Absorber	-	(Karimirad, 2014)
		Monopile + Oscillating Body	-	(Pérez and Iglesias, 2012)
		Monopile + OWC	-	(Pérez and Iglesias, 2012)
		Monopile + OWSC	WEGA	(SeaForLife, 2016)
		Jacket Frame + Point Absorber	Wave Catcher	(Offshore Islands LTD, 2016)
		Jacket Frame + Oscillating Body	Wave Treader	(Power Technology, 2016)
		Jacket frame + OWC	-	(Pérez and Iglesias, 2012)
Water depth >50m	Floating Combined Hybrid	**Single Horizontal Turbine**		
		Spar + Point Absorber	Spar-Torus Combination	(Muliawan, 2013)
		TriFloater + Point Absorber	-	(Roddier et al, 2012)
		TriFloater + OWSC	-	(Roddier et al, 2012)
		Trifloater + OWC	-	(Roddier et al, 2012)
		TLP + Point absorbers	TLPWT+PA	(Bozo et al, 2015)
		SemiSub + OWSC	SFC	(Peiffer, 2012)
		Multiple Horizontal Turbines		
		Overtopping + Point Absorber	Poseidon P80	(Floating Power Plant, 2016)
		SemiSub + Attentuator	2Wave1Wind	(OWWE Ltd, 2016)
		SemiSub + Buoys	W2 Power	(Pelagic Power, 2016)
		SemiSub + Point Absorber	Wavestar	(WaveStar, 2016)
		SemiSub + *Solar*	WindLens	(Maine Int. Consulting, 2013)
		Hexicon + WEC	-	(Fraunhofer, 2014)
		Single Vertical Turbine		
		SemiSub + WEC	VAWT	(Borg, 2013)
		SemiSub + WEC	SKWID	(MODEC, 2016)

3.3 Chosen concept for this research

Now that known concepts are classified and the pros and cons of various existing concepts are stated, several concepts can be looked into more extensively in order to find the design with the most potential for further investigation. As mentioned in subsection 3.1.4, both WindFloat and Hywind are in the most advanced design phase namely the (pre-) commercial phase. In order to be entitled to this phase; concept development, scale testing and full prototype tests are all successfully done and thus the design has proven that it has potential. For the WindFloat concept, four different ways of adding wave energy converters are possible which have been known and investigated under the name WindWaveFloat (Roddier, 2012). The four types are shown in Figures 10a until and 10d.

(a) Oscillating Water Column (b) Spherical Wave Energy Device (c) Oscillating Vertical Flaps (d) Point Absorbers

Figure 10 WindWaveFloat with different wave energy devices (Weinstein, 2012)

It was shown by (Weinstein, 2012) that the addition of wave energy converters to the existing WindFloat platform had limited to no effect on the platform motions and its stability. Total power production by both wind and wave of these different designs is listed in Table 4.

The other floating wind turbine which is currently in (pre-) commercial phase is the Hywind. Due to its spar type body, limited possibilities are there for the addition of wave energy converters. One possibility however is the addition of a torus around the core of the spar, known as the Spar Torus Concept (STC) which can be seen in Figure 11. This concept has been proposed by Muliawan in 2012 and several studies have followed to describe its power production, platform motions and behavior in extreme weather conditions (Muliawan, 2012) (Muliawan et al, 2013a) (Muliawan et al, 2013b) (Muliawan et al, 2013c). Relevant results of these studies have been summarized in Table 4.

The previous two main designs were respectively based on a semi-submersible and a spar type floating construction. As mentioned in subsection 3.1.4, there are three main floating wind turbine types from which the third one is a tension leg platform. In order to have a more complete overview, a TLP is also added to the comparison while the development of such a type is still some process steps away from commercial implementation as can be seen from Figure 8. The tension leg platform can be combined with rotating flaps or point absorbers which can be seen in Figures 12 and 13 (Gao et al, 2016) (Bachynski et al, 2013). Motivation for less than three flaps is because of the fact that the third flap has almost no influence on the produced power, since the power production is heavily dependent on the wave direction. Motivation for having three flaps is that it can produce the same amount of power, independent of the wave direction. This design choice and its effect on power production are visualized in Figure A2.

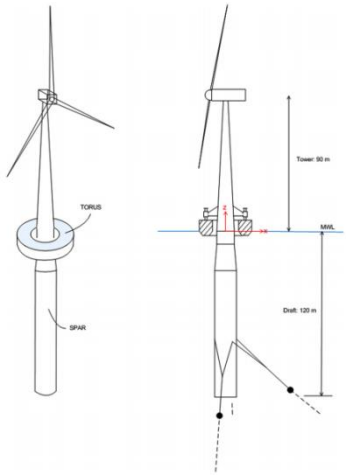

Figure 11 Spar Torus Concept (Muliawan, 2013)

Figure 12 TLP with rotating flap combination (Gao et al, 2016)

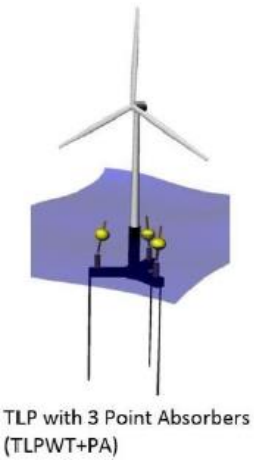

Figure 13 TLP with Point Absorbers (Bachynski et al, 2013)

The aforementioned wind wave hybrid concepts have been investigated in terms of total energy production, wind energy production, platform motions and forces, to find out which concept holds the most potential. The different types are listed in Table 3 and the results of the comparison can be found in Table 4.

Table 3 Different types of wind wave hybrid systems for comparison

Semi-submersible	Spar	Tension Leg Platform
WindWaveFloat	Hywind	TLP
Oscillating Water Column	Spar Torus Combination (STC)	Rotating Flaps (SFC2)
Spherical Wave Energy Device (SWEC)		Rotating Flaps (SFC3)
Oscillating Vertical Flaps (OVF)		Point Absorbers (TLP-PA2)
Point Absorbers (PA)		Point Absorbers (TLP-PA3)

Table 4 Overview of the comparison between different hybrid concepts

	Total Energy production	Wind Energy production	Platform motions	Platform forces
WindWaveFloat OWC (Weinstein, 2012)	(± 3%)	Not affected	Slightly decreased	-
WindWaveFloat Buoy (Weinstein, 2012)	(± 1%)	Not affected	Minimally affected	-
WindWaveFloat Flaps (Weinstein, 2012)	(± 2%)	Not affected	Minimally affected	Slightly increased
STC (Mulianwan, 2013)	(± 10-15%)	(+5%)	Slightly increased	Slightly increased
SFC (2 flaps) (Gao, 2014)	(± 1-4%)	Not affected	Minimally affected	Slightly increased
SFC (3 flaps) (Gao, 2014)	(± 1-4%)	Not affected	Minimally affected	Slightly increased

From Table 4 several things can be noted. First of all, the total energy production only increases slightly, between 1 and 15% from which the wave energy contribution is between 1 and 10%. This was something which was mentioned in the introduction and subsection 3.1.5. While with most of the designs, the wind energy production stays the same, it increased for the STC because the torus led to increase vertical stability, while the overall platform motions increased slightly. Platform forces increase for all concepts due to the higher hydrodynamic loads which are applied on the platform due to the addition of a wave energy converter. The WindWaveFloat with point absorbers and the TLP with two and three point absorbers have not been included in Table 4 due to insufficient useful information.

Since the Hywind concept is less stable than the WindFloat and the SFC only generates very small proportions of energy, it is chosen to use the WindFloat for further investigation. In addition, it is easier to couple a wave energy converter to the WindFloat than the Hywind because of the platform shape. Due to the limited power production of all three different WindWaveFloat types, the buoy is taken for research due to its simplicity of the system. Furthermore, the power take off (PTO) system can be placed above the buoy and thus outside the water which makes operation and maintenance easier. For this design, the WindFloat construction would need limited changes. There should only be an attachment in order to move the buoy in heave mode in the center between the columns. The buoys movement in heave mode should be maximized; this can be accomplished by matching the natural frequency in heave mode of the buoy in heave mode to that of the peak frequency of the sea. First chapter 4 will describe the modeling of ocean waves before the corresponding dynamics related to the wave energy converter movement is described.

4. Ocean Wave Modelling

In this chapter the modelling of ocean waves is described. This explanation is given for both regular and irregular wave conditions. First the general wave characteristics are explained in subsection 4.1, followed by the proposal of wave spectrums for both frequency and time domain in subsection 4.2. Then a method for solving the wave Equation is given in subsection 4.3. At last, the description of wave trapping and the initial concept design is described in subsection 4.4.

4.1 General wave characteristics

In order to describe the ocean waves, first the basic wave theory is explained. Most of the basic terms can be seen in Figure 14. In Figure 14, waves move from left to right, with the wavelength λ defined in meters which is the distances between two crests or two troughs. The wave movement expressed in meters per second is named wave speed. The wave amplitude ζ is half of the wave height which is the difference between crest and trough. The first assumption which has to be made is that the wave height is small compared to the wave length. Other assumptions of the airy wave theory are that the depth is uniform and the fluid flow is inviscid, incompressible and irrotational (Krogstad, 2000).

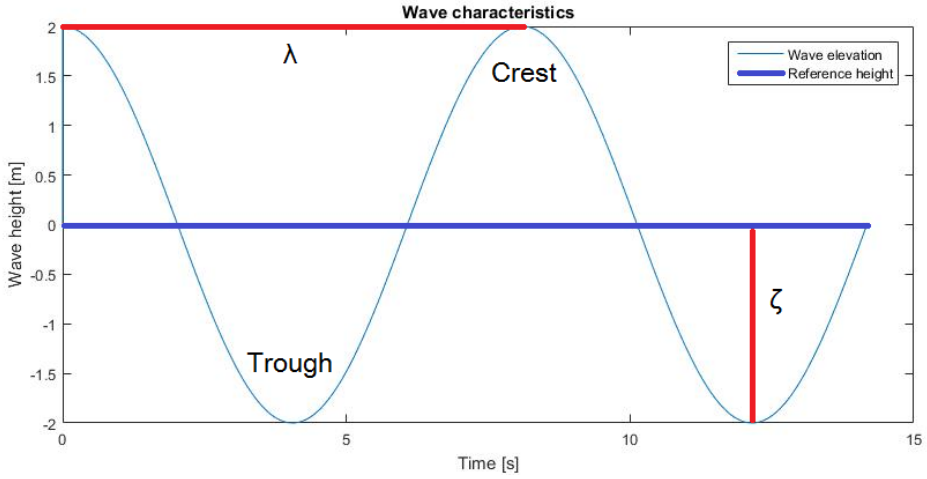

Figure 14 General wave characteristics

The wave height in one dimension at any point and time can be given by Equation 4.1:

$$y = h(x,t) = H_w \cos(kx - \omega t) \tag{4.1}$$

with ω the wave frequency in [rads^{-1}] and k the wave number [-] which are related according to Equation 4.2:

$$\omega = \sqrt{g\, k \tanh(kD)} \tag{4.2}$$

with g as gravity constant in [ms^{-2}], D the depth of the ocean in [m]. Since in reality waves are not ideal cosine waves, a more realistic spectrum can be made by the addition of several cosine functions according to Equation 4.3.

$$y = \sum_i^{\infty} h_i(x,t) = \sum_i^{\infty} H_{wi} \cos(k_i x - \omega_i t) \tag{4.3}$$

with the angular frequency given according to Equation 4.4:

$$\omega_i = \sqrt{g\, k_1 \tanh(k_i D)} \tag{4.4}$$

the wave length λ [m] is related to the wavenumber k according to Equation 4.5:

$$\lambda_w = \frac{2\pi}{|k|} \tag{4.5}$$

While the wave period T_p [s] is related to the wave frequency according to Equation 4.6:

$$T_p = \frac{2\pi}{\omega} \tag{4.6}$$

Finally, the group velocity C_g [ms^{-1}] is given by Equation 4.7 (Cornet, 2008):

$$C_g = \frac{\omega}{2k}\left(1 + \frac{2k_w D}{\sinh(2k_w D)}\right) \tag{4.7}$$

The wave frequency, Equation 4.4, is a general one which can be used for both deep and shallow water. What can be noted is that for deep water waves and thus a large H, the term kD is much larger than 1 which makes the hyperbolic tangent function in Equation 4.4 reduce to 1. This results in a new equation for the radial wave frequency given by Equation 4.8:

$$\omega = \sqrt{gk} \tag{4.8}$$

In general ocean wave environment is dominated by two main parameters, respectively the specific wave height H_s and wave period T_p. Given these two parameters, it is sufficient to create a certain wave field. However, it should be noted that the summation of several cosine terms is not linearly spread. For this different wave spectrums are set up which incorporates the probability of occurrence waves with certain wave height and period. This is explained in more detail in subsection 5.2. The wave energy level is usually expressed as power per unit length, as can be seen in Equation 4.9. Typical values for suitable offshore locations, based on annual average, range between 20 and 70 [kWm^{-1}] and occur mostly in moderate to high latitudes (Falcao, 2009)

$$P_{avail} = \left(\frac{1}{2}\right)\rho g H_w^2 C_g \tag{4.9}$$

The wave energy level, dependent on wave height and period is calculated in order to see its effect on power production. For this the wave height is varied between 0 and 3.5 meter while the wave period is varied between 1 and 15 seconds, which are both typical ranges for these parameters (Edge and Hemsley, 2001). As can be seen in Figure 15, the quadratic effect of the height is clearly visible. Another interesting thing which can be noted is that for a suitable offshore location the annual average of the wave height should at least be 1.6 meter.

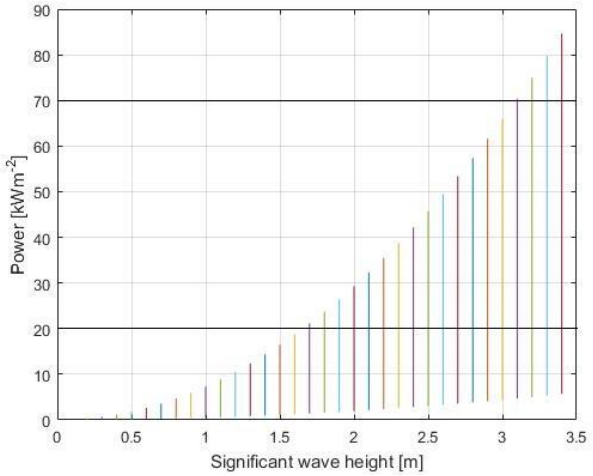

Figure 15 Wave energy density

4.2 Wave Spectrum in frequency and time domain

As mentioned in subsection 4.1, ocean waves show irregular behavior but their occurrence can be visualized according to a specific wave spectrum. Several wave spectrums have been introduced, for this research the JONSWAP spectrum is used (Hasselman, 1973), which is an extension of the Pierson Moskowitz (Pierson and Moskowitz, 1963).

For this radial wave spectrum a range for the frequency is chosen between 0.2 and 2 [rads^{-1}] with 500 intermediate steps. The JONSWAP spectrum is given by Equation 4.10:

$$S(\omega) = \alpha_s H_s^2 \frac{\omega_p^4}{\omega^5} \exp\left(-\frac{5}{4}\frac{\omega}{\omega_p}^4\right) \gamma^{C_x} \tag{4.10}$$

With H_s as wave height [m], ω_p as peak radial frequency [rads^{-1}], γ as JONSWAP constant taken as 3.3 [-] and α_s[-] and C_0 [-] according to Equations 4.11 and 4.12:

$$\alpha_s = \frac{0.0624}{0.230+0.0336\gamma-\left(\frac{0.185}{1.9+\gamma}\right)} \tag{4.11}$$

$$C_x = \exp\left(-\frac{(\omega-\omega_p)^2}{2\sigma^2{\omega_p}^2}\right) \tag{4.12}$$

With σ as the spectral width parameter which is frequency dependent according to:

$$\sigma = 0.07 \; for \; \omega < \omega_p$$

$$\sigma = 0.09 \; for \; \omega \geq \omega_p$$

The JONSWAP wave spectrum given in the frequency domain can be seen for different wave heights and periods in Figure 16. Corresponding sea states are shown in Table 5 (De Backer, 2009).

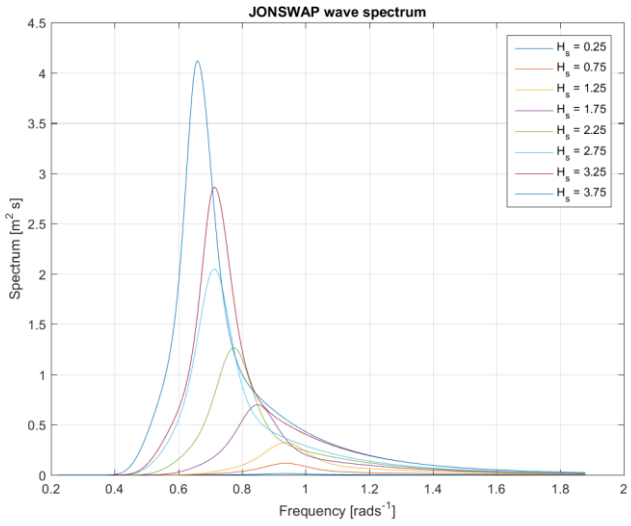

Figure 16 JONSWAP wave spectrums for different wave heights and periods

Sea state	H_s [m]	T_p [s]	ω_p [rads^{-1}]
1	0.25	6.70	0.9378
2	0.75	6.70	0.9378
3	1.25	6.70	0.9378
4	1.75	7.40	0.8491
5	2.25	8.11	0.7747
6	2.75	8.81	0.7132
7	3.25	8.81	0.7132
8	3.75	9.52	0.6599

Table 5 Different sea states

An example of such a JONSWAP theoretical wave spectrum for a specific sea state is shown in Figure 17.

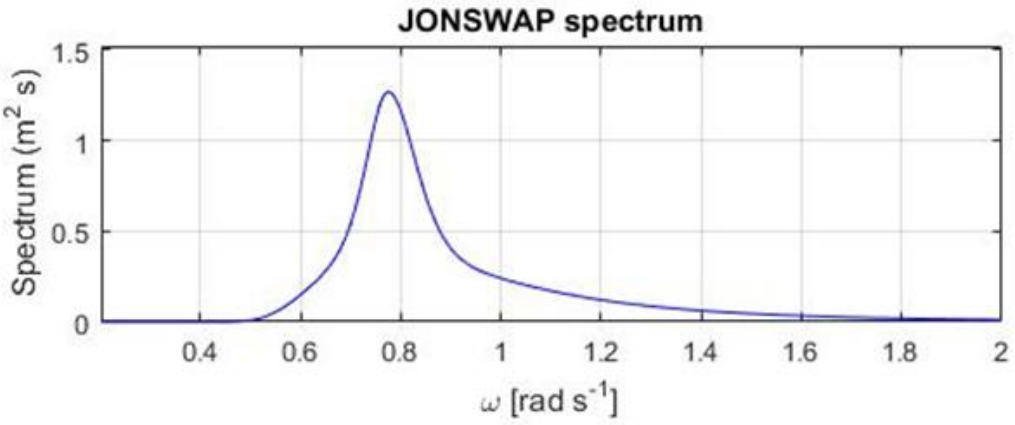

Figure 17 JONSWAP Wave spectrum for H_w = 2.25 [m] and T_p = 8.70 [s]

Using the Fourier transformation in order to convert the frequency domain to the time domain, a MATLAB function is made which is named Freq2Time and can be found in Appendix E. The script is based on the inverse Fourier transformation which is given by Equation 4.13:

$$fft(t) = \frac{1}{\sqrt{2\pi}} \int_{-\infty}^{\infty} F(\omega) e^{i\omega t} d\omega \tag{4.13}$$

For this transformation, the fast Fourier algorithm (FFT) is used for efficiently calculating the discrete Fourier transformation. The advantage of the FFT approach is that it rapidly computes the transformations by factorizing the Discrete Fourier Transformation matrix into a product of sparse factors. Therefore, it reduces the complexity of computing the Discrete Fourier Transformation (DFT) from order n^2 to the order n log n, which n as the size of the data (Van Loan, 1992). Furthermore, Hamming windowing is used in order to reduce spectral leakage (Harris, 1978). The result of this transformation from Figure 17 to the time domain can be seen in Figure 18.

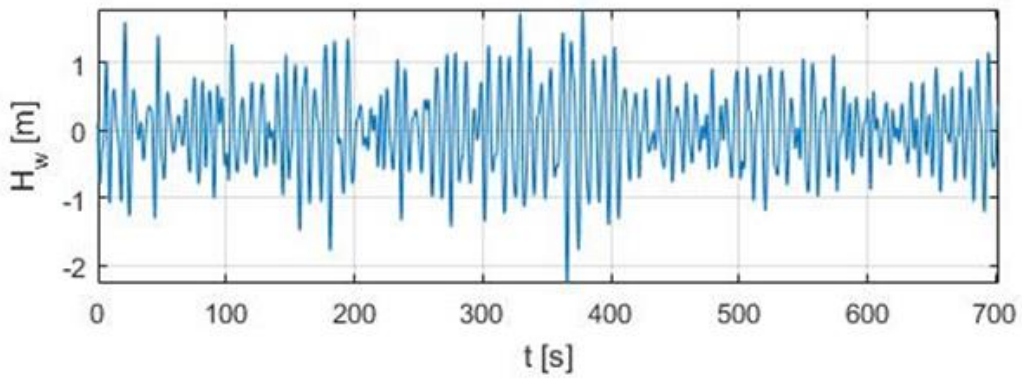

Figure 18 Wave spectrum converted to time domain for H_s = 2.0 [m] and T_p = 8.0 [s]

4.3 Modelling of waves in time by solving wave equation

As mentioned in subsection 4.1, wave movement can be described using the wave Equation. Solving the wave Equation will first be done in one dimension and then extended to two dimensions. Assuming that the function which describes the wave movement is only dependent on position x and time t, function y, be written as $y = h(x,t)$.

This function will then satisfy the linear ordinary differential Equation 4.14:

$$\frac{d^2h}{dt^2} = c^2 \frac{d^2h}{dx^2} \tag{4.14}$$

In order to solve this second order partial differential Equation, the wave Equation is discretized. Discretization is the process of transferring continuous functions into discrete counterparts. This is usually carried out as first step in order to make these functions suitable for numerical evaluation.

The second derivative of h, both in respect to t and x can be approximated by the central difference according to Equation 4.15:

$$f''(x) = \frac{f(x+\Delta x)-2f(x)+f(x-\Delta x)}{\Delta x^2} \tag{4.15}$$

This then results in Equations 4.16 and 4.17:

$$\frac{d^2h}{dt^2} = \frac{h(x,t+\Delta t)-2h(x,t)+f(x,t-\Delta t)}{\Delta t^2} \tag{4.16}$$

$$\frac{d^2h}{dx^2} = \frac{h(x+\Delta x,t)-2h(x,t)+f(x-\Delta x,t)}{\Delta x^2} \tag{4.17}$$

Using Equations 4.16 and 4.17 as approximations, the wave equation can be written as Equation 4.18:

$$\frac{h(x,t+\Delta t)-2h(x,t)+f(x,t-\Delta t)}{\Delta t^2} = c^2 \frac{h(x+\Delta x,t)-2h(x,t)+f(x-\Delta x,t)}{\Delta x^2} \tag{4.18}$$

As can be seen from Equation 4.18, this approximation contains values of h in three different time steps, respectively: future time by (t+Δt), current time (t) and past time (t-Δt). Solving h in terms of future time (t+Δt) by rewriting Equation 4.18 results in Equation 4.19:

$$h(x,t+\Delta t) = r_x{}^2\big(h(x+\Delta x,t)+h(x-\Delta x,t)\big) + 2(1-r_x{}^2)h(x,t) - h(x,t-\Delta t) \tag{4.19}$$

where $r_x = c\,\frac{\Delta t}{\Delta x}$. In order to obtain numerical stability, Δt should be chosen small enough so that r_x < 0.5. Now that the wave equation is discretized, parts of Equation 4.19 are renamed in order to implement them for numerical coding. $h(x,t+\Delta t)$ is future time, $h(x,t)$ is current time and $h(x,t-\Delta t)$ is past time, the script can be found in Appendix D.

As can be noted from Equation 5.19, the calculation of future values starts at n = 2 and ends at n−1. The reference to index i−1 would cause an error for i less than 2. Similarly, the reference to index i+1 is invalid for i greater than n−1. This update rule thus cannot be used on end points for which other terms are introduced. For this case, it is necessary that wave heights are introduced at x=0 and that they reflect back at x=L. Visual representation of the domain is shown in Figure 19.

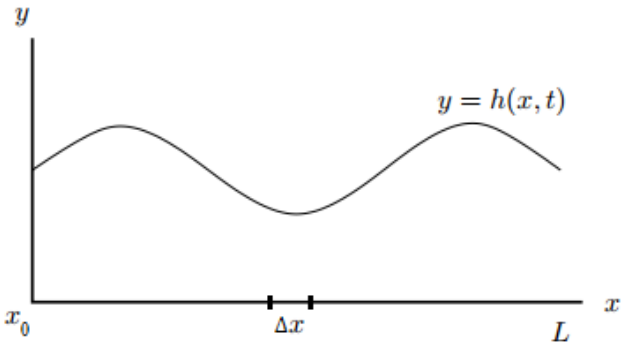

Figure 19 Introduced domain for the two dimensional wave equation

The introduction of waves at x = 0 can be done by introducing and updating values for future values, these values are dependent on the chosen wave spectrum discussed in subsection 4.2. In order to have waves perfectly reflected at x = L and knowing that a reflected wave is perpendicular to the boundary at all times the two following conditions are introduced:

$$\frac{\mathrm{dh}}{\mathrm{dx}}(x = 0) = 0$$
$$\frac{\mathrm{dh}}{\mathrm{dx}}(x = L) = 0$$

By combining these conditions with the wave equation, using the central difference approximation and substituting L for values of x results in Equations 4.20 and 4.21:

$$\frac{h(L,t+\Delta t)-2h(L,t)+f(L,t-\Delta t)}{\Delta t^2} = c^2 \frac{h(L+\Delta \mathrm{x},t)-2h(L,t)+f(L-\Delta \mathrm{x},t)}{\Delta x^2} \quad (4.20)$$

$$\frac{h(\Delta \mathrm{x},\mathrm{t})-h(-\Delta \mathrm{x},\mathrm{t})}{2\Delta \mathrm{x}} = 0 \quad (4.21)$$

From Equation 4.21 can be noted that the term $h(-\Delta \mathrm{x}, \mathrm{t})$ has no physical meaning since the x coordinate is not negative in the proposed domain. However, from Equation 4.21 can be used that $h(\Delta \mathrm{x}, \mathrm{t}) = h(-\Delta \mathrm{x}, \mathrm{t})$, using this in Equation 4.20 results in the following statement for future(n), as can be seen in Equation 4.22:

$$h(L, t + \Delta t) = 2{r_x}^2 h(L - \Delta \mathrm{x}, \mathrm{t}) + (1 - {r_x}^2)h(L, t) - h(L, t - \Delta t) \quad (4.22)$$

Similar derivation is also possible for two dimensions for which the domain is extended and an extra coordinate z is introduced as can be seen in Figure 20.

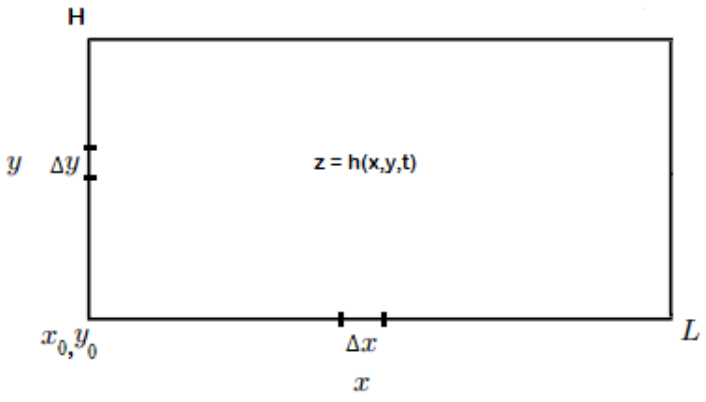

Figure 20 Introduced domain for three dimension wave equation

Performing the same steps as described in the beginning of this subsection, but now for two dimensions, the wave equation can be written according Equation 4.23:

$$h(x,y,t+\Delta t) = r_x{}^2\,[h(x+\Delta x,y,t)+h(x-\Delta x,y,t)] + r_y{}^2[h(x,y+\Delta y,t)+h(x,y-\Delta y,t)] + [2-2r_x{}^2-2r_y{}^2]h(x,y,t) - h(x,y,t-\Delta t) \quad (4.23)$$

With $r_x = c\,\frac{\Delta t}{\Delta x}$ and $r_y = c\,\frac{\Delta t}{\Delta y}$. Results of such an ocean wave field is visualized in Figure A4.

4.4 Wave Trapping

As mentioned in subsection 4.3, a concept is proposed which excites the vertical displacement of the point absorber. This WEC is placed in the center between the three columns of the WindFloat wind turbine as can be seen in Figure 10b (WindFloat, 2016). In order to maximize energy production of the buoy point absorber, maximal wave energy must be absorbed and the waves should be trapped. A point absorber is a floating system that absorbs energy in all direction through its movements at the water surface. A point absorber is usually designed to resonate so that its harnessed power is maximized. In this study, the wave energy converter is placed in the middle of the WindFloat triangle. Subsection 5.4.3 evaluates the best buoy geometry which could be used for this configuration. Since platform movement should be minimized in order to guarantee stability, the buoy should therefore buoy resonate maximally in heave movement. Different translations and rotations, such as the aforementioned heave mode, are shown in Figure 21. The energy is produced using a power take off system which is explained in subsection 6.6.

The initial design which is considered is shown in Figure 10c, dimensions of this concept are listed in Table 6 (WindFloat, 2016). The diameter of the wave energy converter is determined in subsection 5.4.3.

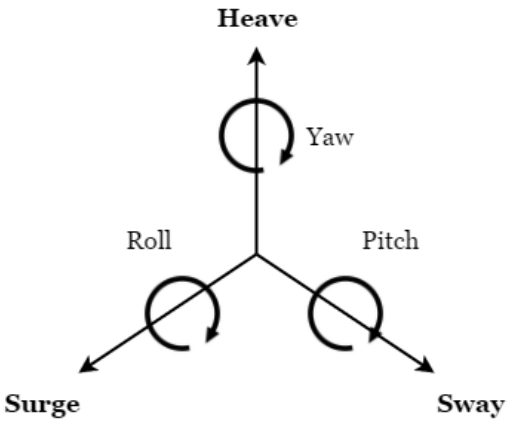

Figure 21 Six degrees of freedom

WindFloat	Dimension	Unit
Column diameter	10	[m]
Column center to center	46	[m]
Pontoon diameter	2.1	[m]
Operation draft	10	[m]
Displacement	4.832.000	[kg]

Table 6 WindFloat main dimensions

5. Wave energy converter

In this chapter the modeling of the wave energy converter is explained. First numerical simulations are done and described in subsection 5.1, in order to increase the understanding of a buoy point absorber behavior in different weather conditions. Then, the buoy is modeled as a simple mass spring damper system in subsection 5.2. Then by adding the power take off system the mass spring damper system becomes more complex and motions relative to a fixed reference are described in subsection 5.3. The process of maximizing energy production is described in subsection 5.4. The hydrodynamic parameters of this optimal buoy are given in subsection 5.5 and its steady state response is given in subsection 5.6.

5.1 Numerical simulations buoy in openWEC

In this subsection the numerical simulations which are done using openWEC is explained. OpenWEC is an all-in-one WEC simulation tool. It is written in python and uses Qt design language for GUI development (McNatt, 2016). Validation of this program is given by Babarit and Delhommeau (2015). In general, the larger the buoy, the more energy can be absorbed because the contact area of the buoy and wave increases. However, if the buoy becomes too large, the diffraction forces increase and they dominate the loading and responses. Thus, the buoy will not work anymore as a point absorber (Engstrom, 2011). Since the dimensions of the support structure of the Wind Float are set, the buoy is limited to a certain size. The experiments are done in order to get an idea behind the possible power extraction of a buoy with a diameter of 5 meter with regular and irregular wave input conditions. A diameter of 5 meter is chosen because the state of art wave energy sector is using small scale applications. The water depth is assumed to be 100 [m], water density 1020 [kgm^{-3}] and 500 mesh panels were used to construct the spherical buoy. Figure 22 shows the intersection of the used mesh profile.

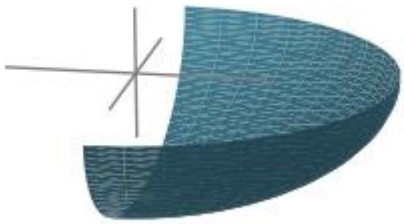

Figure 22 Mesh used for openWEC numerical simulations

Results of these numerical simulations can be found in Appendix C. General buoy behavior which was found during these simulations was that the power extraction increased with wave height. The optimal wave period was around 8 seconds and regular waves produce significantly higher power production than irregular waves. If the wave period is 8 seconds, the wave height should be at least 2.26 meter for a suitable offshore location as can be seen from Figure 15 or solving Equation 4.9 for $T_p = 8$. Equation 4.9 does not directly show its dependence on the wave period but this is incorporated by the wave number in the group velocity which is dependent on λ_w and thus ω. However, when coupling both the wave energy converter with the ocean wave model, sizing the buoy is taken into account in order to maximize energy yield, this will later be done in subsection 5.4.3. Since the buoy which was used for these numerical simulations has a different shape than the eventually chosen buoy, the outcome of these simulations is only used as indication for power production and to study the relevant parameters which influence this power production.

5.2 Modelling buoy responses as simple mass spring damper in time domain

This subsection will describe the modelling process of the wave energy converter. The behavior of a heaving point absorber can be modeled as a mass-spring-damper system with one degree of freedom as can be seen in Figure 23. The system is excited in the heave mode by the waves which can be simplified to an external force.

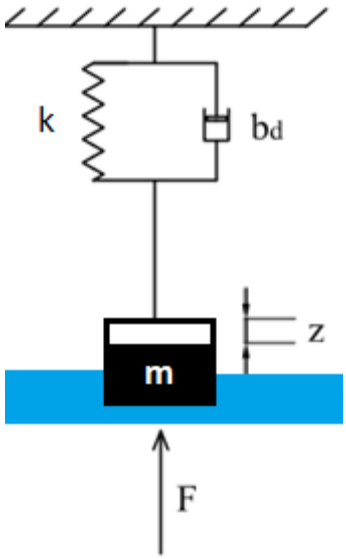

Figure 23 Mass spring damper system

The system contains a spring with stiffness coefficient k [kgs^{-2}] and is linearly damped with damping coefficient b_d [kgs^{-1}]. Furthermore, the buoy has a mass, m [kg], which can move in the vertical direction introduced as z [m], this movement is due to the waves and can be modeled according to Equation 5.1:

$$F = F_a \sin(\omega t) \tag{5.1}$$

Setting up a force balance and using Newton's second law to derive the equation of motion gives Equation 5.2:

$$m\frac{d^2z}{dt^2} + b_d\frac{dz}{dt} + kz = F_A sin(\omega t) \tag{5.2}$$

In order to describe the solution, first the homogeneous solution, where the external force is set to zero, is calculated. Equation 5.2 then reduces to Equation 5.3:

$$m\frac{d^2z}{dt^2} + b_d\frac{dz}{dt} + kz = 0 \tag{5.3}$$

The solution of this ordinary differential equation can be assumed in the form of Equation 5.4:

$$z = z_A e^{qt} \tag{5.4}$$

with z_A and q as unknown constants [-]. Substituting of z into Equation 5.3 results in Equation 5.5:

$$(mq^2 + b_d q + k) z_A e^{qt} = 0 \tag{5.5}$$

In order for Equation 5.5 to fulfill for all time, this can be simplified to Equation 5.6:

$$mq^2 + b_d q + k = 0 \tag{5.6}$$

With q as solution for the quadratic problem according to Equation 5.7:

$$q_{1,2} = -\frac{b_d}{2m} \pm \sqrt{\left(\frac{b_d}{2m}\right)^2 - \frac{k}{m}} \tag{5.7}$$

If the system is critically damped, it would mean that it returns to its equilibrium position directly without vibrating. The corresponding damping coefficient, b_c [kgs^{-1}], is equal to Equation 5.8:

$$b_c = 2\sqrt{km} = 2m\omega_n \tag{5.8}$$

With the natural frequency of the system equal to Equation 6.9:

$$\omega_n = \sqrt{\frac{k}{m}} \tag{5.9}$$

named the natural frequency of the system [rads^{-1}]. The ratio between the actual damping coefficient b_d [kgs^{-1}] and b_c [kgs^{-1}] is called the damping ratio which is thus equal to Equation 5.10:

$$\zeta_d = \frac{b_d}{b_c} \tag{5.10}$$

A heaving point absorber can be considered as an underdamped mechanical oscillator and thus the $b_d < b_c$. This will eventually be checked in subsection 7.2. For an underdamped system the values for q, as written before in Equation 5.7, can now be rewritten as Equation 5.11:

$$q_{1,2} = -\zeta_d\omega_n \pm i\omega_n\sqrt{1 - {\zeta_d}^2} \tag{5.11}$$

According to Equation 5.4 and 5.11, the solution of z becomes:

$$z = A_1\, e^{q_1 t} + A_2\, e^{q_2 t} \tag{5.12}$$

The constants A_1 [-] and A_2 [-] are determined by the initial conditions of the system. Replacing A1 and A2 by the expressions in Equation 5.13 and Equation 5.14, according to de Backer (2009) results in an equivalent expression for the motion given by Equation 5.15:

$$A_1 = \frac{1}{2} z_{Af} \left(sin(\beta_f) - icos(\beta_f)\right) \tag{5.13}$$

$$A_1 = \frac{1}{2} z_{Af} \left(sin(\beta_f) + icos(\beta_f)\right) \tag{5.14}$$

$$z = z_{Af} e^{-\zeta_d \omega_n t} \sin\left(\sqrt{1 - {\zeta_d}^2}\, \omega_n t + \beta_f\right) \tag{5.15}$$

The exponential function in Equation 5.15 is responsible for the decreasing amplitude. The sine function causes the oscillations at a frequency equal to the damped natural angular frequency which is equal to Equation 5.16:

$$\omega_d = \sqrt{1 - {\zeta_d}^2}\, \omega_n \tag{5.16}$$

The damped free oscillations of a system disappear after a number of oscillations. The number of oscillations depends on the damping in the system.

When an external force is applied on the system, as in Equation 5.2, the complete solution of the equation of motion consists of the addition of the free oscillation, dependent on the initial conditions, and the forced oscillation or steady-state oscillation, which is called the particular solution of the differential equation. This particular solution of Equation 5.2 is of the form Equation 5.17:

$$z = z_{As} \sin(\omega t + \beta_s) \tag{5.17}$$

with z_{As} [m] the amplitude of the steady-state oscillation given in Equation 5.18:

$$z_{As} = \frac{F_A}{\sqrt{[(k-m\omega^2)^2+(b\omega)^2]}} \tag{5.18}$$

and β_s the phase angle [rad] between the external force and the motion of the system is given as Equation 5.19

$$\beta_s = \operatorname{atan}\left(\frac{-b_d\omega}{k-m\omega^2}\right) \tag{5.19}$$

To conclude, the complete response of a mass-spring-damper system subjected to a regular external force is given by the addition of the free oscillation and steady state solution resulting in Equation 5.20:

$$z_t = z_{free} + z_{forced} = z_{Af} e^{-\zeta_d \omega_n t} \sin\left(\sqrt{1-{\zeta_d}^2}\,\omega_n t + \beta_f\right) + z_{As} \sin(\omega t + \beta_s) \tag{5.20}$$

Visual representation of Equation 5.20 can be seen in Figure A3.

5.3 Buoy response modelling frequency domain fixed reference

As described in subsection 5.2, the wave energy converter can be described by a mass-spring-damper system. However, in previous calculations the power take off system has not been taken into consideration. This system can be modeled as an external damper and a supplementary mass, as can be seen in Figure 24 (De Backer, 2009), where the buoy is now represented by a slightly different but more realistic shape. Note that the PTO system has a fixed reference while in the case of a hybrid wind wave system, the platform itself moves as well. The translation from fixed to floating reference is made in chapter 7.

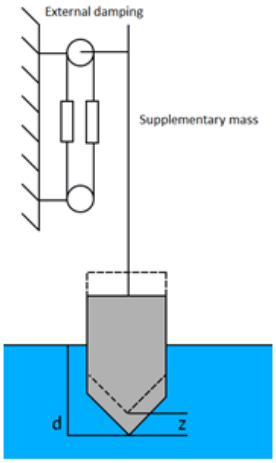

Figure 24 Schematic representation of a heaving point absorber

In equilibrium position the floater has a draft *d* [m]. Due to the vertical wave motion, the floater now has a position *z* from its equilibrium position. The equation of motion of this point absorber can again be described by Newton's second law which results in Equation 5.21:

$$m\frac{d^2z}{dt^2} = F_{ex} + F_{rad} + F_{res} + F_{damp} + F_{tun} \quad (5.21)$$

where m is the mass of the buoy [kg] and $\frac{d^2z}{dt^2}$ the buoy acceleration [ms^{-2}]. F_{ex} *is* the exciting wave force in [N], F_{rad} the radiation force in [N]. This radiation force can be decomposed using linear theory according to van Paepegem et al (2009), in a linear added mass term and a linear hydrodynamic damping term as shown in Equation 5.22:

$$F_{rad} = -m_{added}(\omega)\frac{d^2z}{dt^2} - b_{hyd}(\omega)\frac{dz}{dt} \quad (5.22)$$

The hydrostatic restoring force, F_{res}, is the difference between the buoyance and the force due to the floaters weight and is given in [N]. This force corresponds to the spring force in Equation 5.2. With a linear spring coefficient k [Nm^{-1}], the hydrostatic restoring force can be expressed as Equation 5.23:

$$F_{res} = \rho V - mg = -kz \quad (5.23)$$

where V is the submerged buoy volume [m^3]. The hydrostatic restoring coefficient given in [Nm^{-1}] is expressed as Equation 5.24:

$$k = \rho g A_w \quad (5.24)$$

where A_w is the waterline area [m^2]. F_{damp} is the external damping force [N], exerted by the PTO system and F_{tun} the tuning force to phase-control the buoy [N]. The damping and tuning forces are determined by the PTO and control mechanism, respectively, and are in practical applications typically non-linear. However, for simplicity, they are often assumed linear. In that case the damping force becomes as written in Equation 5.25:

$$F_{damp} = b_{ex}\frac{dz}{dt} \quad (5.25)$$

with b_{ext} the linear external damping coefficient originating from the PTO and enabling power extraction given in [kgs^{-1}].

In order to maximize the power production, the buoy should oscillate as much as possible. In order to oscillate the buoy as much as possible the natural frequency of the buoy should be equal to the wave peak frequency. However, in general the natural frequency is higher than the wave frequency and thus should be lowered as can be seen from Equation 5.9. This can be done by adding supplementary mass. Adding supplementary mass can be done by mechanically coupling a flywheel to the vertical motion of the buoy. A representation of the supplementary mass, m_{sup}, is given in Figure 24. The supplementary inertia is designed by adding two equal masses at both sides of a rotating belt. In that way, the inertia of the system can be increased without changing the draft of the floater. The tuning force is expressed as Equation 5.26:

$$F_{tun} = m_{sup}\frac{d^2z}{dt^2} \quad (5.26)$$

The effect of the tuning force can be seen in Figure 25. This line would correspond to the buoy position if the mass of the buoy were negligible. The dashed line illustrates the position of the buoy in case the inertia of the point absorber is increased so that the natural frequency of the buoy matches the wave frequency which is called tuning.

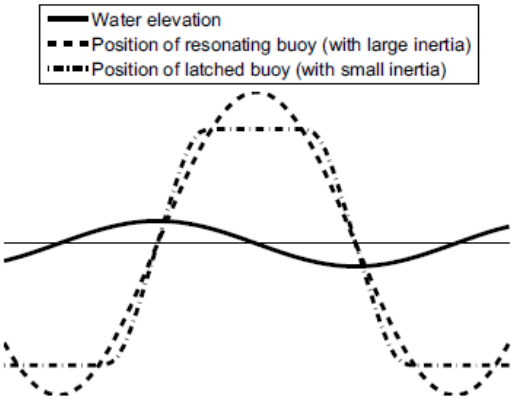

Figure 25 Effect of phase control (Falnes, 2002)

When taking into account the previous considerations, the equation of motion of the presented heaving point absorber can be rewritten as Equation 5.27:

$$\left(m_{buoy} + m_{added}(\omega)\right)\frac{d^2z}{dt^2} + m_{sup}\left(\frac{d^2z}{dt^2}\right) + b(\omega)\frac{dz}{dt} + b_{ex}\left(\frac{dz}{dt}\right) + kz = F_{ex}(\omega, t) \quad (5.27)$$

The two external parameters b_{ext} [kgs^{-1}] and m_{sup} [kg] have to be optimized in order to maximize the absorbed power which is done in subsection 5.6.

5.4 Power production wave energy converter

In this subsection the power production of the wave energy converter is described. First the absorbed power is calculated, followed by a brief description of how the maximum power can be achieved. At last, the optimal buoy dimensions; both size and shape is chosen.

5.4.1 Power absorption

In this subsection the power production of the buoy is explained. For this the buoy is seen as a harmonically oscillating body with velocity v [ms^{-1}] and a time dependent force F [N] according to Equations 5.28 and 5.29:

$$F(t) = F_A\cos(\omega t + \beta_f) \quad (5.28)$$
$$v(t) = v_A\cos(\omega t + \beta_v) \quad (5.29)$$

The average absorbed power of the buoy is equal to the average excited power minus the average radiated power according to Equation 5.30:

$$P_{abs,av} = P_{ex,av} - P_{rad,av} \quad (5.30)$$

The power averaged over a time period T can then be found according to Equation 5.31 (de Backer, 2009):

$$P_{ex,av} = \frac{1}{2}F_A v_A\cos(\mu) \quad (5.31)$$

With μ as the phase shift between the exciting force and the velocity according to Equation 5.32:

$$\mu = \beta_{Fex} - \beta_v \quad (5.32)$$

The average radiated power is equal to Equation 5.33:

$$P_{rad,av} = \frac{1}{2} b_{hyd} v_A^2 \tag{5.33}$$

When filling in Equation 5.30, the average absorbed power of the buoy can be written as Equation 5.34:

$$P_{abs,av} = \frac{1}{2} F_A v_A \cos(\mu) - \frac{1}{2} b_{hyd} v_A^2 \tag{5.34}$$

The power absorbed by the power take off system can thus be written as Equation 5.35 (De Backer, 2009):

$$P_{abs,av} = \frac{1}{2} b_{ex} v_A^2 = \frac{1}{2} b_{ex} \omega^2 z_A^2 \tag{5.35}$$

5.4.2 Maximizing power production

In this subsection the relationship for optimizing the absorbed power of the buoy is given. In subsection 5.4.1, the derivation of the absorbed power is given. Its maximum occurs when the derivative of Equation 5.34 with respect to buoy's velocity is taken and set equal to zero. The found maximum velocity is then equal to Equation 5.36:

$$v_{A,max} = \frac{F_{exA}}{2 b_{hyd}} \cos(\mu) \tag{5.36}$$

Substituting this result in Equation 5.31 results in Equation 5.37:

$$P_{abs,av,max} = \frac{|F_{exA}|^2}{8 b_{hyd}} \cos^2(\mu) \tag{5.37}$$

From this can be directly noticed that the optimal phase shift, which was introduced in subsection 5.4.1, is optimal when equal to zero. The velocity of the buoy should therefore be in phase with the exciting force in heave mode. The amplitude of this force can be rewritten as Equation 5.38:

$$F_{exA} = f_x \, \zeta_A \tag{5.38}$$

Where f_x is a transfer function [-]. In addition, the hydrodynamic coefficient in heave mode can be analytically determined according to Falnes (2002) with Equation 5.39:

$$b_{hyd} = \frac{\omega k_w}{2 \rho g^2 D_f} f_{x,A}^2 \tag{5.39}$$

Where k_w is the wavenumber [-] and D_f the so called depth function [-] which is equal to Equation 5.40 (Falnes, 2002):

$$D_f = \tanh(k_w D) + k_w D - k_w D \, tanh^2(k_w D) \tag{5.40}$$

When substituting Equations 5.39 and 5.40 into Equation 5.37, the following expression for the average absorbed power in regular waves is found according to Equation 5.41:

$$P_{abs,av,max} = \frac{\rho g^2 D_f}{4 \omega k_w} \, {\zeta_A}^2 \tag{5.41}$$

The total available power in the waves can be found by substituting Equations 4.2 and 4.7 in Equation 4.9 resulting in Equation 5.42:

$$P_{avail} = \frac{\rho g^2 D_f}{4\omega} \zeta_A{}^2 \tag{5.42}$$

The ratio between the absorbed and the available power per unit crest length is named the capture width. Practical application for this term is that when it's divided by the diameter of the buoy, the absorption efficiency can be determined. This efficiency is thus not the total efficiency of the WEC which should include losses in power production of the PTO system. The maximum capture width is thus equal to Equation 5.43:

$$\lambda_p = \frac{P_{abs,av,max}}{P_{avail}} = \frac{1}{k_w} = \frac{\lambda_w}{2\pi} \tag{5.43}$$

This maximal capture width can also be obtained from Equation 5.44 according to (Vantorre et al, 2004):

$$\lambda_p = \frac{P_{abs}}{P_{avail}} = \left(\frac{2\lambda_w}{\pi}\right) \frac{b_{hyd}(\omega) b_{ex} \omega^2}{\sqrt{\left(k - (m_{buoy} + m_{added} + m_{sup})\omega^2\right)^2 + (b_{hyd}(\omega) + b_{ex})\omega)^2}} \tag{5.44}$$

Maximum values for Equation 5.44 are reached when the numerator is maximal and the denominator is minimal and thus can be set to zero. The denominator is minimal when the natural frequency is equal to Equation 5.45:

$$\omega_n = \sqrt{\frac{k}{m_{buoy} + m_{added} + m_{sup}}} \tag{5.45}$$

This is in line with previous assumptions mentioned in subsection 4.4 but is now again proved. In other words, a point absorber that is a good damper at an angular frequency ω_n is also a good receiver for waves with the same frequency. However, the theoretical optimum which is found is Equation 5.45 only holds when the system is slightly simplified, in reality second order effects become important and should be taken into account as well; this will then result in a smaller capture width. At last, as mentioned in chapter 4, ocean waves show irregular behavior. In an irregular wave field, the response in irregular waves is obtained by super imposing the responses of regular waves. The wave amplitude of is derived from the JONSWAP spectrum of Equation 4.10, which results in Equation 5.46:

$$\zeta_A = 2\sqrt{S_\zeta(w)\Delta w} \tag{5.46}$$

The spectrum of the amplitude of the buoy position is equal to Equation 5.47:

$$S_z(w) = S_\zeta(w)\left(\frac{z_A^2}{\zeta_A^2}\right) \tag{5.47}$$

When a Rayleigh distribution is assumed for the motion amplitude of the floater motion, the significant amplitude of the buoy's motion can be written as Equation 5.48:

$$z_{A,sign} = 2\sqrt{\int_0^\infty S_z \, d\omega} \tag{5.48}$$

The available power over the diameter of the point absorber is expressed according to Equation 5.49 (Crabb, 1980):

$$P_{avail,D} = D \int_0^\infty \rho g C_g(\omega) S_\zeta(w) d\omega \tag{5.49}$$

By applying linear superposition of the buoy responses, the power absorption in irregular waves is found to be equal to 5.50 (de Backer, 2009):

$$P_{abs} = \int_0^{\infty} b_{ex}\omega^2 \left(\frac{z_A}{\zeta_A}\right)^2 S_{\zeta}(w)d\omega \tag{5.50}$$

The absorption efficiency for irregular waves can still be found using Equation 5.43 and dividing it by the buoys diameter. It should be noticed that the power absorption efficiency can be higher than 100. A maximum of 140% was found according to Vantorre et al (2004) in small amplitude waves. This shows the point absorber performance in which the absorption length can be larger than the physical length of the absorber. With increasing wave height, more power can then be captured, but at a lower efficiency. This means that increasing the size of the buoy would result in higher power absorption because the power for both longer and shorter wave periods is obtained at nearly the same efficiency (Vantorre et al, 2004).

5.4.3 Effect different buoy types on power production

In this subsection the effect of different buoy geometries is given. As can be seen from Equation 5.38, the absorbed power is dependent on b_{ext} and the velocity of the buoy which itself is dependent on b_{ext} and m_{supp}. Both of these values are dependent on the shape and mass the buoy. To find these values for given buoy shapes, Vantorre et al (2004) determined optimal values as a function of the waterline radius for each chosen spectrum restricted to two conditions; the power absorbed by the external damping system should be maximized and the probability of slamming due to excessive vertical motions of the buoy relative to the free water surface should be limited. First, the optimal buoy shape was numerically calculated with respect to maximized power absorption performance (Vantorre, 2002). An optimum appeared to be found by a bi-conical shape with a diameter of 5.0 [m]. Current wave energy converters are, due to their costs, mostly still quite small. In subsection 7.4, investigation will be done to see the effect when sizing up the buoy. The physical explanation of the bi-conical shape is that most of the wetted area is located near the free surface, which improves the buoy's response to wave movement. Furthermore, the lower part increases the draft which lowers the possibility of slamming. Slamming is a phenomenon that occurs when the buoy re-enters the water, after having lost contact with the water surface. When the buoy experiences such a slam, high hydrodynamic pressures and loads can be subjected to the buoy. The time period of these impacts are usually in the order of magnitude of milliseconds. Fatigue by repeated slamming pressures can the reason for structural material damage and should thus be prevented (De Backer, 2009).

However, when Vantorre et al (2004) did experiments with testing the bi-conical buoy shape it appeared that non-linear effects due to the variability of the waterline surface with draft and free surface instabilities significantly affect the efficiency of power absorption for that buoy. Therefore, the buoy shape had to be modified in order to realize a compromise between the sensitivity to the vertical wave forces, linearity in restoring force, and the limitation in the hydraulic losses during the motion as observed during the first tests. For the three different drafts, it turned out that the cone-cylinder performs slightly better than the hemisphere cylinder shape, however, the difference between both shapes is very small. The most optimal shape in that respect seems to be a hemisphere coupled with a cylinder. But the application of such a shape would result in a significant decrease in hydrodynamic damping, as was concluded as a result of the computational study (Vantorre et al, 2004). Therefore, the modified form, a conical shape with top angle of 90 degrees is expected to give the optimum solution for the conditions which were mentioned earlier (De Backer, 2009). This proposed shape is used further on for this research; hydrodynamic coefficients of this type of buoy are derived in subsection 5.5. The different proposed and compared shapes can be seen in Figure 26.

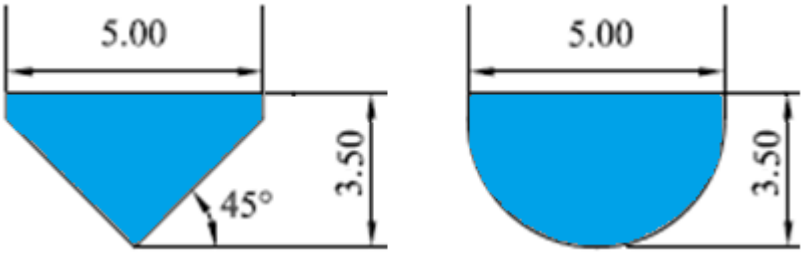

Figure 26 Different buoy shapes

Now that the shape of the buoy is proposed, the size and thus diameter of the buoy must be determined. The effect on power absorption of different drafts and sizing the diameter can be seen in Figure 27.

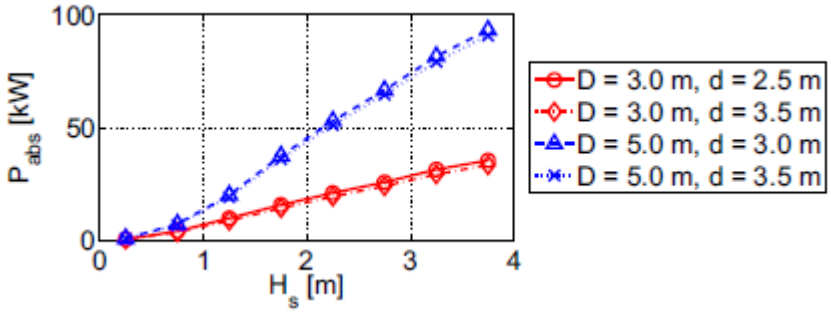

Figure 27 Effect of the diameter on power absorption for cone shaped cylinder (De Backer, 2009)

Since the hydrodynamic damping coefficient and heave exciting force are larger for smaller drafts, the power absorption is larger for smaller drafts. However, as can be seen by Figure 27, this difference is very small. While the selected drafts seemed to limitedly influence the power absorption, changing the diameter has a significant effect on the absorbed power. De Backer (2009) compared two buoys with the same draft (d = 3.5 m), when the volume ratio is 2.0, the ratio of the absorbed power varies between a factor of 1.8 (smallest sea state) and 2.7 (largest sea state). So it was concluded that the smallest diameter is only beneficial in the two smallest sea states, assuming the volume is a measure for the material cost. However, since each unit is assumed to be equipped with its own PTO-system, important additional costs per unit will exist, most probably making the larger diameter also economically more attractive in the smaller sea states. This will be looked into in subsection 7.4.

Finally, when designing and sizing a buoy some restrictions should be taken into account. To avoid too large strokes, excessive control forces and slamming problems, several general restrictions can be imposed on the buoy motions which are:

- Slamming restriction: intended to reduce the occurrence probability of rising out of the water.
- Stroke restriction: limits the maximum buoy displacement
- Force restriction: limits the control forces generated by the power take-off system.

When the force restriction is taken into account, advantage of the larger diameters is almost negligible, since larger diameters involve larger forces, resulting in an increased penalty when the same force restrictions are applied as for the smaller buoys. Hence, this force restriction should be related to the dimensions of the buoy but will not be taken as restriction in this research. To conclude, the optimum diameter has to be determined for a particular device and a particular location, taking into account the relevant restrictions and incorporating a cost assessment. The optimal buoy shape with respect to costs is something which is recommended for

upcoming research and is not part of the scope of the project. For this research a conical shape with top angle of 90 degrees and a diameter of 5 meter is used and only stroke restrictions are taken into consideration. The mass of this buoy was found to be 26200 [kg] (De Backer, 2009).

5.5 Hydrodynamic parameters of the wave energy converter

In this subsection the hydrodynamic parameters of the wave energy converter as described in chapter 5.4.3 is derived. The chosen type was a conical shape with top angle of 90 degrees. Values for added mass, hydrodynamic damping, exciting force F_{exA} and the phase angle θ_{ex} have been taken from de Backer (2009) who used WAMIT in order to obtain these hydrodynamic parameters. WAMIT is a software program developed for the computation of wave loads and motions of floating or submerged offshore structures and based on linear (and second-order) potential theory (WAMIT, 2016). Graphs for these parameters are shown in Figures 28 until and 31. Marked points are values derived from de Backer (2009) through which a fit is modeled in order to obtain the dependency of these hydrodynamic parameters for all frequencies in between the frequency range. The hydrodynamic damping is compared in Figure 29 with the analytical value which was proposed in Equation 5.39. It can be concluded that this matches the output of WAMIT and shows similar behavior in the given frequency range.

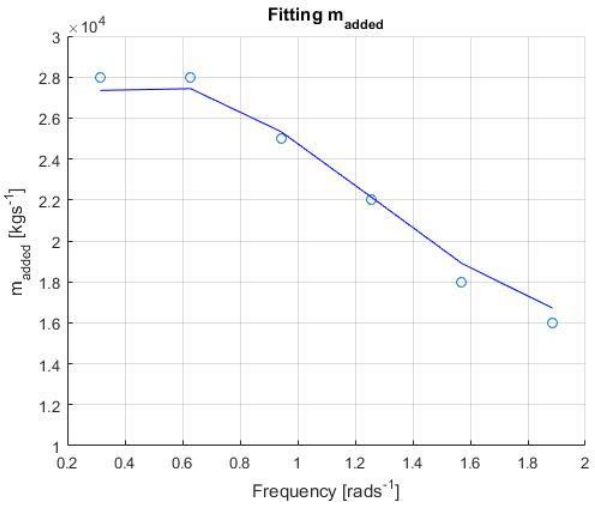

Figure 28 Added mass of the wave energy converter

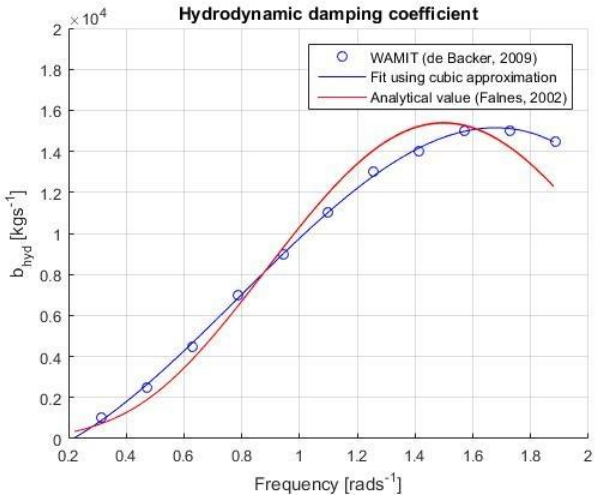

Figure 29 Hydrodynamic damping

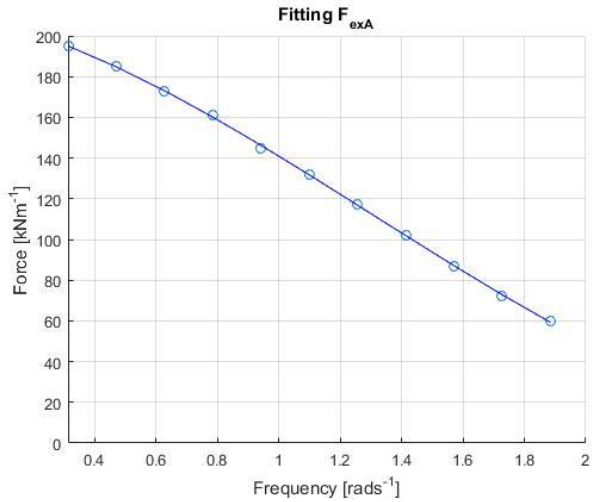

Figure 30 Excitation force per unit wave amplitude

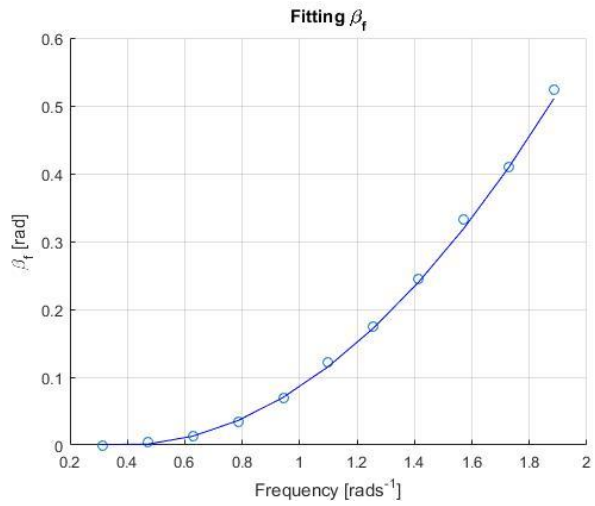

Figure 31 Phase angle of excitation force

These results from de Backer (2009) have been validated with openWEC which uses Nemoh as BEM solver (Babarit and Delhommeau, 2015). The hydrodynamic parameters found using openWEC can be found in Appendix D, it can be concluded that the found values match with WAMIT. The hydrodynamic parameters shown in Figures 28 until and 31 however do not take into account the coupling with the WindFloat structure as proposed in subsection 3.3. In order to find out the effect of the physical presence of the WindFloat structure, additional hydrodynamic parameter calculations are done. For the eight investigated sea states the corresponding wave lengths are calculated using Equation 5.51 and then listed in Table 7.

$$\lambda_w = \frac{gT_p^2}{2\pi} \tag{5.51}$$

Table 7 Wave lengths different sea states

Sea state	H_s	T_p	Wave length	Unit
1	0.25	6.70	70.09	[m]
2	0.75	6.70	70.09	[m]
3	1.25	6.70	70.09	[m]
4	1.75	7.40	85.50	[m]
5	2.25	8.11	102.69	[m]
6	2.75	8.81	121.18	[m]
7	3.25	8.81	121.18	[m]
8	3.75	9.52	141.50	[m]

As can be seen from Table 7, the wave lengths are significantly higher than the lengths between the columns of the WindFloat construction stated in Table 6. Therefore, it is expected that the presence of the WindFloat has influence on the behavior of the wave energy converter. This influence could in theory be both negative as positive since it depends of the refracted waves will either be in or out of phase with other incoming waves at the location where the wave energy converter is placed. The effect of wave refraction is not in the scope of this thesis but the influence of the WindFloat is described in more detail in chapter 8 when the coupling of both systems is taken into account.

5.6 Steady state solution buoy movement

In this subsection the steady state solution of the buoy is described. Since displacement and power production are directly linked the optimization process will here be summarized. The general solution to the buoy movement of Equation 5.30 is given by Equation 5.52:

$$x_t(t) = x_h(t) + x_p(t) \tag{5.52}$$

For the scope of the thesis only the steady state solution of the buoy movement is taken into account. The exponential function of Equation 5.20, goes to zero when time becomes so large that it approaches infinity. This means that transient behavior, described in subsection 5.1 will not be taken into account. If sufficient time has passed, the motion of the total system will thus be given to the steady state solution. As mentioned in subsection 5.3, the two external parameters b_{ext} [kgs^{-1}] and m_{sup} [kg] have to be optimized in order to maximize the oscillation and thus absorbed power. First of all, the supplementary mass is optimized by rewriting Equation 5.45 into Equation 5.53, so that the natural frequency of the system is equal to the peak frequency of the sea state.

$$m_{sup} = -\left(m_{buoy} + m_{added}\right) + \frac{k}{\omega_p^2} \tag{5.53}$$

As can be seen from Equation 5.53, the supplementary mass is both dependent on the sea state and the frequency. This is because the added mass is dependent on the frequency as shown in Figure 28, in order to calculate the supplementary mass depended on only the sea state, the added mass is taken at the peak frequency of the relevant sea state. The peak frequency of the waves is dependent on the wave height according to Equation 4.6. This is visualized in Figure 32, showing the dependency between the supplementary mass and the different sea states.

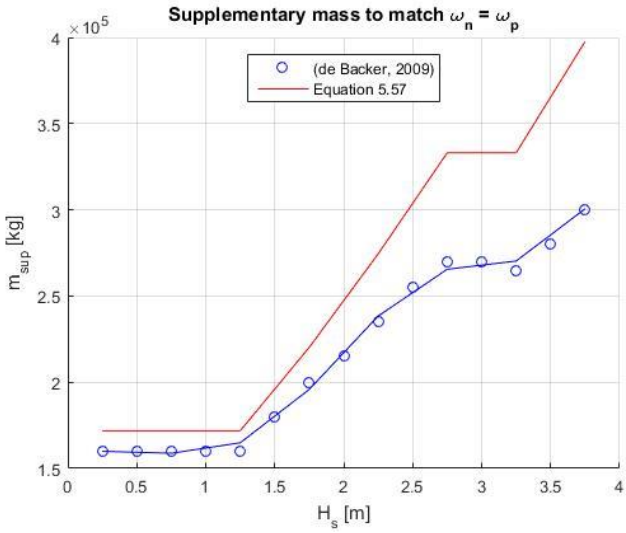

Figure 32 Supplementary mass analytical according to Equation 6.52 and compared to de Backer (2009)

Now that the optimal supplementary mass is known, the external damping coefficient, b_{ex}, can be optimized. Equation 5.44 shows the contradicting influence of b_{ex} on absorbed power; a higher damping coefficient increases the term b_{ex} but reduces the amplitude of the buoy. The optimal is iteratively determined taking some proposed restrictions into consideration in order to avoid unrealistic solutions. Filling in Equation 5.50, results in Figure 33. The corresponding absorption efficiency is found by dividing Equation 5.43 by the diameter of the buoy, its result is shown in Figure 34.

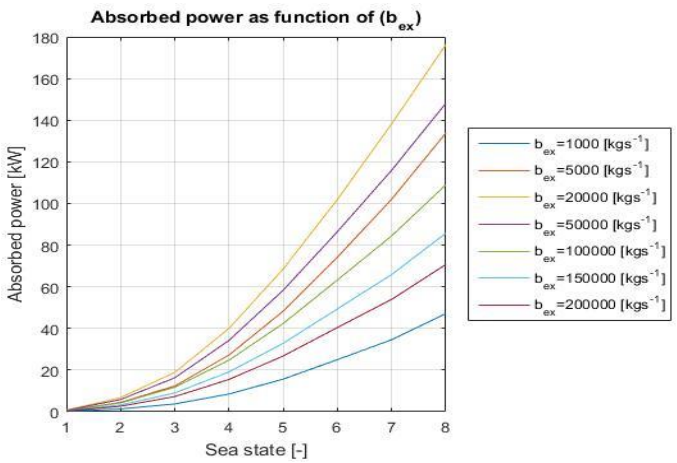

Figure 33 Absorbed power as function of hydrodynamic damping

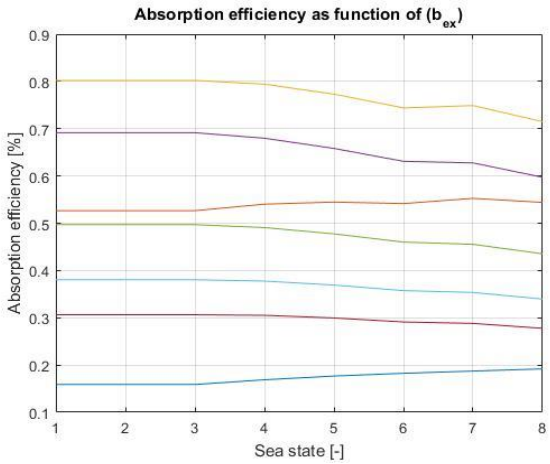

Figure 34 Corresponding absorption efficiency

It can be seen from Figures 33 and 34 that the optimal hydrodynamic damping coefficient is around 20.000 [kgs^{-1}] for maximal power production and thus also maximal absorption efficiency. However, this should be carefully interpreted since the hydrodynamic coefficient also has influence on the significant amplitude of the buoy. As can be seen from Figure 35, such a low damping value leads to unrealistic amplitudes in the buoys movement. In order to realize a realistic optimization, it is assumed that the maximum significant amplitude of the buoys motion, Equation 5.48, is set to 2 [m]. Assuming Rayleigh distribution of the buoy motions, this

would mean that for 4.39% of the waves, a stroke of 5 [m] is exceeded. This was found to be a realistic constraint within the SEEWEC project (Kaasen and Solaas, 2008). In this way the found values can be easily validated with (De Backer, 2009) Corresponding values for these hydrodynamic damping can be found in Figure 36, these values match with the values found by de Backer (2009) which are marked as circles in blue.

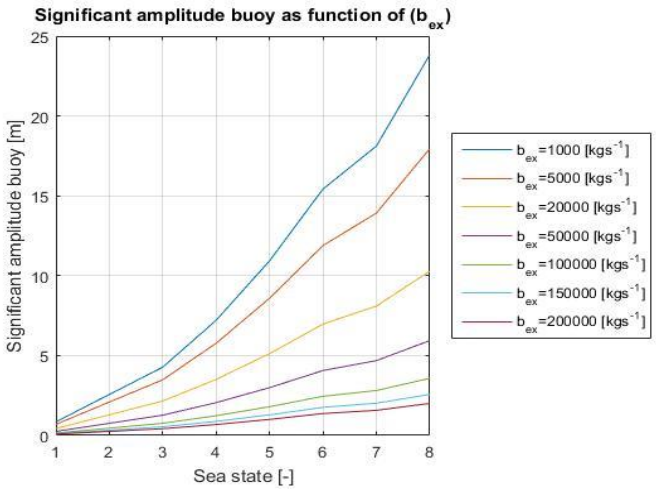

Figure 35 Significant amplitude of the WEC

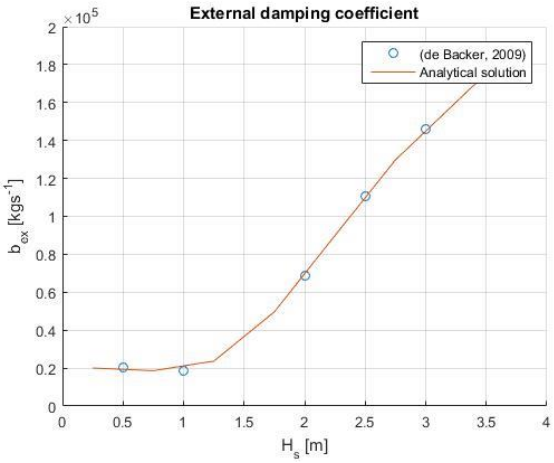

Figure 36 External damping coefficients for z_{Asign} = 2.0 [m]

Now that all hydrodynamic parameters for the wave energy converter are found, the power production and corresponding capture width can be calculated. The absorbed power is calculated using Equation 5.50, the available power using Equation 5.49 and the capture width is the ratio between the absorbed power and the available power. When dividing the capture width by the diameter of the buoy the absorption efficiency can be calculated. Results of the absorbed power in both regular and irregular waves, available power and absorption efficiency in irregular waves can respectively be seen in Figures 37 until and 39 and are listed in Table 8.

Table 8 Produced power regular and irregular waves

	Significant wave height							
	1	2	3	4	5	6	7	8
P_{AVAIL} [kW]	1.74	15.69	43.57	85.40	141.19	211.02	294.73	393.01
P_{ABS} regular [kW]	1.0	9.10	25.17	55.34	101.32	165.56	222.90	322.71
P_{ABS} irregular [kW]	0.80	7.25	20.17	37.73	51.36	65.1	75.33	92.76
η_{ABS} [-]	0.80	0.80	0.80	0.68	0.51	0.39	0.34	0.29

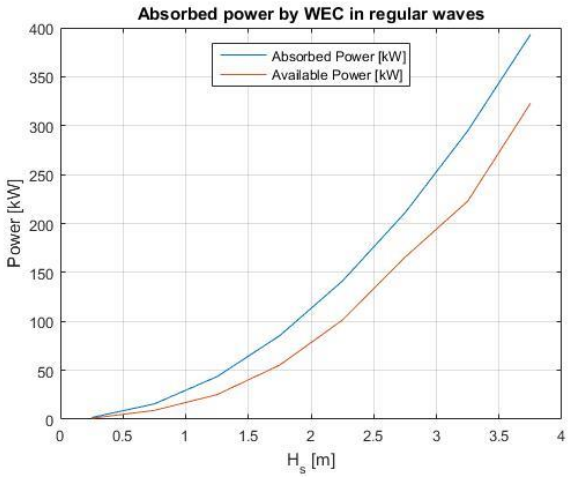

Figure 37 Absorbed power WEC in regular waves

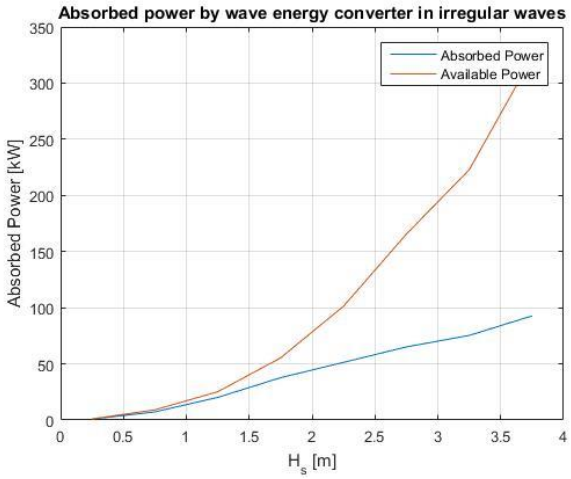

Figure 38 Absorbed power WEC in irregular waves

Figure 37 shows the absorbed power of the wave energy converter in regular waves. Interesting thing to notice is that the absorbed power is higher than the available wave power on the length of the buoys diameter. This phenomenon is called the 'point-absorber effect' and is explained by the fact that the point absorber is able to absorb a larger fraction of the power than what is available over its diameter. Theoretical maximum absorption width is equal to Equation 5.43.

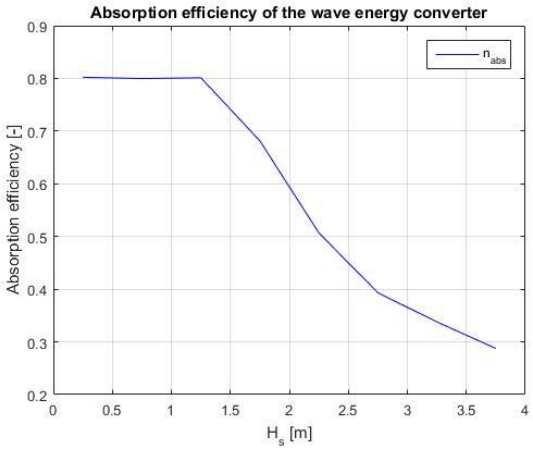

Figure 39 Absorption efficiency WEC in irregular waves

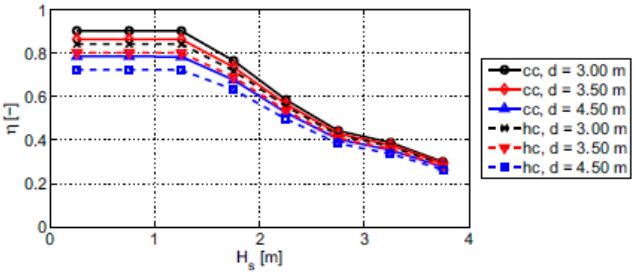

Figure 40 Absorption efficiency (de Backer, 2009)

What can be seen from the comparison between the absorption efficiency of the wave energy converter in irregular waves between Figures 39 and 40, is that it can be concluded that the found values are validated when comparing them to the cone cylinder with a draft of 3.50 [m] by de Backer (2009). So far, only a stroke restriction is taken into account. As mentioned in subsection 5.4.3, the occurrence of slamming must be minimized. This slamming restriction can be modeled by Equation 5.54:

$$z_{A,sign} - \zeta_{A,sign} \leq d_r$$

In words, Equation 5.54 restricts the significant amplitude of the buoy's position relative to the free water surface elevation to be smaller or equal to the draft of the buoy, in this way the buoy stays intact with the water and slamming is prevented. The effect of the three possible restrictions is investigated by de Backer (2009) and the result in shown in Figure 41 and 42. Since the same buoy size and type is used, the results of this study are relevant to look into.

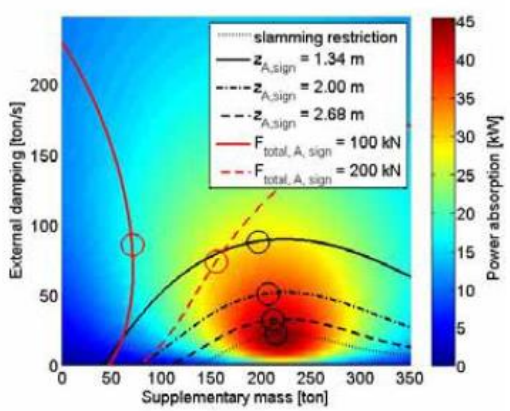

(a) H_s = 1.75 [m], T_p = 7.40 [s]

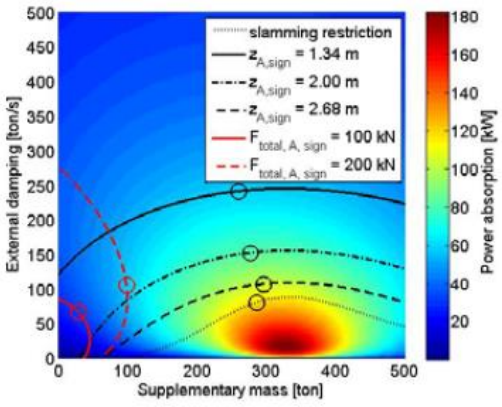

(b) H_s = 3.25 [m], T_p = 8.80 [s]

Figure 41 Slamming, stroke and force restrictions (de Backer, 2009)

From this could be concluded that the stroke restriction has the least influence on the power production. In addition it is interesting to notice how the values of b_{ex} and m_{sup} are optimized in order to hold the restrictions. For the stroke restriction the damping coefficient is increased for higher sea states while for the force constraint the damping is kept constant but the supplementary mass is decreased significantly. Now the buoy behavior and the power production of the wave energy converter is known for all sea states, the coupling to the WindFloat and its effect can be looked into. First, chapter 6 will describe the modelling of floating wind turbines in the time domain and the derivation of the platform movements of the WindFloat in the frequency domain.

6. Floating wind turbine modelling

In this chapter the floating wind turbine modelling is explained. First, subsection 6.1, describes the behavior of four different offshore floating wind turbines in the time domain using Fast v8.1. In subsection 6.2 the movements of the WindFloat is described in the frequency domain, followed by the corresponding power production in the frequency domain which is described in subsection 6.3.

6.1 Time domain modelling FWT responses

In order to improve insight in the response and dynamic behavior of floating wind turbines, an analysis was done on four different types. For this analysis, aero elastic tool Fastv8.1 was used (NREL, 2016). Validation of this tool can be found in (Lloyd WindEnergie, 2005). Scripts were compiled using MATLAB 2014b. The four different floating wind turbines were respectively: ITI Barge, MITNREL, Hywind, DeepCWind. Geometries of these designs were made available since the update Fast v7. The different designs shown in Figures 42 until and 45 were visualized using the mesh generated by Fast v8.1 which was loaded into ParaView 5.1.2.

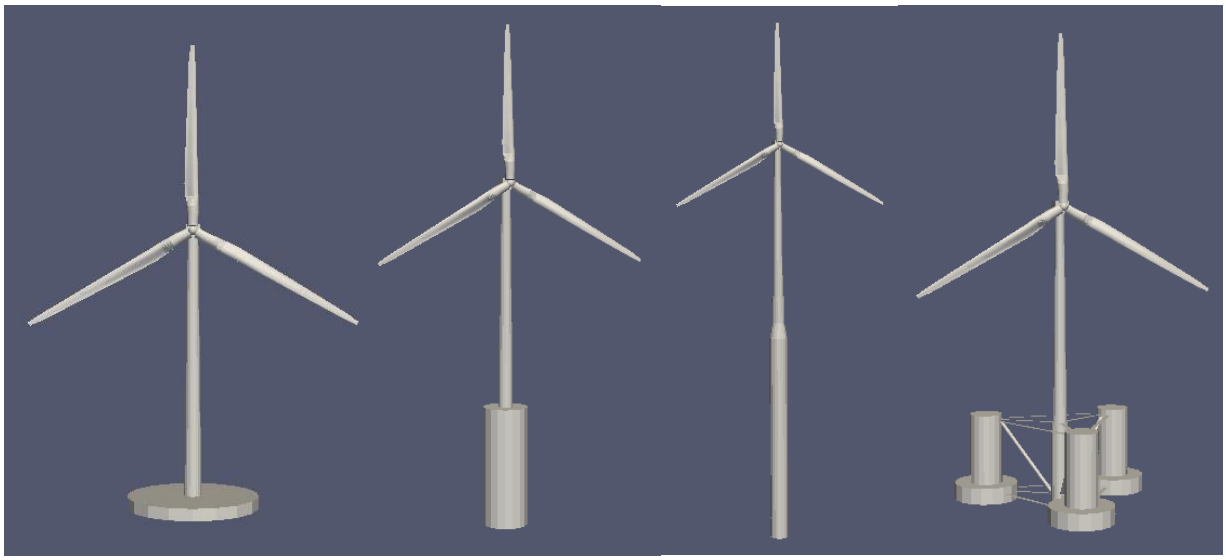

Figure 42 ITI Barge Figure 43 MIT-NREL Figure 44Hywind Figure 45 DeepCWind

In order to compare the different designs, similar environmental input conditions were being imposed on the constructions. For this, a rated wind speed with an average of 14 [ms^{-1}] and an average wave height of 2.0 [m] was set, as can be seen in Appendix B.

Power production and responses in all 6 degree of freedoms can also be found in Appendix B. An additional calculation was done to compare the power production when it would always produce the rated power. In other words, values for rated efficiency were found. From all these results, it be seen how different types of floating wind turbines respond to given aero- and hydrodynamic forces. In general, MITNREL shows the least responses except for yaw where the DeepCWind has the lowest platform movement. MITNREL has the highest rated wind speed efficiency. The DeepCWind concept is based on a similar concept as the WindFloat which makes this comparison worth mentioning. Due the low platform motions which this concept has, is favorable for the wave energy production since the WEC is attached to the platform and the relative movement between the waves and the platform are essential. More reasons for choosing the WindFloat have been mentioned in subsection 4.4. Additional information about the relative movement between the WindFloat and the WEC is described in subsection 7.1.

6.2 WindFloat principle and platform motions in frequency domain

The main dimensions of the floating wind turbine WindFloat have been listed in Table 6. The WindFloat technology consists of a column-stabilized offshore platform with water-entrapment plates and an asymmetric mooring system. A wind turbine mast is positioned directly above one of the stabilizing columns. The WindFloat construction, as can be seen in Figure 46, consist the following parts (Roddier et al, 2010):

1) The three columns which are marked in red and gray in Figure 46 provide buoyancy to support the turbine and stability from the water plane inertia.

2) Horizontal plates at the bottom of the columns, which increase the added mass by shifting the natural frequency away from the wave energy. In addition, the viscous damping is increased in roll, pitch, and heave. The water-entrapment plates provide additional hydrodynamic inertia to the structure due to the large amount of water displaced as the platform moves. In addition, vortices generated at the edge of the plates generate large damping forces that further hinder platform motion.

3) In order to lower the platform to its operational draft, permanent water ballast is put inside the bottom of the columns. An active ballast system moves water from column to column to compensate for the mean wind loading on the turbine. This movable ballast compensates for significant changes in wind speed and directions.

4) Six mooring lines made of conventional components such as drag-embedment anchors, chains, shackles, fairleads, and chain jacks.

5) Wind turbine rated at 5 MW, in this report the 5 MW NREL wind turbine is used for calculations (Jonkman, 2009). More information about this wind turbine is given in subsection 6.3.

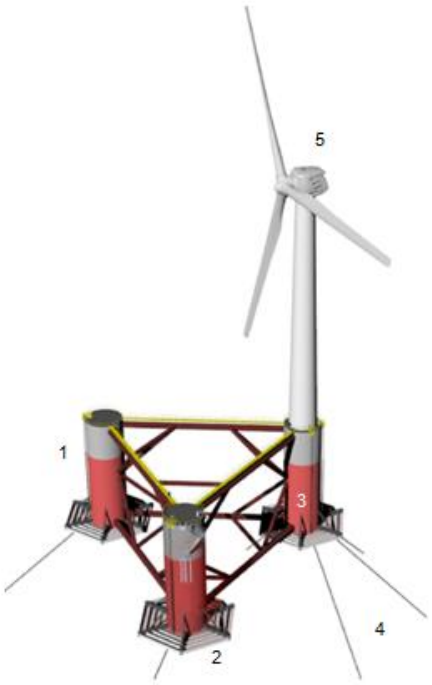

Figure 46 WindFloat (Roddier et al, 2010)

The platform motions of the WindFloat, which can be extracted from the response amplitude operator in heave and pitch mode, are given in Figure 47 and 48. These figures have been taken from Roddier et al (2010), who used both experiments and the software TIMEFLOAT to compute these graphs. Since both methods show similar responses it is assumed that these values are validated.

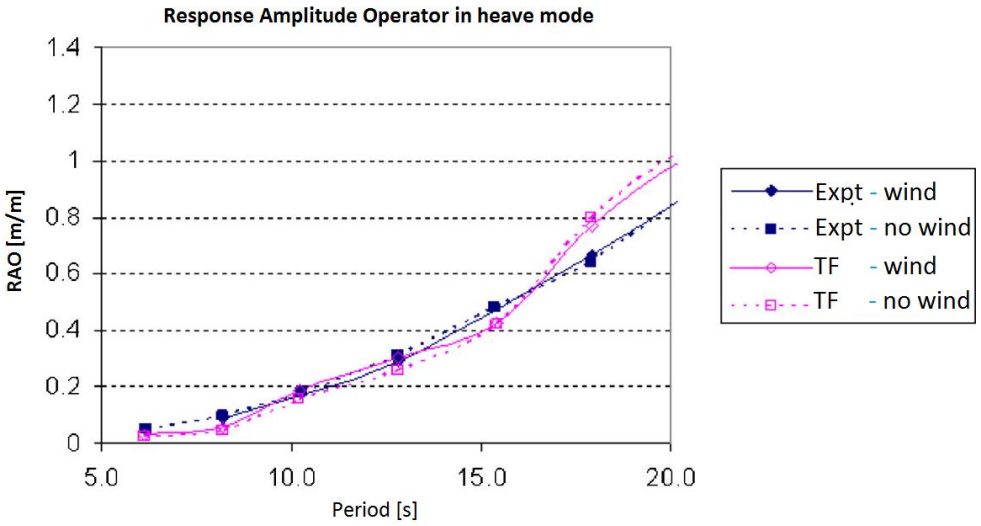

Figure 47 Response Amplitude Operator in heave mode of the WindFloat (Roddier et al, 2010)

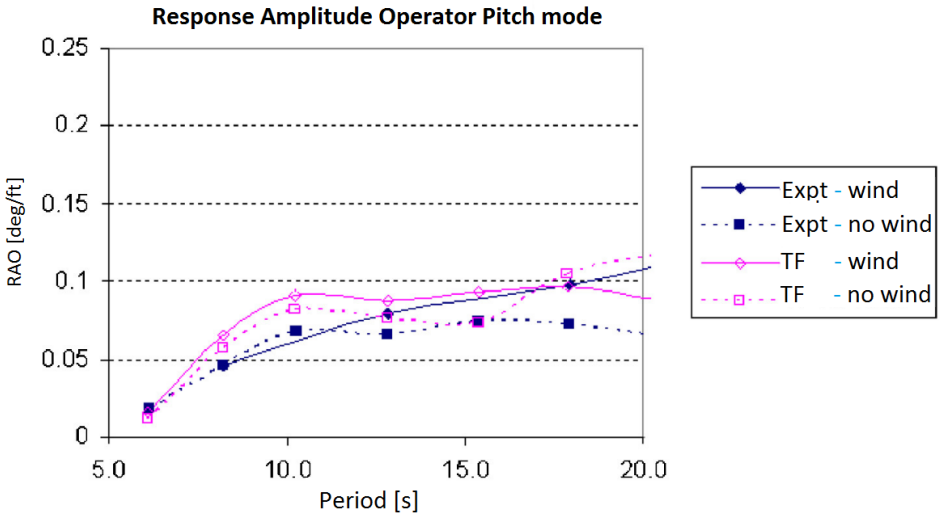

Figure 48 Response Amplitude Operator in pitch mode of the WindFloat (Roddier et al, 2010)

In order to get the platform motions for different sea states, the response amplitude operator (RAO) in heave and pitch mode must be multiplied with the wave amplitude according to Equations 6.1 and 6.2:

$$z_{pl} = \zeta_a \, RAO_{heave} \tag{6.1}$$

$$\beta_{pl} = \zeta_a \, RAO_{pitch} \tag{6.2}$$

6.3 WindFloat power production

In this subsection the power production of the wind turbine of the WindFloat is described. As mentioned in subsection 6.2, the wind turbine which is used on the WindFloat is the standard 5 MW NREL turbine (Jonkman, 2009). Turbine properties are listed in Table 9:

Table 9 5 MW NREL wind turbine properties

	Value	**Units**
Hub height	90	[m]
Blade diameter	126	[m]
Blade area	12469	[m^2]
Rated wind speed	11.4	[ms^{-1}]
Rated power	5	[MW]

The power delivered by the wind turbine can be calculated using the Rankine–Froude theory, which was also mentioned in chapter 2 according to Equation 6.3:

$$P_w = \frac{1}{2}\,\rho_{air}\,c_p\,A_T\,U_w^3 \tag{6.3}$$

The density of the air at a height of 90 meter is calculated using a MATLAB script. The input values are the temperature and pressure at the water surface, respectively taken as $p_0 = 1.018e5\ [Pa]$ and $T_0 = 283.15\ [K]$. Furthermore, the specific heat constant of air under constant pressure is assumed to be 1006 [$Jkg^{-1}K^{-1}$] and the specific gas constant of air is assumed to be 287 [$Jkg^{-1}K^{-1}$]. Temperature as function of height is given by Equation 6.4 when using hydrostatic equilibrium and the gas law (Boeker and Grondelle, 2011):

$$T(h) = T_0 - \frac{(gh)}{cp_{air}} \tag{6.4}$$

Pressure as function of height can then be calculated using Equation 6.5:

$$P(h) = \frac{p_0}{1+\left(\frac{gh}{R_d T(h)}\right)} \tag{6.5}$$

Eventually the density as function of height can be calculated using the local temperature and pressure using Equation 6.6:

$$\rho_{air}(h) = \frac{p(h)}{R_{air}\,T(h)} \tag{6.6}$$

The result is shown in Figure A4. Since variation dependent on height is negligible small, the air density is assumed to be 1.244 [kgm^{-3}]. The power coefficient,c_p, of the turbine is given according to Equation 6.7 (Hansen, 2015):

$$c_p = 4\,a\,(1-a)^2 \tag{6.7}$$

With a, which is the axial induction factor, taken as one third which in theory yields maximal production. It is assumed that the hub height of the WindFloat is also 90 meters. The velocity, dependent on height, is calculated using the power law wind profile, which is most suited for height above 60 meter and given by Equation 6.8:

$$U_w\,(h) = U_w\,\left(h_{ref}\right)\left(\frac{h}{h_{ref}}\right)^{\vartheta} \tag{6.8}$$

With ϑ is equal to power law wind constant, taken as 0.11 [-] for sea environment (Hsu et al, 1994). The wind speed at 10 meter height is dependent on the weather conditions and also influences the wave height. The wind speed wave height relation is derived from the Sverdrup-Munk-Bretschneider nomogram which relates wind speed, fetch length and wave height (Bretschneider, 1964). For an assumed fetch length of 100 kilometers, the correlation according to Figure A6 is found. Substituting this wind speed into Equation 7.8 results in the wind speed – sea state relation as can be seen in Figure 49. The horizontal wind speed is the wind speed at the hub height.

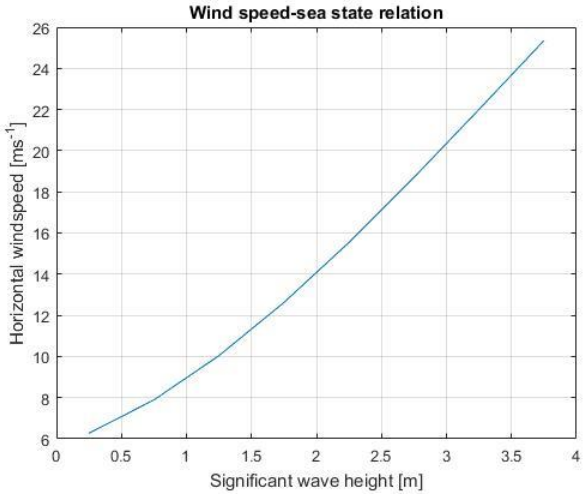

Figure 49 Correlation between wind speed and sea state

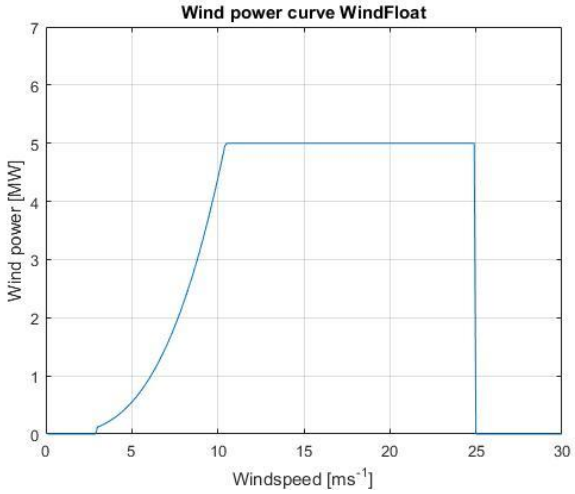

Figure 50 Wind power curve WindFloat including restrictions

Since the WindFloat cut in wind speed is set on 3 [ms^{-1}], cut out wind speed at 25 [ms^{-1}] and the rated power is set on 5 [MW], the wind speed power curve of the WindFloat can be seen in Figure 50 (WindFloat, 2016). As can be from Figure 48, the rated wind speed is already reached at a sea state with a significant wave height of 1.5 [m]. Since the rated power of the WindFloat is 5 [MW], it can be concluded that the WindFloat will thus generate 5 [MW] for sea states with significant wave height of 1.5 [m] and higher.

7. Coupled hybrid system in frequency domain

In this chapter the coupled hybrid system response in the frequency domain is described. First the correlation between the buoy responses relative to the platform is derived in subsection 7.1. Then, the influence in response of the coupling of the wave energy converter to the WindFloat is described in subsection 7.2. Moreover, the power production by both wind and wave of the hybrid system is given and their ratio is determined in subsection 7.3. At last, the potential contribution of wave energy is looked into in subsection 7.4 by scaling up the buoy size.

7.1 Buoy response modelling frequency domain floating platform

As described in subsection 5.3, the buoy and power take of system have been modeled together acting on a fixed reference frame while this is not the case with a floating hybrid system. Because the generator and the supplementary mass move together with the platform, the forces associated with the control parameters, b_{ext} and m_{sup}, are dependent on the buoy velocity relative to the platform velocity, respectively the acceleration relative to the platform acceleration as can be seen in Figure 51.

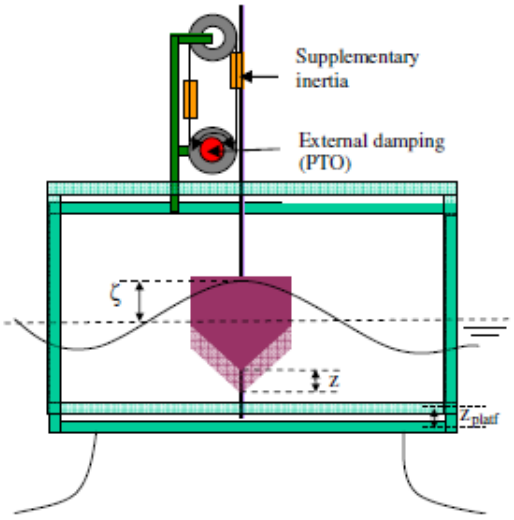

Figure 51 Buoy floater coupled with a floating platform (De Backer, 2009)

With z_{pl} denoting the position of the platform, the equation of motion of Equation 5.24 can be written as Equation 7.1:

$$\left(m_{buoy} + m_{added}(\omega)\right)\frac{d^2z}{dt^2} + m_{sup}\left(\frac{d^2z}{dt^2} - \frac{d^2z_{pl}}{dt^2}\right) + b(\omega)\frac{dz}{dt} + b_{ex}\left(\frac{dz}{dt} - \frac{dz_{pl}}{dt}\right) + kz = F_{ex}(\omega, t) \quad (7.1)$$

Rearranging leads to Equation 7.2:

$$\left(m_{buoy} + m_{added}(\omega) + m_{sup}\right)\frac{d^2z}{dt^2} + \left(b(\omega) + b_{ex}\right)\frac{dz}{dt} + kz = F'_{ex}(\omega, t) \quad (7.2)$$

With the force term equal to Equation 7.3:

$$F'_{ex}(\omega, t) = F_{ex} + m_{sup}\frac{d^2z_{pl}}{dt^2} + b_{ex}\frac{dz_{pl}}{dt} \quad (7.3)$$

In order to find the steady state solution of the buoy motion, the amplitude, $F_{ex,A}$, and phase shift, β_{Fex}, of F_{ex} should be determined. With Equations 7.4, 7.5, the complex amplitude of F_{ex} can be expressed as Equation 7.7:

$$z_{pl} = z_{A,pl}\, e^{i(\omega t+\beta_{pl})} \tag{7.4}$$

$$F'_{ex} = F'_{exa}\, e^{i(\omega t+\beta'_{Fex})} \tag{7.5}$$

$$\boldsymbol{F'_{ex}} = F_{exA}e^{i\beta_{Fex}} + i\omega b_{ex}z_{pl}e^{i\beta_{pl}} - \omega^2 m_{sup}z_{pl}e^{i\beta_{pl}} \tag{7.6}$$

$$\begin{aligned}\boldsymbol{F'_{ex}} = {} & F_{exA}\cos(\beta_{Fex}) - \omega b_{ex}z_{pl}\sin(\beta_{Fex}) - \omega^2 z_{pl}\cos(\beta_{pl}) \\ & +i\,[\,F_{exA}\sin(\beta_{Fex}) + \omega b_{ex}z_{pl}\cos(\beta_{pl}) - m_{sup}\omega^2 z_{A,pl}\sin(\beta_{pl})]\end{aligned} \tag{7.7}$$

where the bold indicates the complex amplitude. The amplitude of the adjusted exciting force F_{ex} becomes equal to Equation 7.8:

$$F'_{exA} = \sqrt{(Re(\boldsymbol{F'_{ex}}))^2 + (Im(\boldsymbol{F'_{ex}}))^2} \tag{7.8}$$

which after filling in results in Equation 7.9:

$$\begin{aligned}F'_{exA} = {} & [\,F_{exA}^2 + \omega^2 z_{pl,A}^2 {b_{ex}}^2 + \omega^4 z_{pl}^2 m_{sup}^2 + 2\omega z_{pl}b_{ex}F_{exA}\sin(\beta_{Fex}-\beta_{pl}) - \\ & 2\omega^2 z_{pl}m_{sup}F_{exA}\cos(\beta_{Fex}-\beta_{pl})]^{\frac{1}{2}}\end{aligned} \tag{7.9}$$

and the phase angle β_{Fex} can be computed by Equation 7.10:

$$\beta'_{Fex} = atan\left[\frac{F_{exA}\sin(\beta_{Fex}) + \omega\, b_{ex}z_{A,pl}\cos(\beta_{pl}) - m_{sup}\omega^2 z_{A,pl}\sin(\beta_{pl})}{F_{exA}\cos(\beta_{Fex}) - \omega\, b_{ex}z_{A,pl}\sin(\beta_{pl}) - m_{sup}\omega^2 z_{A,pl}\cos(\beta_{pl})}\right] \tag{7.10}$$

In this way, the steady state solution for the buoy motion relative to the platform written in the form of Equation 5.20 becomes equal to Equation 7.11 and 7.12:

$$z_a(\omega) = \frac{F'_{exA}(\omega)}{\sqrt{[(k-(m+m_{sup}+m_{added}(\omega)\omega^2)^2+(b(\omega)+b_{ex})\omega)^2]}} \tag{7.11}$$

$$\beta_{mot} = \beta'_{Fex} - atan\left[\frac{(b(\omega)+b_{ex})\omega}{(k-(m+m_{sup}+m_{added}(\omega)\omega^2)}\right] \tag{7.12}$$

7.2 Coupled hybrid system response frequency domain

In this subsection the coupled motions of the wave energy converter and the WindFloat is described. In order to describe these motions, the found steady state solution according to Equations 5.20, 7.11 and 7.12 is used. Platform motions and the phase angle of the platform are derived using Equations 6.1 and 6.2 respectively. It is assumed that the wave energy converter will not influence the response of the WindFloat construction. This assumption holds because the significant amplitude of the PTO forces of the wave energy converter is negligible small compared to the added mass of the WindFloat construction. The force spectrum is equal to Equation 7.13:

$$S_{F_A} = \frac{F_A^2}{2\Delta\omega} \tag{7.13}$$

With the significant amplitude of the force given by Equation 7.14:

$$F_{A,sign} = 2\sqrt{\int_0^\infty S_{FA}(\omega)d\omega} \tag{7.14}$$

Thus the significant amplitude of the damping and turning force which were introduced in subsection 6.3, are given by Equation 7.15 and 7.16. The addition of both terms results in Equation 7.17 (de Backer, 2009).

$$F_{bex,sign} = 2\sqrt{\int_0^\infty S_{bex}(\omega)d\omega} \tag{7.15}$$

$$F_{msup,sign} = 2\sqrt{\int_0^\infty S_{msup}(\omega)d\omega} \tag{7.16}$$

$$F_{t,sign} = 2\sqrt{\int_0^\infty [S_{bex}(\omega) + S_{msup}(\omega)]d\omega} \tag{7.17}$$

Adding the damping force and supplementary mass force together for the different sea states using Equation 7.17, results in Figure 52. When comparing this to the added mass of the WindFloat which is shown in Figure 53, it shows indeed that the effect of the wave energy converter on the platform is negligible.

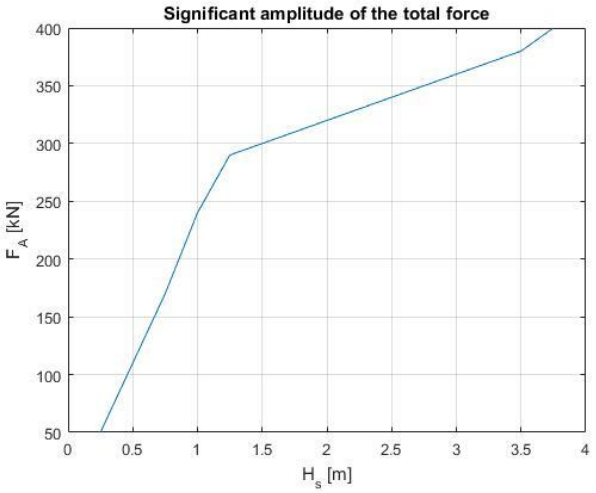

Figure 52 Significant amplitude of the total control force

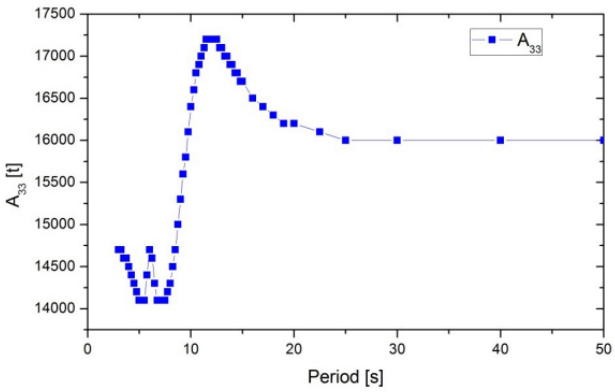

Figure 53 Added mass WindFloat (Wang, 2014)

In addition, to double validate the effect of the presence of the wave energy converter on the WindFloat, its hydrodynamic parameters are looked into. For this, the BEM solver Nemoh will be used. The wave energy converter will be modeled as a cone cylinder with a height of 3.50 [m] and a diameter of 5.0 [m]. The WindFloat construction will be heavily simplified to three columns with height and diameter of 10.0 [m] with distances of 46 [m] between the column centers. The mesh of both situations can be seen in Figure 54a and b.

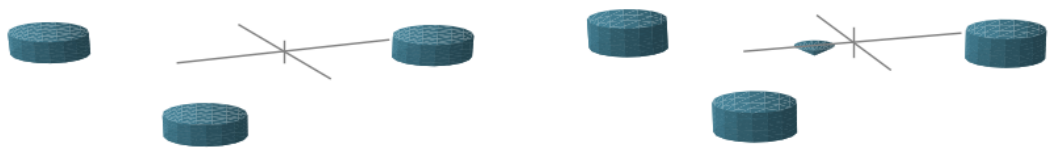

(a) Columns without WEC

(b) Columns with WEC

Figure 54 Mesh used for Nemoh simulations

The effect on the hydrodynamic parameters in heave mode can be seen in Figure 55, where the exciting wave force is shown for both situations. The red line indicates the coupled subsystems while the blue line represents only the columns. The comparison for added mass and hydrodynamic damping is shown in Figure C2.4 until and C2.7. It can be noticed from the hydrodynamic parameters that the influence of the wave energy converter is very small. However, ideally the columns should be modeled as fixed boundaries while the wave energy converter moves in heave mode. However, this heavily simplified comparison is done in order to see the aforementioned effect.

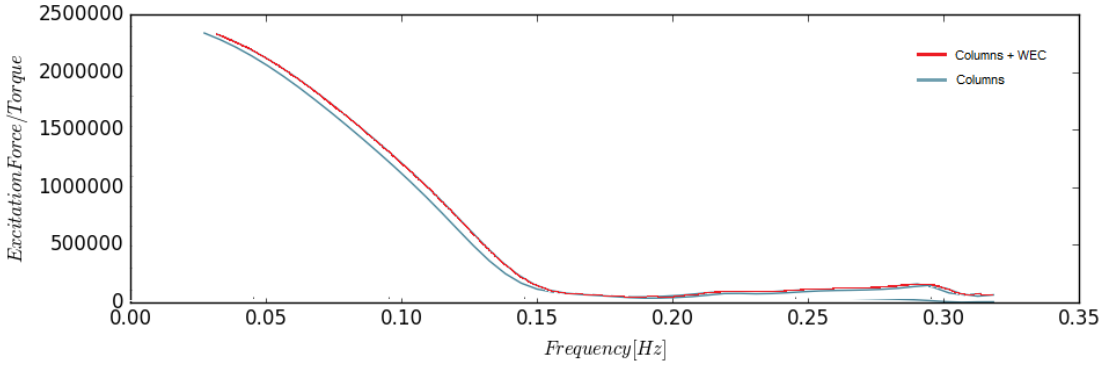

Figure 55 Wave exciting force for columns with and without wave energy converter

Until now, the wave energy converter is maximized in heave response, coupled to the WindFloat and assumed the coupling has no influence on the WindFloat motion. However, a wave energy converter can also be used in order to reduce platform motions of floating wind turbines. Maximum motion reduction of the FOWT is then achieved by shifting the WEC to a lower frequency than the FOWT natural frequency (Borg et al, 2013). This interesting phenomenon however is not investigated in this report since it is written from an energy production point of view and not a motion suppressing standpoint.

Now that all assumptions are known and validated, the effect of the coupling can be investigated. First, the response amplitude operator in heave mode of the coupled system is derived and can be seen in Figure 56. Comparing it to the response amplitude operator of the wave energy converter alone, as seen in Figure A7, shows that the RAO is slightly reduced due to the motion of the WindFloat. The RAO graphs have the frequency on the x axis normalized by dividing it to the corresponding natural frequency. The effect of a reduced heave response amplitude operator is clearer when plotting both heave response amplitude operators of one sea state, in this case the third sea state, in one graph as can be seen in Figure 57. The effect of reduction is only visible for low frequencies because the WindFloat has higher heave responses for low frequencies which can be derived from Figure 57.

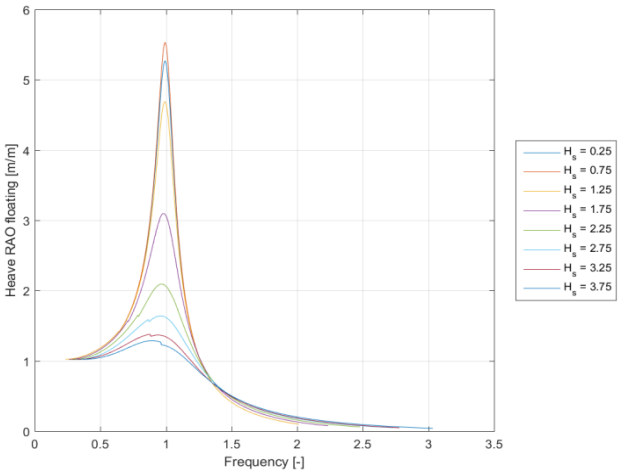

Figure 56 Heave RAO of the coupled WEC and WindFloat

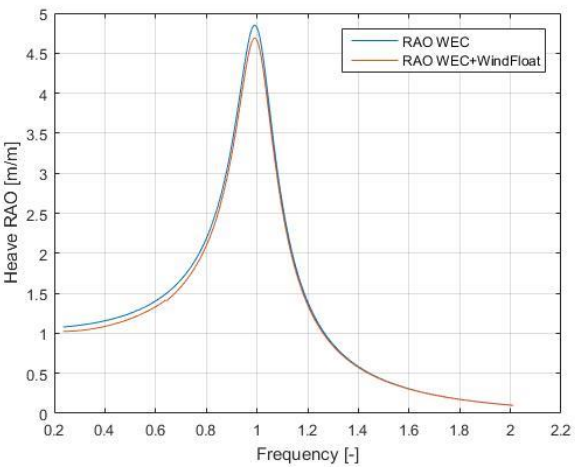

Figure 57 RAO in heave mode for the third sea state

What also can be noticed from Figure 56 is that the peaks of the response amplitude operator in heave mode for the different sea states are not directly above 1 but slightly shifted to the left. This is because, due to the presence of the damping, the system actually oscillates at the damped natural frequency as given by Equation 5.16. Damping ratios for the different sea states can be seen in Figure A8. As stated in subsection 5.2, for damping ratios was lower than 1, the system is underdamped, which is true for all sea states. In subsection 7.3, the derived motions are used to calculate the corresponding produced power for the coupled hybrid system in different sea states.

7.3 Coupled hybrid power production

In this subsection the power production of the coupled hybrid system is described. Since it was found in subsection 7.2, that the relative motions of the wave energy converter were slightly reduced it is expected that the power production will also be slightly lower. The absorbed power is calculated with Equation 6.54 and the corresponding absorption efficiency is calculated using Equation 5.45. Results of both calculations can be respectively seen in Figure 58 and 59. Both graphs also have their previously calculated values from subsection 5.6 for a fixed reference as comparison.

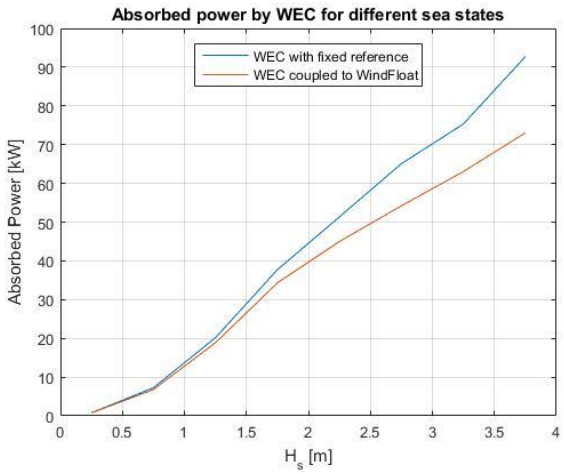

Figure 58 Absorbed power of the WEC when coupled

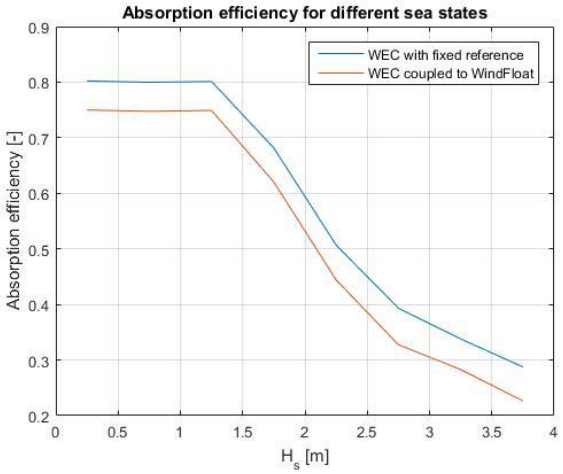

Figure 59 Absorption efficiency of the WEC when coupled

As can be concluded from Figures 58 and 59, is that the reduced relative motion indeed results in a lower power production of the wave energy converter and thus also a lower absorption efficiency for the different sea states. Therefore, while it is assumed that the wave energy converter has no influence on the WindFloat but that the presence of the WindFloat has influence on the wave energy converter. This is in line with what was assumed in subsection 7.1. However, it must be noted that the comparison with a completely fixed reference at a water depth of 100 [m] is quite unrealistic. Normally the wave energy converter is coupled to a floating reference which will, just as the WindFloat, move in heave mode. The actual reason for a difference in power production between a separate wave energy converter and one which is coupled to the WindFloat is the effect of the diffraction of waves due to the WindFloat construction. This can have both positive as negative effect on the power production since the waves at the location of the wave energy converter can either be in phase or cancelling each other out. However, this effect is not in the scope of this project.

Now a sensitivity case for the heave motion and power absorption will be done. For this, a base scenario with significant wave height of 2.0 [m] is taken into account, corresponding absorbed power is marked yellow in Figure 60. Then, four new scenarios are looked into to see the sensitivity of heave motion and power production by introducing an addition and reduction in wave energy converter motion of ±20 and ±40 % while the response in heave mode for the WindFloat stays the same. The power which is related to these motions can be found in Figure 60. Figure 61 shows the relation between reduction in significant wave height and its

corresponding reduction in power, the five dots shows the base scenario and the four other scenarios, the effect seems to be linear for small differences but has a slightly significant effect for higher reductions or additions.

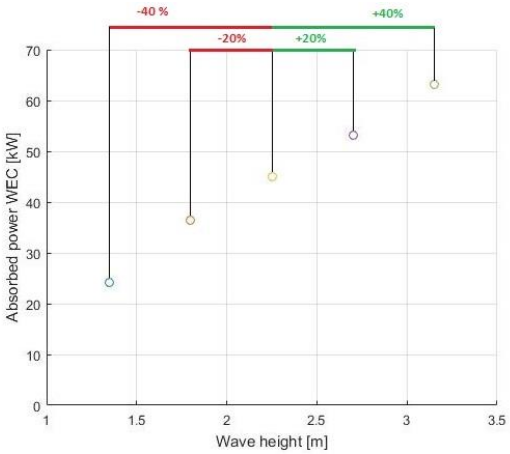

Figure 60 Increase and decrease in wave height ±20 and 40 %

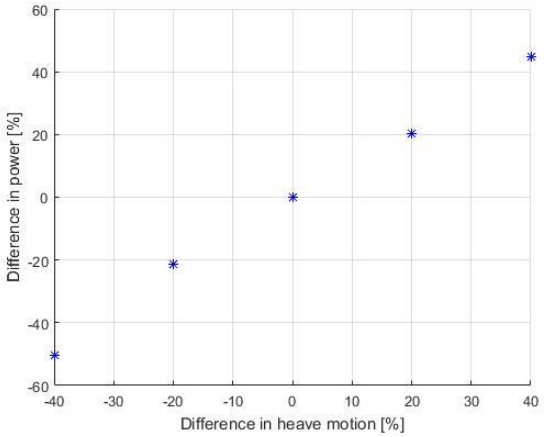

Figure 61 Effect of motion and power

As already mentioned in subsection 4.1.5, the contribution of the wave energy converter is low relative to the produced wind power. When combining the results found in Figure 49 and 58, the percentage of the contribution of the wave energy converter in comparison to wind energy is equal to Equation 7.18:

$$PR_{ww} = 100 \frac{P_{abs}}{P_{abs} + P_W} \tag{7.18}$$

The contribution for all eight different sea states are listed in Table 10 and shown in Figure 62.

Sea state	P_{ABS} [kW] coupled d = 5.0 [m]	PR_{WW} [%] coupled d = 5.0 [m]
1	0.75	0.07
2	6.78	0.31
3	18.86	0.42
4	34.34	0.68
5	45.0	0.89
6	54.22	1.10
7	63.10	1.25
8	73.07	1.44

Table 10 Produced wave power and its contribution

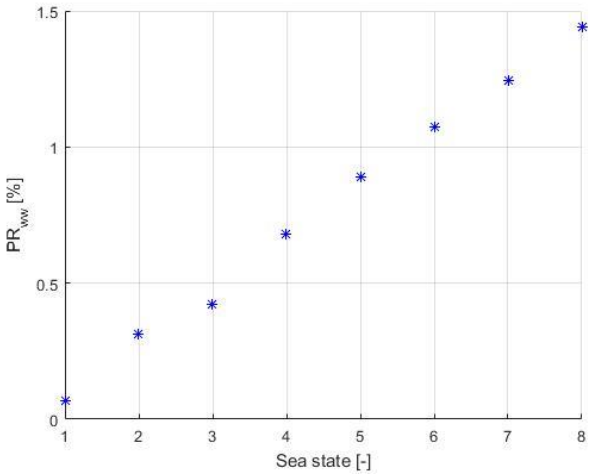

Figure 62 Produced wave power and its contribution

It is found that the contribution is in the order of 1 [%] which is quite low, which is in line with the prediction of Weinstein (2012) as can be seen in Table 4. It should be noticed that the actual absorbed power will be even lower since mechanical friction, viscous losses, neither turbine nor generator losses in the conversion system are not taken into consideration. Reasons for adding a wave energy converter have already been mentioned in the introduction of this report. In addition, it should be taken into account that the buoy only has a diameter of 5.0 [m] while the blades of the wind turbine are 128.0 [m], low percentage of power contribution is therefore logical and expected. In order to determine the economic feasibility of the addition of a wave energy converter to a WindFloat, research must be done into the costs of the wave energy converter.

Since the proposed hybrid system is composed of two subsystems which both are not in fully commercial phase it should be taken into account that while both technologies develop their combined technical and economic feasibility will increase in time. Especially the wave energy technology still has to prove itself but its potential is already described in chapter 2. According to JRC (2014), currently the highest contribution in research and development of wave energy is done in the improvement of point absorbers. As described in chapter 2, floating offshore wind turbines will probably have low contribution until 2030, during which point absorbers have time to develop. Although wave energy is relatively expensive in comparison to offshore wind energy and limited wave energy production is advised, subsection 7.4 will look into the way of increasing the contribution of the wave energy production.

7.4 Increasing wave energy contribution

In this subsection the wave energy contribution is altered by increasing the size of the buoy. Until now, it has been taken as 5 meter because the wave energy sector is still seeking for designs which are both technical and economical feasible which is done using small scale applications. Furthermore, in similar literature studies the same buoy diameter is used which made the validation of results easier. As shown in Table 6, the distance between the centers of two columns is 45 while the diameter of each column is 10 meter. This means that the distance is between the edges of both columns is 35 meter. To see the effect on power production as function of the diameter, the buoy is scaled up to 25 meter. It should be taken into account that for the current status of wave energy converter this size will not be feasible due to the enormous forces the system then has to hold. However, in order to see the potential of the contribution of wave energy, the effect of scaling up the buoy is investigated. For this, new hydrodynamic parameters are found using Nemoh, from which the results can be seen in Appendix C. The volume of a cone is equal to Equation 7.19:

$$V_c = \frac{1}{3}\,\pi\,R^2\,h_c \tag{7.19}$$

Increasing the buoy size from 5 to 25 meter and scaling up the height in similar ways, the volume and thus mass increases by factor $(5)^3$ in comparison to the original buoy mass which was found to be 26300 [kg]. The hydrostatic force, given by Equation 5.27, scaled up with the waterline area. This means that increasing the buoy diameter from 5 to 25 meter results in an increase of waterline area with $(5)^2$. In addition, it is found that the added mass increases around $(5)^3$ times, the hydrodynamic damping with factor 100, while the wave excitation force only increases by around $(5)^2$. The dynamics of the system will thus change for all sea states. It can be noticed that the difference in scaling factors for several parameters will result in a different sort of mechanical oscillator. First of all, when calculating the natural frequency with Equation 5.48 but neglecting the supplementary mass it is found that the natural frequency lies already between 0.75 and 0.86 [$rads^{-1}$]. When comparing these values with the values found for the peak frequencies, as can be seen in Table 5, it can be noticed that for low sea states, the mass even needs to be lowered or the spring coefficient needs to be reinforced in order to match the natural frequency to the wave peak frequency. The optimal external damping coefficient was found iteratively and similar for all sea states and equal to 1.75e6 [kgs^{-1}]. When using these values, the absorbed power per sea state is shown in Figure 63, while the wave energy contribution is shown in Figure 64. It is noticed that for high sea states the increase is quite significant, up to factor 8, while for low wave heights the contribution only doubles. As can be seen from Table 11, for sea states with higher significant wave height the increase in absorbed power is significant and a contribution of 11 % wave energy can be reached. Furthermore, the significant amplitude of the buoy is below 2.0 meter for all sea states which means that if the stroke was limited, it would already be within limits. It must be noted that the coupling of such a big buoy to the WindFloat will have effect on the platform motions and the stability of the floating structure.

Table 11 Absorbed wave power for buoy with d = 25.0 [m]

Sea state	PR_{avail} [kW] coupled d = 25.0 [m]	P_{ABS} [kW] coupled d = 25.0 [m]	η_{abs} [%] coupled d = 25.0 [m]	PR_{ww} [%] coupled d = 25.0 [m]	$Z_{A,sign}$ [m] coupled d = 25.0 [m]
1	5.03	1.54	0.29	0.14	0.06
2	45.32	13.87	0.29	0.64	0.19
3	125.89	38.53	0.29	0.86	0.31
4	276.83	94.40	0.34	1.85	0.54
5	506.60	185.63	0.38	3.58	0.85
6	827.78	313.75	0.42	5.90	1.24
7	1145.0	414.44	0.41	7.65	1.41
8	1613.5	599.30	0.44	10.70	1.90

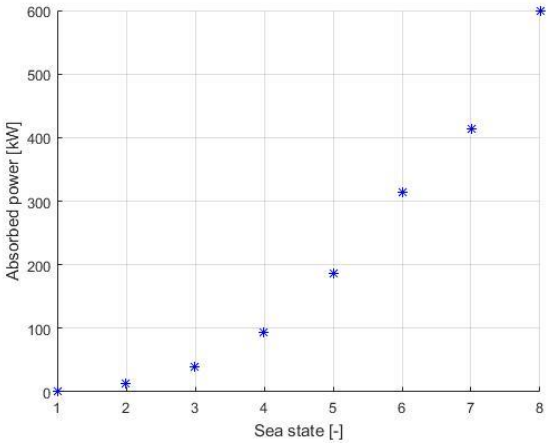

Figure 63 Absorbed power WEC for d = 25.0 [m]

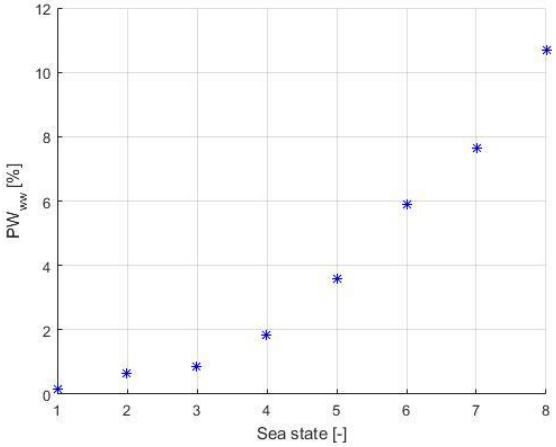

Figure 64 Contribution wave energy for d = 25.0 [m]

From Table 11 can also be concluded that scaling up might only be feasible for environments with high wave height, since for low sea states the increase is minimal with respect to the buoy size increase. However, technical feasibility for this scenario will be interesting since enormous buoys in strong wave environment result in expensive structures which need to withhold all the corresponding wave forces. The effect of scaling up is only done in order to see its effect on power production and to see what percentage could potentially be reached within the WindFloat support structure, technical and economic feasibility of such a concept is not in the scope of this project and will also be difficult to find out since current wave energy projects are based on small scale applications.

Another way to increase the wave energy contribution could be to combine the concept designs of Figures 10a and 10b. The oscillating water column, which is a simple technique, could result in a platform which is even more stable while producing additional power. Combining this with a point absorber will have two positive effects, since the relative heave motion between the platform and WEC will increase, the power would increase as well. At last, several small point absorbers can also be coupled to the columns of the WindFloat, for this sufficient space is there due to the size of the three columns. Several other designs, apart from the proposed design, could be interesting to research; this is something which is recommended for further research.

8. Conclusion

It can be concluded that a shift to a more sustainable energy society is inevitable due to the depletion of fossil fuels and the increase of total worldwide energy demand. Ocean energy technologies will play a role into this shift and its potential exceeds the current and future demand. Combining offshore wind and wave energy devices could reduce system costs through shared infrastructure, load reduction and increase in energy yield. The progress of wave energy converters depends on several crucial factors, including efficient technical performance; economic manufacture, installation and operation; high reliability and survivability in extreme conditions; and acceptable environmental impact. While offshore wind energy has proven its potential in limited depths. Floating wind turbines are starting to prove their technical feasibility in deep water regions. When combining offshore wind and wave energy devices, it is advised to make minimum changes to the wind turbine support structure in order limit extra costs.

A classification for wind wave hybrid systems is proposed based on several sub classifications. First, the integration of a single turbine was proved to be the best option to minimize the LCOE. Second, horizontal wind turbines higher efficiency and power output compared to similar sized vertical wind turbines. Another property of horizontal wind turbines is that it produces well in turbulent wind fields and if wind dominates from one specific direction. Therefore, a horizontal wind turbine will be used. Because the current status of wave energy is still yet mostly in the demonstration phase sharing certain common costs with offshore wind applications could increase its potential and make wave energy more attractive. A floating wind turbine is chosen because it provides access to a significantly larger market than traditional offshore wind. In order to get an overview of the current proposed floating wind turbines, a classification has been made. In addition, to give an overview of ongoing wind wave hybrid concepts, most of the different known concepts are listed and then compared in terms of total energy production, wind energy production, platform motions and forces. Since only the WindFloat and the Hywind are in (pre-) commercial phase and the WindFloat is expected to have better overall stability, it is chosen as floating structure. Due to the limited power production of all three different WindWaveFloat, the buoy is taken for research due to its simplicity of the system. The PTO can be placed above the buoy and thus outside the water, which makes operation and maintenance easier. For this design, the WindFloat construction would need limited changes.

State of art software is used for numerical wave energy simulations to see the effect of damping, wave height and wave period on the power production. Numerical simulations are also done for four different types of floating wind turbines to see how different types of floating wind turbines respond to given wind and wave conditions. In general, MITNREL shows the least responses except for yaw where the DeepCWind has the lowest platform movement. In addition, MITNREL also has the highest rated wind speed efficiency.

The JONSWAP spectrum is chosen as wave spectrum and eight sea states are investigated for this research. A heaving point absorber can generally be considered as an underdamped mechanical oscillator, which was proved for all sea states. The buoy itself can be modeled as a mass spring damper system when adding a supplementary mass and hydrodynamic damper. A point absorber that is a good damper at an angular frequency is also a good receiver for waves with the same frequency. With increasing wave height, more power may be captured, but at a lower efficiency. The absorbed power is dependent on b_{ext} and the velocity of the buoy which itself is dependent on b_{ext} and $m_{sup.}$ The conical shape with top angle of 90 degrees is expected to give the optimum solution. Supplementary mass is chosen such that the natural frequency of the buoy matches the peak frequency of the waves. The hydrodynamic damping coefficient is chosen such that the significant amplitude of the buoy is maximal 2 meter; this is done to avoid unrealistic buoy movements. Slamming, stroke and force restrictions, fixed and dependent on wave height, have also been looked into by using results of found literature. From this could be concluded that the stroke restriction has the least influence on the power production. In addition, it is interesting to notice how the values of b_{ex} and m_{sup} are optimized in order to hold

the restrictions. For the stroke restriction, the damping coefficient is increased for higher sea states while for the force constraint the damping is kept constant but the supplementary mass is decreased significantly. The values which were found for absorbed power in regular and irregular waves do not take into account mechanical friction, viscous losses, neither turbine nor generator losses in the conversion system. The found values were in line with the values found in current literature conducting similar research.

Platform motions of the WindFloat in heave and pitch mode were determined in the frequency domain. The power production for the WindFloat in the eight sea states was derived and found to be between 0.75 and 73.07 [kW]. It can be concluded that the WindFloat will generate 5 [MW] for sea states with significant wave height of 1.5 meter and higher. When coupling the wave energy converter to the WindFloat, it results in a slightly lower power production in comparison to the fixed reference case. The presence of the WindFloat has thus influence on the wave energy converter. However, it must be noted that the comparison with a completely fixed reference at a water depth of 100 meter is quite unrealistic. Normally the wave energy converter is coupled to a floating reference which will, just as the WindFloat, move in heave mode. Finally, the contribution of the wave energy compared to the total produced energy is between 0.07 and 1.5 %. Scaling up to a buoy diameter of 25.0 [m] might only be feasible for environments with high wave heights because the wave energy contribution increases with factor 8, while for low sea states this increase is only factor 2.

Recommendations

The proposed theory of the steady state behavior of the buoy should be validated using scaled experiments. So far, this validation of the theory is done with the comparison to values found in literature. Furthermore, a study should be done in order to determine the magnitude of the mechanical friction, viscous losses and turbine and generator losses in the conversion system in order to get an idea of the actual absorbed power.

Also, the influence of the WindFloat on the behavior of the wave energy converter should be looked into in more detail. For now, only its potential influence is investigated but since the wave length is higher than the space between the columns, waves will be refracted and therefore the heave motion at the location of the wave energy converter will be influenced. This effect can be both positive when the waves are in phase, or negative when they are out of phase. The hydrodynamic coefficients of the wave energy converter in the presence of the WindFloat should be derived and in case there is any difference, its effect can be easily found by substituting these values into the proposed theory.

In addition, it is strongly recommended to investigate the economic feasibility of the addition of the wave energy converter to the existing WindFloat structure in order to make the general conclusion about the overall feasibility of the hybrid system.

At last, three possible options to increase the power production of the wave energy converter have been proposed. Increasing buoy size, combining different WindWaveFloat concepts and maximally using the WindFloat structure for attaching wave energy converters. Further research should determine the feasibility of the different options based on increased power production, platform motions, platform forces and cost assessment. The combination of a WindFloat platform with an oscillating water column and point absorber could be interesting since the oscillating water column would work as a platform stabilizer while producing additional wave energy.

Appendices

Appendix A Additional figures

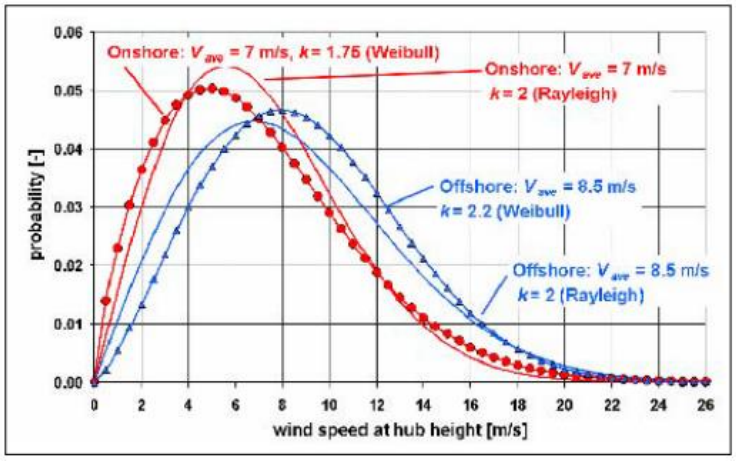

Figure A1 Strong offshore wind environment (Kuhn, 2001)

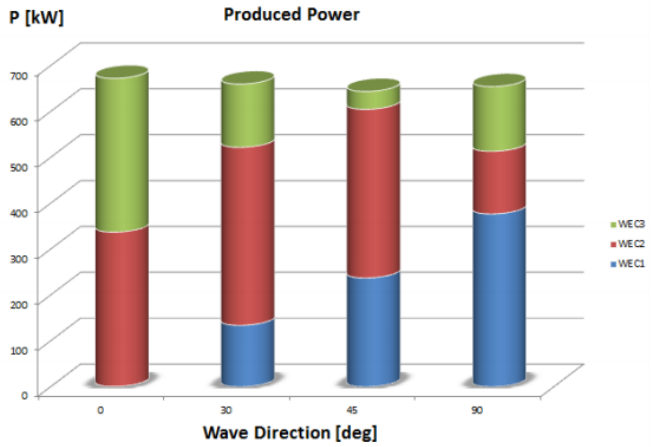

Figure A2 SFC power production with three flaps and their particular contribution (Xing, 2014)

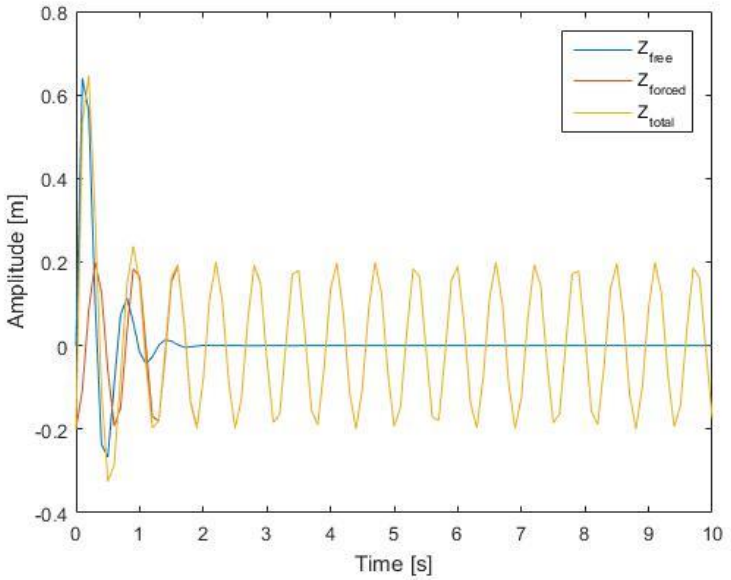

Figure A3 Mass spring damper free, forced and total response for F_a = 10 [N], m =1 [kg], k = 100 [Nm^{-1}], c = 5 [kgs^{-1}], ω_n = 0.7 [$rads^{-1}$] and initial conditions u(0) = 0 and $\frac{du}{dt}(0) = 0$

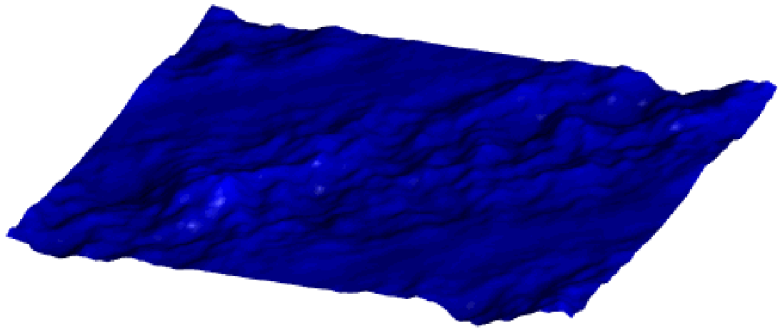

Figure A4 Ocean wave field

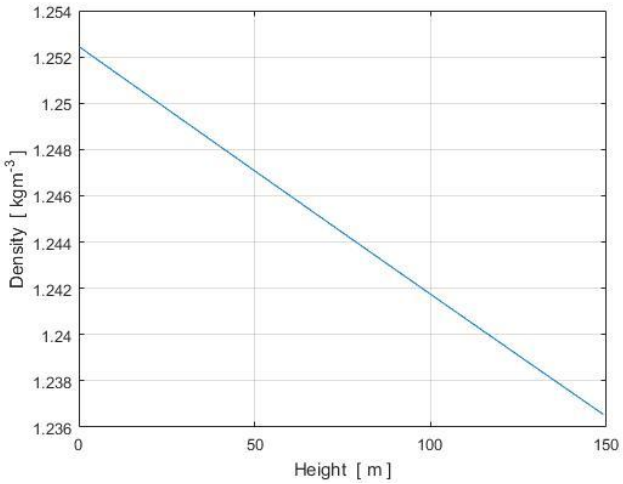

Figure A5 Height dependent air mass density

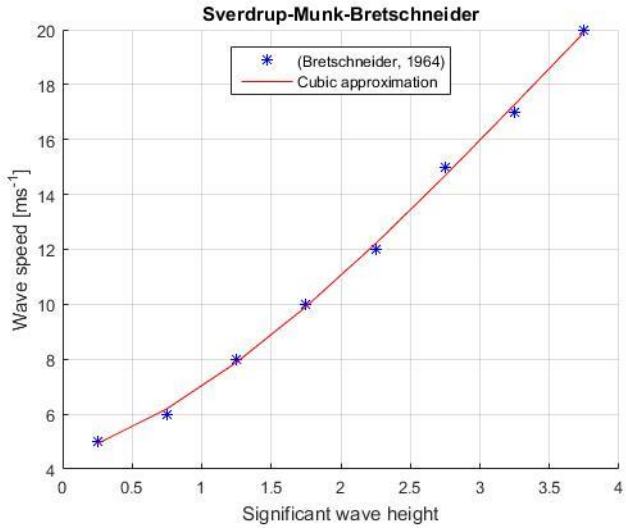

Figure A6 Approximation used for determining wind speed – wave height relation

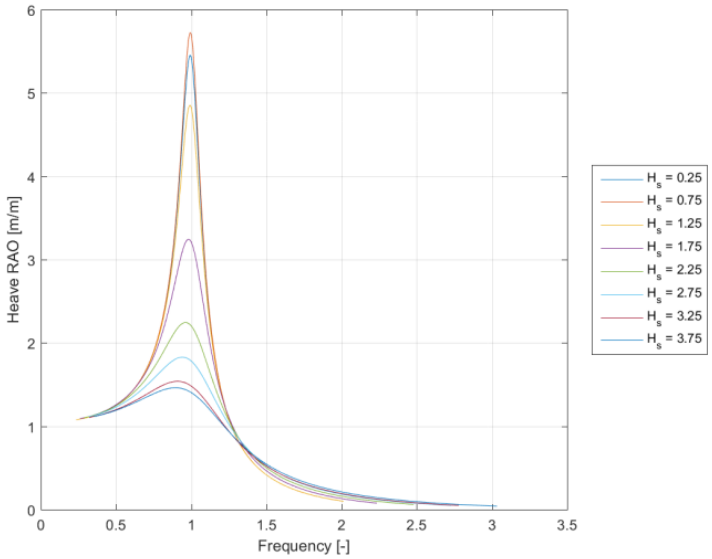

Figure A7 Heave RAO of the wave energy converter

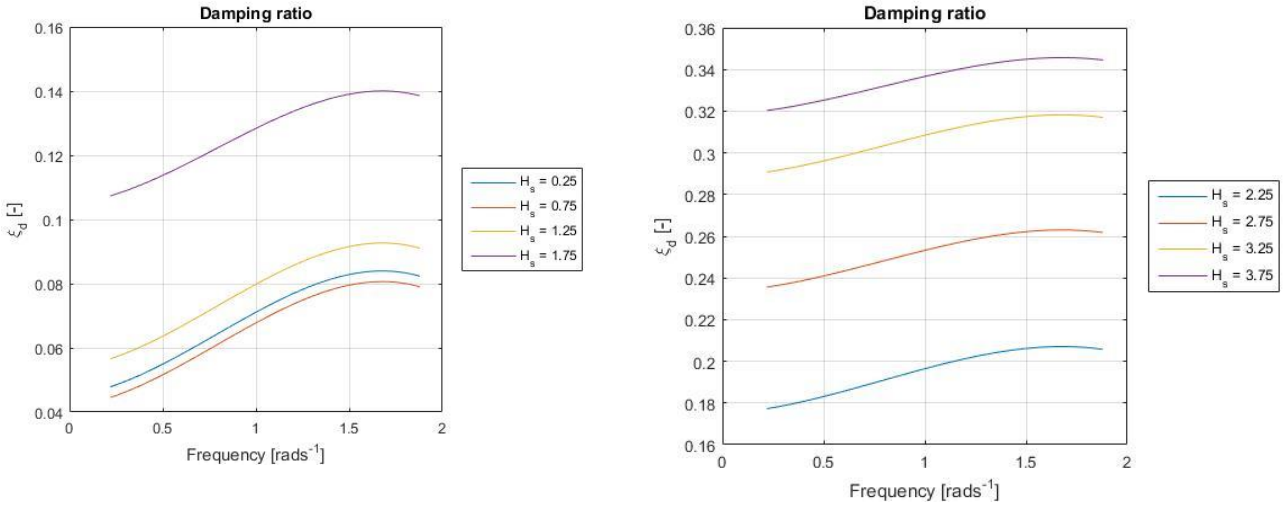

Figure A8 Damping ratios different sea states

Appendix B Numerical simulations of floating wind turbine response

Input conditions Wind(X,Y,Z) and Wave

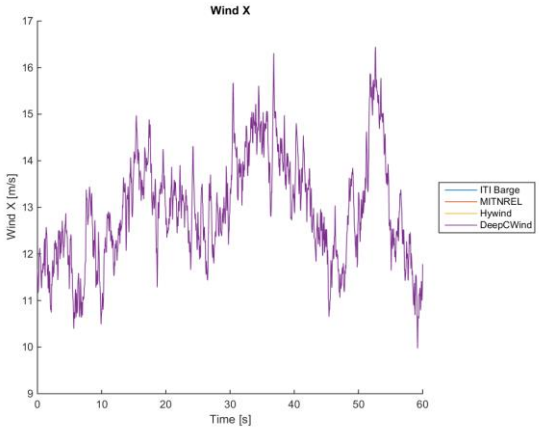

Figure B1 Wind data X direction

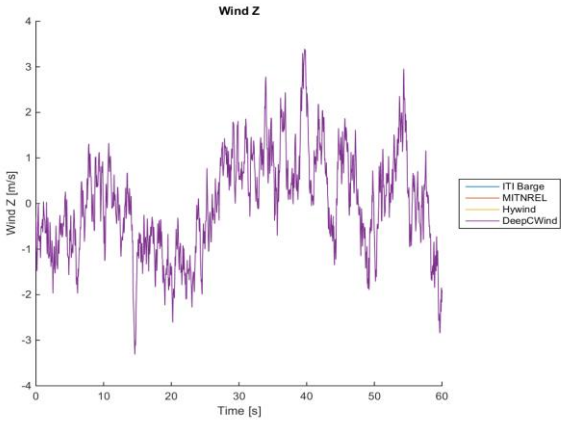

Figure B2 Wind data Z direction

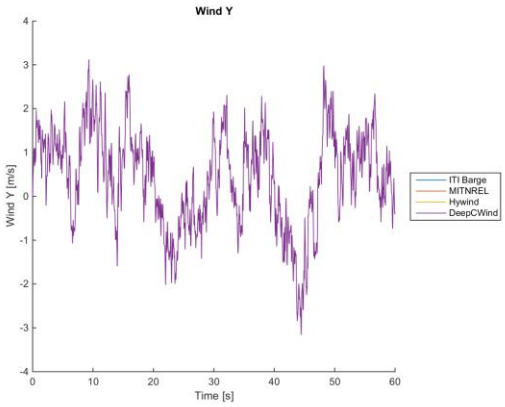

Figure B3 Wind data Y direction

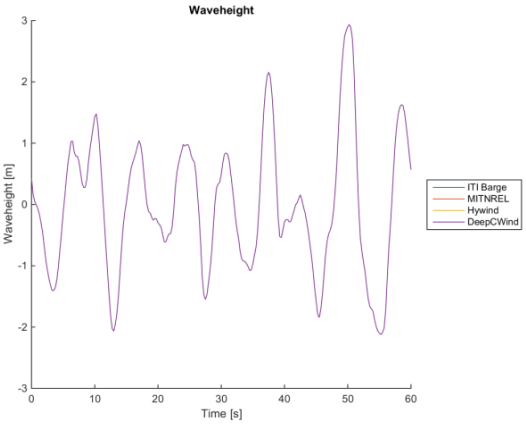

Figure B4 Wave height

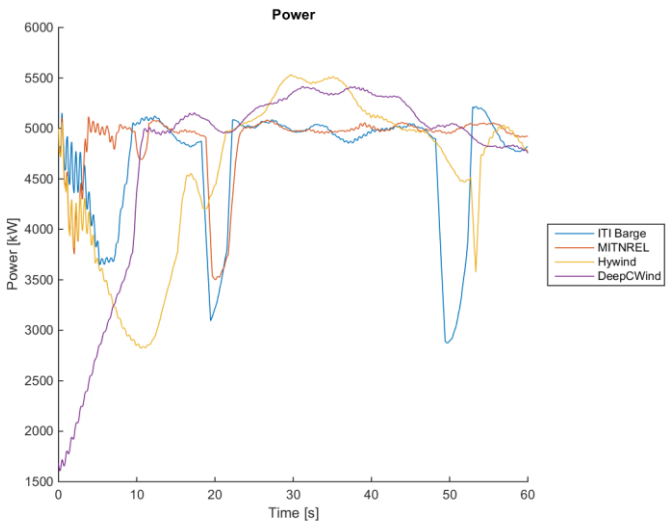

Figure B5 Power production floating wind turbines

Concept	η [-]
ITI Barge	0.9348
MIT-NREL	0.9760
OC3 Hywind	0.9307
OC4 DeepC Wind	0.9443

Table B1 Rated power efficiency

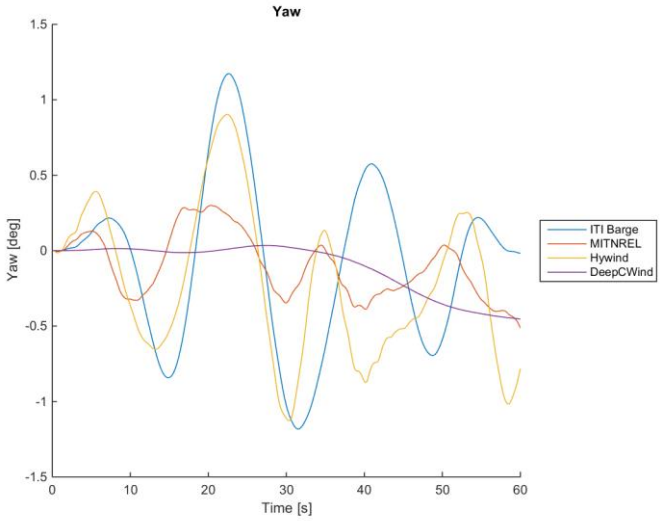

Figure B6 Yaw response floating wind turbines

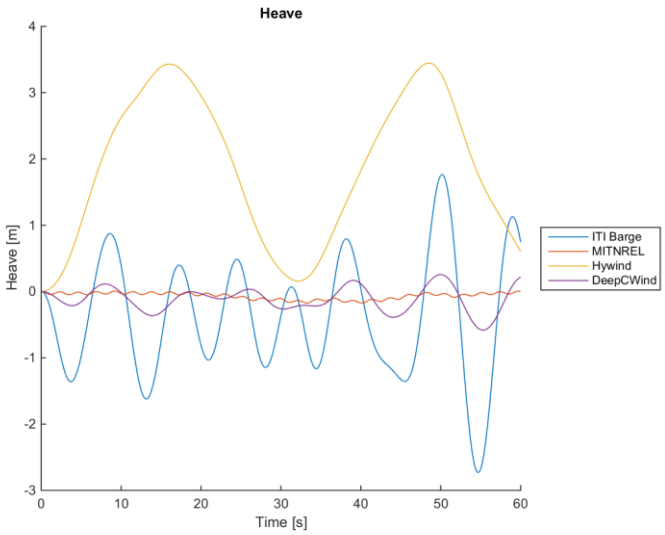

Figure B7 Heave response floating wind turbines

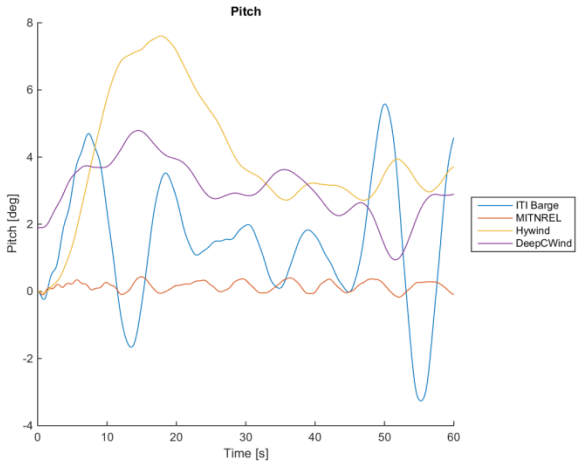

Figure B8 Yaw response floating wind turbines

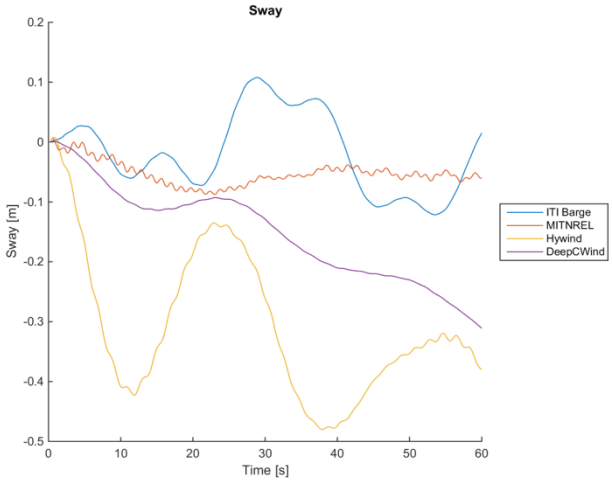

Figure B9 Heave response floating wind turbines

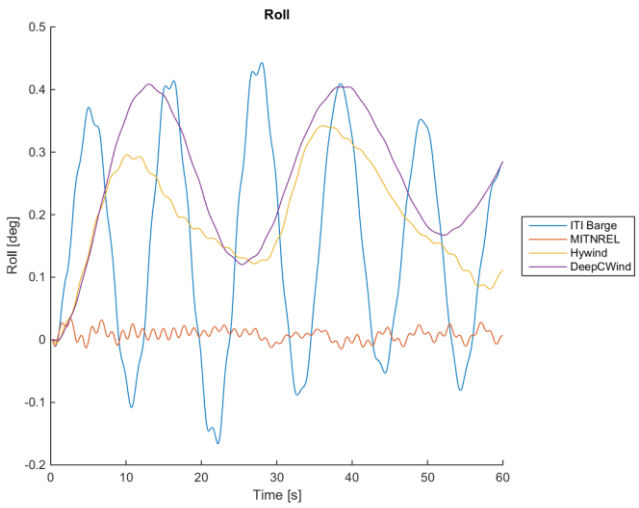

Figure B10 Yaw response floating wind turbines

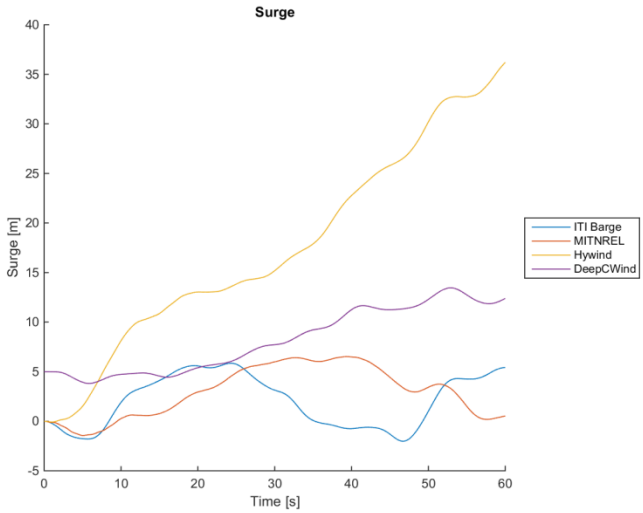

Figure B11 Heave response floating wind turbines

Appendix C Numerical simulations of WEC power production

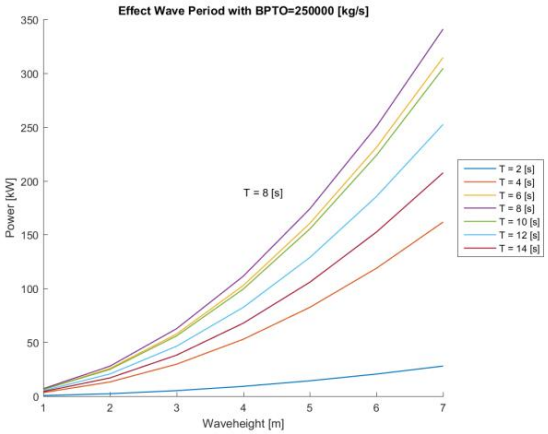

Figure C1 Effect wave period with fixed damping

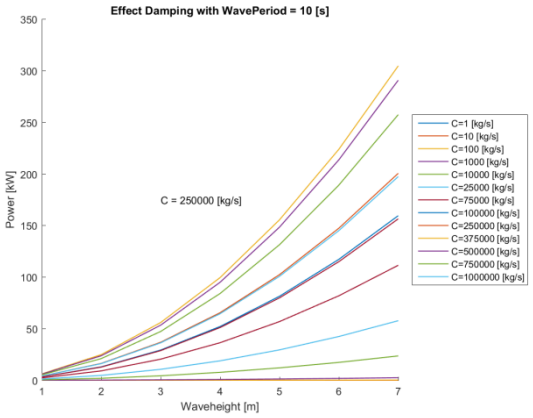

Figure C2 Effect damping with fixed wave period

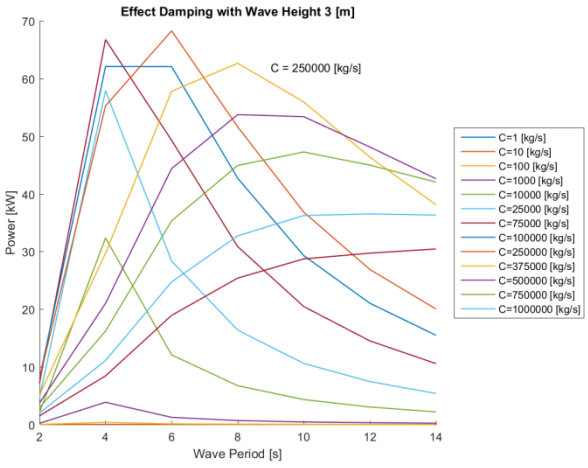

Figure C3 Effect damping with fixed wave height

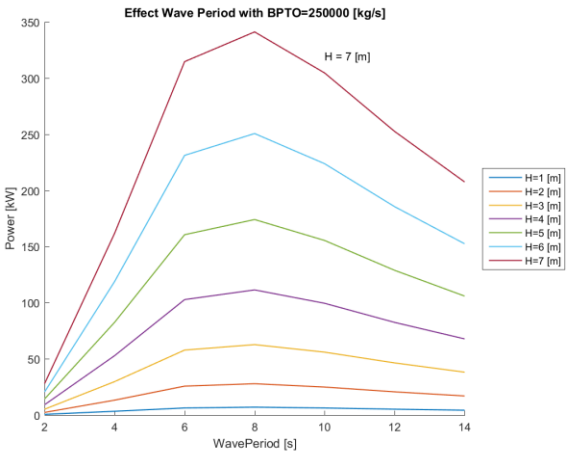

Figure C4 Effect wave height with fixed damping

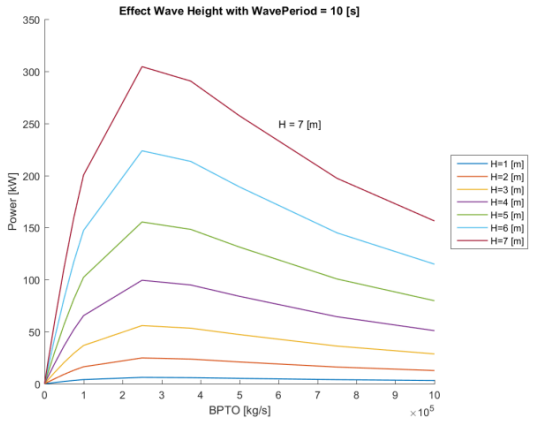

Figure C5 Effect wave height with fixed wave period

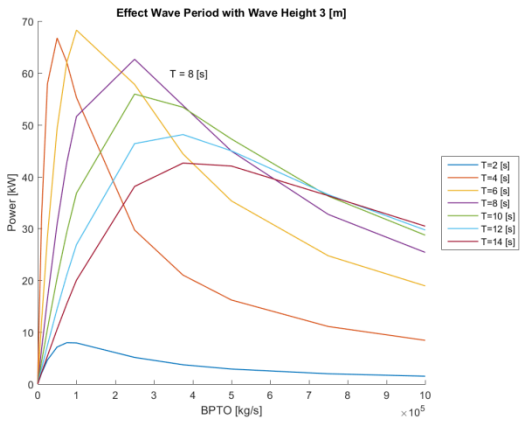

Figure C6 Effect wave period with fixed wave height

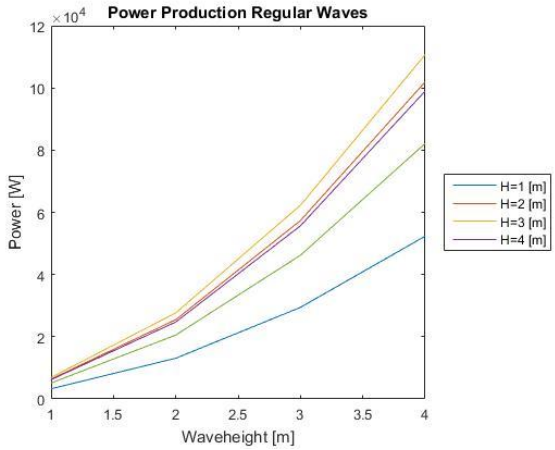

Figure C7 Power production in regular waves

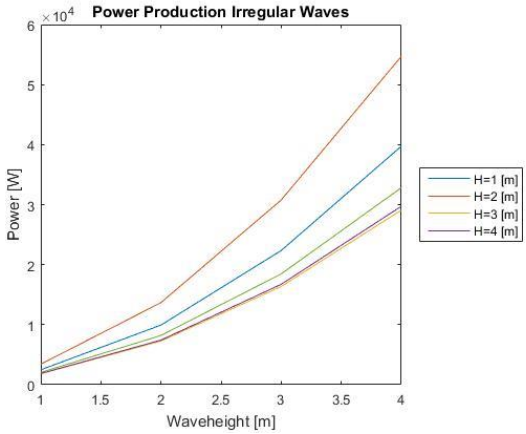

Figure C8 Power production in irregular waves

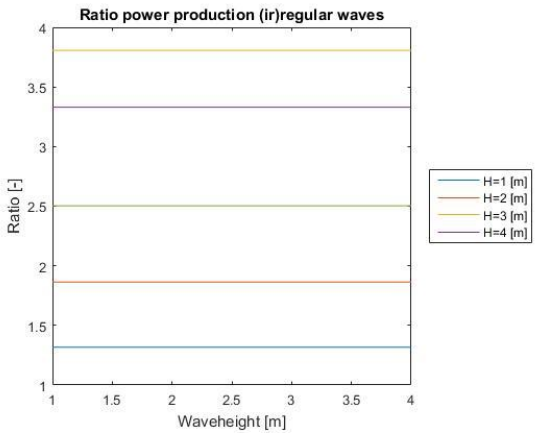

Figure C9 Ratio regular and irregular power production

Appendix D Hydrodynamic parameters using Nemoh

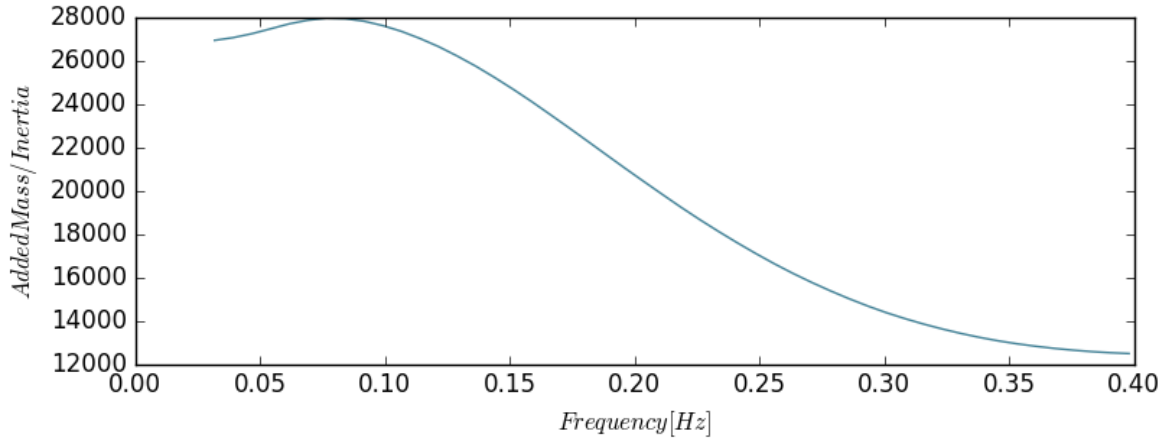

Figure D1 Added mass wave energy converter with buoy diameter = 5.0 [m]

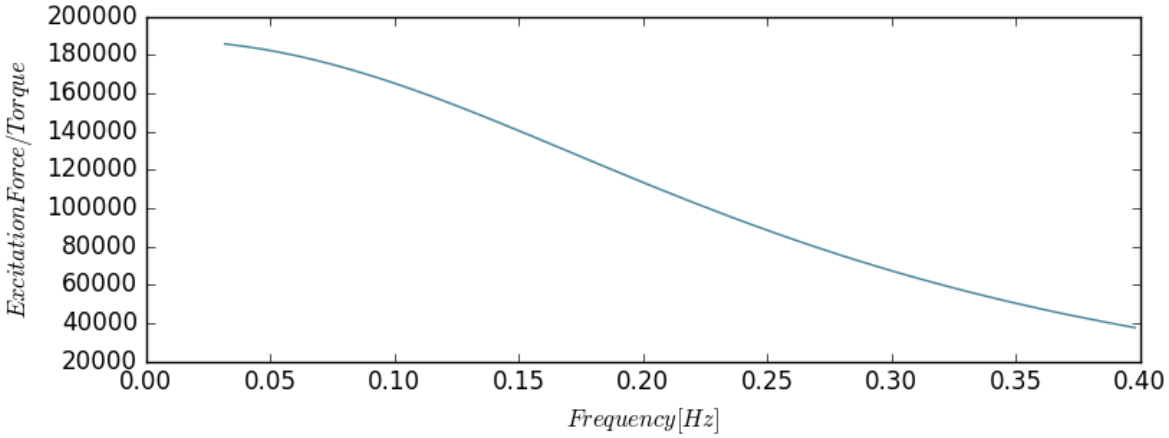

Figure D2 Wave excitation force wave energy converter with buoy diameter = 5.0 [m]

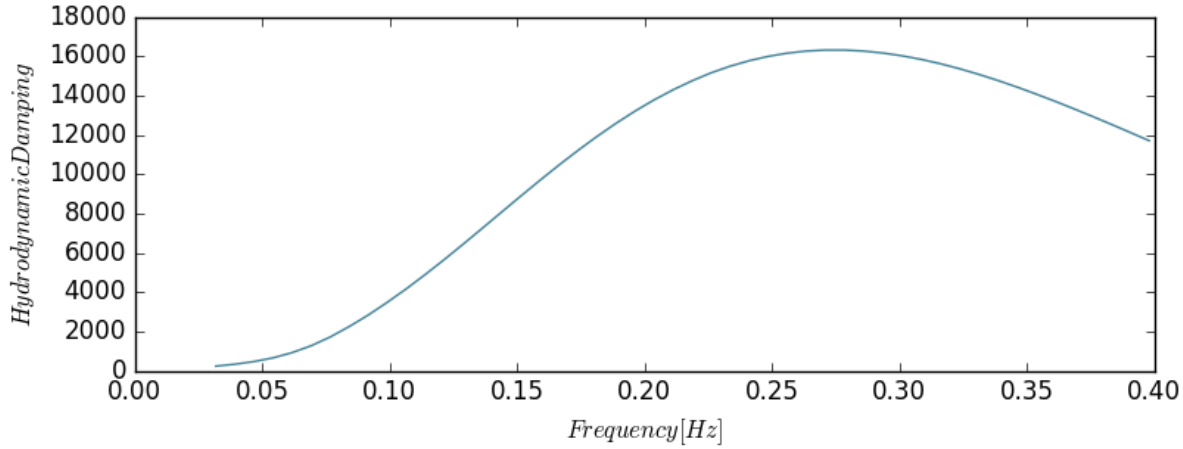

Figure D3 Hydrodynamic damping force wave energy converter with buoy diameter = 5.0 [m]

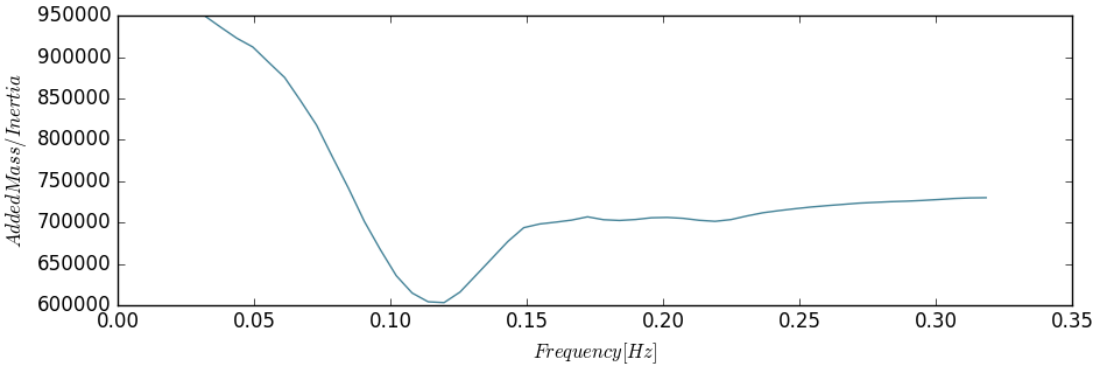

Figure D4 Added mass for columns without wave energy converter

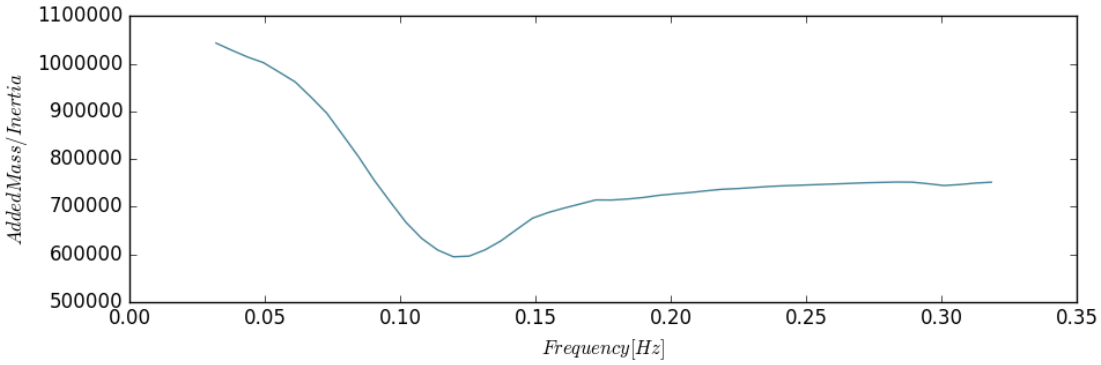

Figure D5 Added mass for columns with wave energy converter

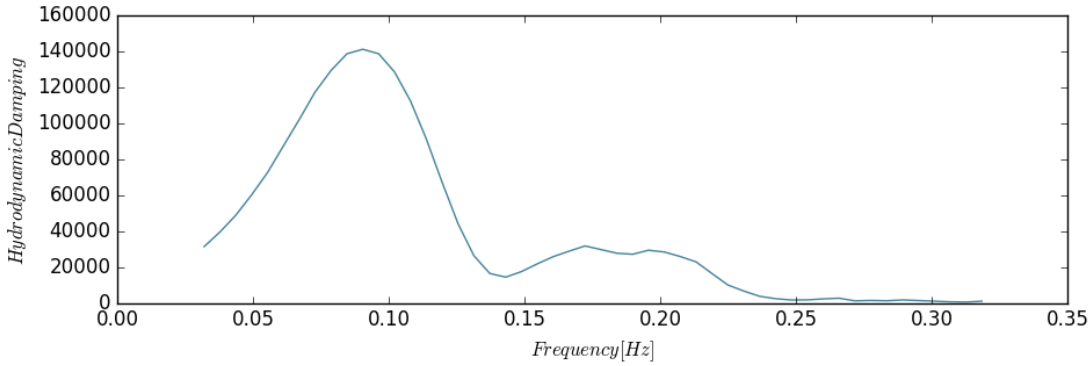

Figure D6 Hydrodynamic damping for columns without wave energy converter

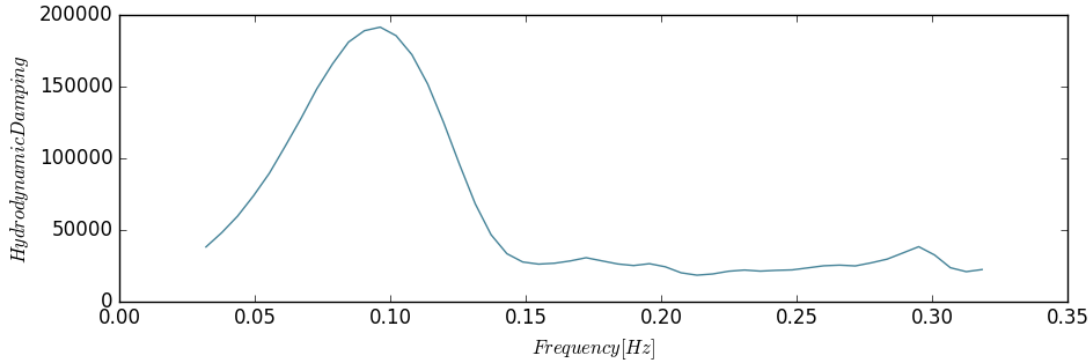

Figure D7 Hydrodynamic damping for columns with wave energy converter

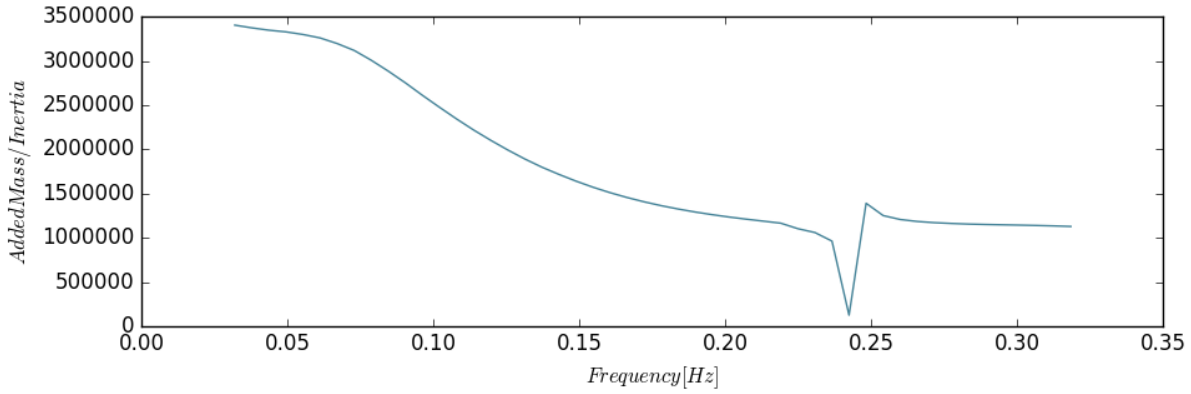

Figure D8 Added mass wave energy converter with buoy diameter = 25.0 [m]

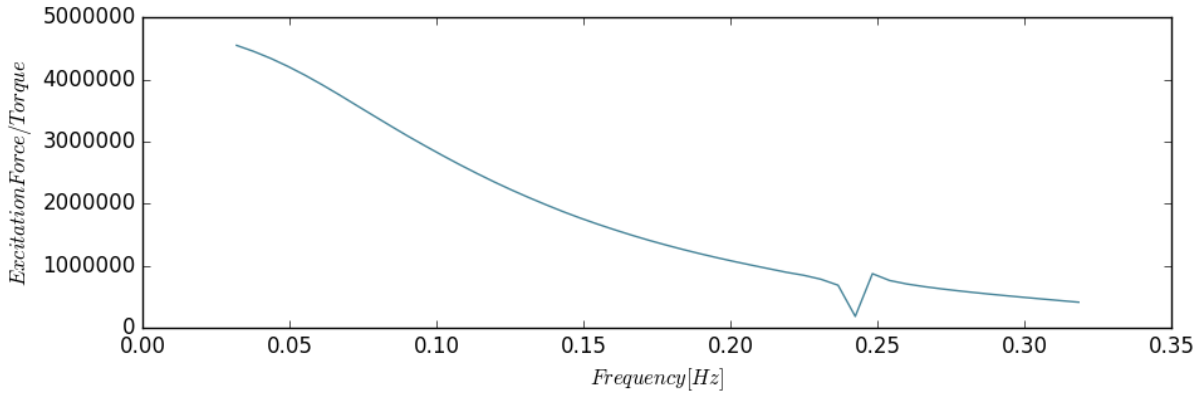

Figure D9 Wave excitation force wave energy converter with buoy diameter = 25.0 [m]

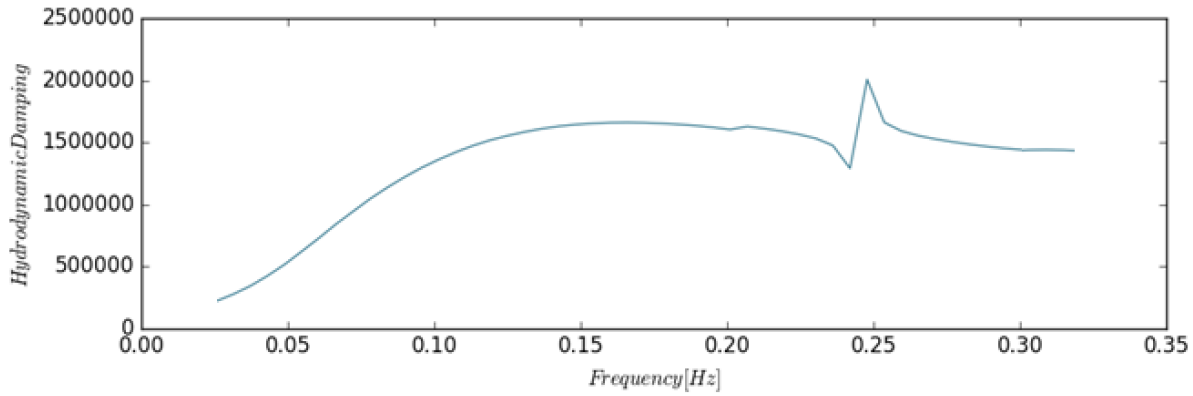

Figure D10 Hydrodynamic damping force wave energy converter with buoy diameter = 25.0 [m]

Appendix E MATLAB Scripts

Script used for Figure 2

Script used for Figure 18

Script used for Figure 21

Script used for subsection 4.3

Script used for Figure A3

Script used for Figure A4

Script used for Figure A5

Script used for Figure A6

Script used for Appendix B

Script used for chapters 6, 7 and 8

Used script for Figure 2

```
i = 1;
cp = 0.593;
rho = 1.2;
g = 9.81;

for v = 1:0.1:15
p = cp*rho*g*v^3;
P(i)=p;
V(i)=v;
i=i+1;
end

figure
plot(V,P)
title('Rankine Froude actuator disk model')
xlabel('Wind speed [ms^{-1}]');
ylabel('Power [Wm^{-2}]')
grid on
```

Used script for Figure 18

```
rho = 1020;
g = 9.81;
j = 1;

H0 = 0;
dH = 0.1;
Hx = 3.5;

T0 = 1;
dT = 0.1;
Tx = 15;

for H = H0:dH:Hx %i
i=1;
    for T = T0:dT:Tx %j
P = (rho*g*g*H*H*T)./(64*pi)/(1000);

p(i,j)=P;
h(i,j)=H;
t(i,j)=T;

i=i+1;
    end
    i=1;
j=j+1;
end
```

Script used for Figure 21

```
function [S,W]=Freq2Time(z,n,m,sfr,skl);
% HitSpek2 : generate wave spectrum from time signal
%
zf = fft(z);
R  = zf.*conj(zf)/n;
fr = (0:n-1)/n*sfr;
P  = 2*R/sfr;
w  = hamming(m) ;
w  = w/sum(w) ;
w  = [w(ceil((m+1)/2):m);zeros(n-m,1);w(1:ceil((m+1)/2)-1)];
w    = fft(w) ;
pavg = fft(P) ;
pavg = ifft(w.*pavg) ;

S = abs(pavg(1:ceil(n/2)));
F = fr(1:ceil(n/2));

S=S/(2*pi)*sqrt(skl);% Spectral (m^2.s)
W=2*pi*F/sqrt(skl); % w (rad/s)
end
```

Used script for subsection 4.3

```
% Constants
g = 9.81;                                                   % gravity constant
[m/s2]
D = 100;                                                    % wave depth [m]
i = 1;                                                      % set numerator X
j = 1;                                                      % set numerator Y

% Define grid [ space (X,Y) and time ]

x0 = 0;                                                     % start x grid
dx = 0.01;                                                  % dx step [m]
L = 100;                                                    % end x grid [m]

n = L/dx + 1;                                               % grid points X

y0 = 0;                                                     % start x grid
dy = 0.1;                                                   % dx step [m]
H = 1;                                                      % end x grid [m]

m = H/dy + 1;                                               % grid points Y

t0 = 0;                                                     % first timestep
dt = (pi/10000);                                            % dt step [s]
T = 10*pi;                                                 % last timestep [m]

%%%%%%%%%%%%%%%%%%%%%%%%%%%%%%%%%%%%%%%%%%%%%%%%%%%%%%%%%%%%%%%%%%%%%%%%%%%%%%%

                              % Input Commands
%prompt1 = '1D [1] or 2D [2] Wave Spectrum? ';
s = input(prompt1);

%prompt2 = 'Regular [1] or Irregular [2] Wave Spectrum? ';
Q = input(prompt2);

% wave properties
%prompt2 = 'Wave Period in [s]? ';
T_p = input(prompt2);

%prompt3 = 'Wave Height in [m]? ';
H_w = input(prompt3);

s = 2;
Q = 2;
T_p = 10;
H_w = 2;

%%%%%%%%%%%%%%%%%%%%%%%%%%%%%%%%%%%%%%%%%%%%%%%%%%%%%%%%%%%%%%%%%%%%%%%%%%%%%%%

if Q == 1                 %%% Regular Wave Spectrum %%%

lambda = (g/(2*pi))*(T_p^2);                                % wave lenght [m]
k = (2*pi/lambda);                                          % wave number [-]
omega = sqrt(g*k*tanh(k*D));                                % angular freq [s-
1]
c = sqrt((tanh(2*pi*D)/lambda))*(g*lambda)/(2*pi);          % wavespeed [m/s]
```

```
% Wave functions f(x)
    for tplot = 0:0.01:T

% Total wave function
fplot = (H_w/2)*cos(omega*tplot);

% Store time values
Tplot(j)=tplot;

% Store wave amplitudes
Fplot(j)=fplot;

% Update numerator
j=j+1;
    end

% Visualize Regular Wave Spectrum
figure(1);
plot(Tplot,Fplot)
xlabel('Time [s]')
ylabel('Waveheight [m]')
axis([0 T -2*H_w 2*H_w])

% Numerical input variables
for i = 1:1:10
current(i,:) = (H_w/2)*cos(omega*pi/L*[0:dx:L]);
past(i,:) = current(i,:);
end

else           %%% Irregular Wave Spectrum %%%     [in progress]

% average wave length and speed for numerical stability
lambda = (g/(2*pi))*(T_p^2);                              % wave lenght [m]
c = sqrt((tanh(2*pi*D)/lambda))*(g*lambda)/(2*pi);        % wavespeed [m/s]

% Define frequency domain
w0 = 0.2;
wx = 2;
w=linspace(w0,wx,50);              % Create frequency spectrum with substeps
dw = w(2)-w(1);                    % Difference frequency
w = w + dw .* rand(1,length(w));   % Random frequency selection
w3=w;                              % Store frequency values

% JONSWAP Irregular Wave Spectrum

y     = 3.3;                       % y-constant JONSWAP
wp    = 2*pi/T_p;                  % Peak period [s] to frequency [s-1]
sigma = (w<=wp)*0.07+(w>wp)*0.09; % sigma-constant JONSWAP

C0    = exp(-((w-wp).^2)./(2*sigma.^2*wp.^2)); % Constant C0
C1  = (320*H_w^2)/T_p^4;           % Constant C1
C2  = w.^-5;                       % Constant C2
C3 = exp(-5/4*(w/wp).^-4);         % Constant C3
C4  = y.^C0;                       % Constant C4

S     = C1.*C2.*C3.*C4;            % S(w) JONSWAP output

%--------------------------------
scale  = 50 ;                      % Scale factor [-]
```

```
Sf   = 50;                          % Sampling frequency (Hz)
t = [t0:10*dt:T];                   % Time vector [-]
phi = 2*pi*(rand(1,length(w))-0.5); % Random phase selection
A = sqrt(2*S.*dw);                  % Frequency Amplitude

wave = zeros(1,(T/(10*dt)));
    for v = 1:length(t)
    wave(v) = sum(A .* cos(w*t(v) + phi));
    end

[Sx]=Freq2Time(wave',length(wave),400,Sf,scale); % 400 :hamming variable,
custom, can be modified
smax=(max(S)<=max(Sx))*max(Sx)+(max(S)>max(Sx))*max(S);

subplot(2,1,1)
plot(w3,S,'r');
xlabel('w [rad/s]');
ylabel('Spectral [m^2.s]');
legend('Theoretical');
grid;
axis([w0 wx 0 max(S)]);
subplot(2,1,2)
plot(t,wave,'b');
xlabel('Time [s]');
ylabel('Waveheight [m]');
grid;
axis([0 T -inf*2 inf*2]);

% Numerical input variables
    for i = 1:1:10
    current(i,:) = wave;
    past(i,:)= current(i,:);
    end

end

%%%%%%%%%%%%%%%%%%%%%%%%%%%%%%%%%%%%%%%%%%%%%%%%%%%%%%%%%%%%%%%%%%%%%%%%%%%%%%%

% numerical stability factor
r_x = (c*dt)/(dx);
r_y = (c*dt)/(dy);
if r_x < 1/(sqrt(s)) && r_y < 1/(sqrt(s))
    disp('Code is numerical stable')
    disp('Start Calculating')
else
end

%%%%%%%%%%%%%%%%%%%%%%%%%%%%%%%%%%%%%%%%%%%%%%%%%%%%%%%%%%%%%%%%%%%%%%%%%%%%%%%

% X and Y definition for 3plot

%// Define the x values
X = (x0:dx:L).';
xMat = repmat(X, 1, 10); %// For plot3

%// Define y values
Y = y0:dy:(H-dy);
yMat = repmat(Y, numel(X), 1); %//For plot3
```

```
%%%%%%%%%%%%%%%%%%%%%%%%%%%%%%%%%%%%%%%%%%%%%%%%%%%%%%%%%%%%%%%%%%%%%%%%%%%%%%%%

for t = 0:dt:T

% Differential Scheme %% 2D

    for i = 1:1:10

        if Q == 1  % Regular Wave Spectrum
        future(i,1) = (H_w/2)*cos(omega*t);
        else       % Irregular Wave Spectrum

                for v = 1:length(t)
                wave(v) = sum(A .* cos(w*t(v) + phi));
                end

                future(i,1) = wave(v);
        end

    future(i,2:n-1) = r_x*r_x*(current(i,1:n-2)+current(i,3:n)) + 2*(1-
r_x*r_x)*current(i,2:n-1)-past(i,2:n-1);
    future(i,n) = 2*r_x*r_x*current(i,n-1)+2*(1-r_x*r_x)*current(i,n)-
past(i,n);

    % Update Past and Current Values
    past(i,:) = current(i,:);
    current(i,:) = future(i,:);

    end % close i loop

        if mod(t/dt, 10) == 0

        %// Define z values
        z1  = current(1,:)';
        z2  = current(2,:)';
        z3  = current(3,:)';
        z4  = current(4,:)';
        z5  = current(5,:)';
        z6  = current(6,:)';
        z7  = current(7,:)';
        z8  = current(8,:)';
        z9  = current(9,:)';
        z10 = current(10,:)';

        zMat = [z1 z2 z3 z4 z5 z6 z7 z8 z9 z10]; %// For plot3

        figure(2);
        plot3(xMat, yMat, zMat, 'b'); %// Make all traces blue
        grid;
        xlabel('Length [dam]'); ylabel('Width [m]'); zlabel('Height [m]');
        axis([0 L 0 H -2*H_w 2*H_w])
        view(40,40); %// Adjust viewing angle
        pause(0.001)

        end % close plotting loop

end % close t loop
```

Used script for Figure A3

```
i=1;

t0 = 0;
dt = 0.1;
T = 10;

F_a = 10;
m = 1;
k = 100;
c = 5;
b_d = c;

w_n = sqrt(k/m);
b_c = 2*m*w_n;
eta_d = (b_d/b_c);

if eta_d <= 1
   disp('Underdamped')
end

w_d = sqrt(1-eta_d^2)*w_n;
w=w_n;

% free response
H_w = 2;
beta_f = 0;
omega_n = 0.7;

for t = t0:dt:T
z_af = (H_w/2)*cos(omega_n*t+beta_f);
z_free = z_af * exp(-eta_d*w_n*t)*sin(sqrt(1-eta_d^2)*w_n*t + beta_f);

%forced response
z_as = F_a / ((((k-m*w^2)^2)+((b_d*w)^2)^(0.5)));
beta_s = atan((-b_d*w)/k-m*w^2);
z_forced = z_as * sin(w*t+beta_s);

%total response
z_t = z_free + z_forced;

Z_free(i) = z_free;
Z_forced(i) = z_forced;
Z_t(i) = z_t;

T(i) = t;
i=i+1;
end
```

Used script for Figure A4

```
clear all;
close all;
clc;

%% // Default parameters
param.meshsize  = 256 ;     %// main grid size (128=default)
param.patchsize = 200 ;
param.windSpeed = 100 ;     %// [m/s]
param.winddir   = 90   ;    %// Azimuth
param.rng = 15 ;            %//
param.A         = 1e-7 ;    %// scaling factor
param.g         = 9.81 ;    %// gravitational constant

param.xLim = [-10 10] ;     %// domain limits X
param.yLim = [-10 10] ;     %// domain limits Y
param.zLim = [-1e-4 1e-4]*2 ;

gridSize = param.meshsize * [1 1] ;

%% // Define the grid X-Y domain
x = linspace( param.xLim(1) , param.xLim(2) , param.meshsize ) ;
y = linspace( param.yLim(1) , param.yLim(2) , param.meshsize ) ;
[X,Y] = meshgrid(x, y) ;

%% // get the grid parameters which remain constants (not time dependent)
[H0, W, Grid_Sign] =  initialize_wave( param ) ;

%% // calculate wave at t0
t0 = 0 ;
Z = calc_wave( H0 , W , t0 , Grid_Sign ) ;

%% // populate the display panel
h.fig  = figure('Color','w') ;
h.ax   = handle(axes) ;                 %// create an empty axes that fills
the figure
h.surf = handle( surf( NaN(2) ) ) ;     %// create an empty "surface"
object

%% // Display the initial wave surface
set( h.surf , 'XData',X , 'YData',Y , 'ZData',Z )
set( h.ax   , 'XLim',param.xLim , 'YLim',param.yLim , 'ZLim',param.zLim )

axis off                                %// make the axis grid and border
invisible
shading interp                          %// improve shading (remove
"faceted" effect)
blue = linspace(0.4, 1.0, 25).' ; cmap = [blue*0, blue*0, blue]; %'//
create blue colormap
colormap(cmap)
%// configure lighting
h.light_handle = lightangle(-45,30) ;   %// add a light source
set(h.surf,'FaceLighting','phong','AmbientStrength',.3,'DiffuseStrength',.8
,'SpecularStrength',.9,'SpecularExponent',25,'BackFaceLighting','unlit')

%% // Animate
view(75,55) %// no need to reset the view inside the loop ;)
```

```
timeStep = 1./25 ;    % 1/25
nSteps = 10000 ;      % 2000
for time = (1:nSteps)*timeStep
    %// update wave surface
    Z = calc_wave( H0,W,time,Grid_Sign ) ;
    h.surf.ZData = Z ;
    pause(0.001);
end
```

```
function sgn = signGrid(n)

    [x,y] = meshgrid(1:n,1:n) ;
    sgn = ones( n ) ;
    sgn(mod(x+y,2)==0) = -1 ;
end
```

```
function P = phillips(Kx, Ky, windDir, windSpeed, A, g)

    K_sq = Kx.^2 + Ky.^2;
    L = windSpeed.^2 ./ g;
    k_norm = sqrt(K_sq) ;
    WK = Kx./k_norm * windDir(1) + Ky./k_norm * windDir(2);
    P = A ./ K_sq.^2 .* exp(-1.0 ./ (K_sq * L^2)) .* WK.^2 ;
    P( K_sq==0 | WK<0 ) = 0 ;
end
```

```
function Z = calc_wave( H0,W,time,Grid_Sign )

    % recalculate the grid sign if not supplied in input
    if nargin < 4
        Grid_Sign = signGrid( param.meshsize ) ;
    end
    % Assign time=0 if not specified in input
    if nargin < 3 ; time = 0 ; end

    wt = exp(1i .* W .* time ) ;
    Ht = H0 .* wt + conj(rot90(H0,2)) .* conj(wt) ;
    Z = real( ifft2(Ht) .* Grid_Sign ) ;
end
```

Used script for Figure A5

```
% Provided data subquestion a
T_air = 283.15;                     % temperature in Kelvin [K]
P_0 = 1.018e5;                      % pressure in Pascal [Pa]
RH = 0.8;                           % relative humidity [%]
CR_air = 1;                         % Cool rate air in Kelvin per hour [K/h]

%saturated water pressure [Pa]
e_sat_0 = 610.78*exp(17.2694*(T_air-273.16)/(T_air-35.86));

%Saturated water mixing ratio
R_d=287.04;                         %gas constant for dry air in [J/kgK]
R_v=461.5;                          %gas constant for water vapour in[J/kgK]

q_sat_0 =(R_d/R_v) * e_sat_0/((P_0)-e_sat_0)    %[kg/kg]

% q_v = q_sat_0;

T_f = ((35.86*ans + 273.16) / (1-ans));

Time = (T_f-T_air) * CR_air * 60    % Cooling down time in [min]

%%%%%%%%%%%%%%%%%%%%%%%%%%%%%%%%%%%%%%%%%%%%%%%%%%%%%%%%%%%%%%%%%%%%%%%%%%%%%%%

% Provided data subquestion b
p_0 = 1.018e5;                      % pressure in Pascal [Pa]
cv_air=719;                         % [J/kgK]
cp_air=1006;                        % [J/kgK]
g=9.81;                             % gravity constant [m/s^2]

R_air_s=287.058;                    % specific gas constant air [J/kgK]

i=1;                                % iteration counter

E1=RH*q_sat_0/(R_d/R_v);

% Calculation
height = 0.1:1:150;  % height vector
for i = 1:length(height)
    % Height [m]
    h = height(i);
    % Local temperature [K]
    T(i) = T_air - ( ( g / cp_air ) * h );

    % Local pressure [Pa]
    p(i) = p_0 / ( ( 1 + ( ( g * h ) / ( R_d * T(i) ) ) ) );

    % Local density
    rho_air(i) = (p(i))/(R_air_s*T(i));

    %find h for which E1=E2
end
```

Used script for Figure A6

```
H_W = [0.25 0.75 1.25 1.75 2.25 2.75 3.25 3.75];
U_W = [5 6 8 10 12 15 17 20];

figure
plot(H_W,U_W)
hold on

% Coefficients:
  p1 = -0.10101;
  p2 = 1.0584;
  p3 = 1.5691;
  p4 = 4.4674;

u_ref = p1*(H_W).^3 + p2*H_W.^2 + p3*H_W + p4;

figure
scatter(H_W,U_W,'*','b')
hold on
plot(H_W,u_ref,'r')
xlabel('Significant wave height')
ylabel('Wave speed [ms^{-1}]')
title('Sverdrup-Munk-Bretschneider')
legend('(Bretschneider, 1964)','Cubic approximation','location','north')
grid on
```

Used script for Appendix B

```
%%%%%%%%%%%%%%%%%%%%%%%%%%%%%%%%%%%%%%%%%%%%%%%%%%%%%%%%%%%%%%%%%%%%%%%%%%%%%%%%
% Open WEC Data
% D = 5 [m]
% Nemoh Regular Waves
% f = 0.2:2.5 (50)
% Time = 100 [s] / dt = 0.1 [s]

%%%%%%%%%%%%%%%%%%%%%%%%%%%%%%%%%%%%%%%%%%%%%%%%%%%%%%%%%%%%%%%%%%%%%%%%%%%%%%%%
% Load variables

                    load('BuoyPowerHeightDamping.mat');
                    load('BuoyPowerHeightTime.mat');
                    load('BuoyPowerTimeDamping.mat');

%%%%%%%%%%%%%%%%%%%%%%%%%%%%%%%%%%%%%%%%%%%%%%%%%%%%%%%%%%%%%%%%%%%%%%%%%%%%%%%%
% Reference values

                    load('ReferenceDamping.mat');
                    load('ReferenceHeight.mat');
                    load('ReferenceTime.mat');

%%%%%%%%%%%%%%%%%%%%%%%%%%%%%%%%%%%%%%%%%%%%%%%%%%%%%%%%%%%%%%%%%%%%%%%%%%%%%%%%
% List of Plots

% (1) X = Damping         Y = Power    Z = Wave Height
% (2) X = Wave height     Y = Power    Z = Damping
% (3) X = Wave Period     Y = Power    Z = Wave height
% (4) X = Wave Height     Y = Power    Z = Wave Period
% (5) X = Damping         Y = Power    Z = Wave Period
% (6) X = Wave Period     Y = Power    Z = Damping

%%%%%%%%%%%%%%%%%%%%%%%%%%%%%%%%%%%%%%%%%%%%%%%%%%%%%%%%%%%%%%%%%%%%%%%%%%%%%%%%
%     X = Damping     Y = Power    Z = Wave Height  (1)

figure;
xlabel('BPTO [kg/s]')
ylabel('Power [kW]')
title('Effect Wave Height with WavePeriod = 10 [s]')
set(gcf,'numbertitle','off','name','5m Buoy Power Production')
hold on

 for ii = 1:7

 Y=(BuoyPowerHeightDamping(:,ii)/1000);
 X=(ReferenceDamping(:,ii));
 plot(X,Y,'LineWidth',1)

 if ii == 7
    text(600000,250,'H = 7 [m]')
 end

 end
legend('H=1 [m]', 'H=2 [m]', 'H=3 [m]', 'H=4 [m]', 'H=5 [m]','H=6 [m]',
'H=7 [m]','Location','Eastoutside')
saveas(gcf,'5mBuoyPowerDampingWaveheight.png');
saveas(gcf,'5mBuoyPowerDampingWaveheight.fig');
```

```
%%%%%%%%%%%%%%%%%%%%%%%%%%%%%%%%%%%%%%%%%%%%%%%%%%%%%%%%%%%%%%%%%%%%%%%%%%%%
%      X = Wave height      Y = Power     Z = Damping   (2)

figure;
xlabel('Waveheight [m]')
ylabel('Power [kW]')
title('Effect Damping with WavePeriod = 10 [s]')
set(gcf,'numbertitle','off','name','5m Buoy Power Production')
hold on

 for ii = 1:14

 Y=(BuoyPowerHeightDamping(ii,:)/1000);
 X=(ReferenceHeight(ii,:));
 plot(X,Y,'LineWidth',1)
     text(3,175,'C = 250000 [kg/s]')
    end

 end

legend('C=1 [kg/s]', 'C=10 [kg/s]', 'C=100 [kg/s]', 'C=1000 [kg/s]',
'C=10000 [kg/s]','C=25000 [kg/s]', 'C=75000 [kg/s]','C=100000
[kg/s]','C=250000 [kg/s]','C=375000 [kg/s]','C=500000 [kg/s]','C=750000
[kg/s]','C=1000000 [kg/s]','Location','Eastoutside')
saveas(gcf,'5mBuoyPowerWaveheightDamping.png');
saveas(gcf,'5mBuoyPowerWaveheightDamping.fig');

%%%%%%%%%%%%%%%%%%%%%%%%%%%%%%%%%%%%%%%%%%%%%%%%%%%%%%%%%%%%%%%%%%%%%%%%%%%%
%      X = Wave Period     Y = Power     Z = Wave height   (3)

figure;
xlabel('WavePeriod [s]')
ylabel('Power [kW]')
title('Effect Wave Period with BPTO=250000 [kg/s]')
set(gcf,'numbertitle','off','name','5m Buoy Power Production')
hold on

 for ii = 1:7

 Y=(BuoyPowerHeightTime(:,ii)/1000);
 X=(ReferenceTime(ii,:));
 plot(X,Y,'LineWidth',1)

  if ii == 7
    text(10,320,'H = 7 [m]')
  end

 end

legend('H=1 [m]', 'H=2 [m]', 'H=3 [m]', 'H=4 [m]', 'H=5 [m]','H=6 [m]',
'H=7 [m]','Location','Eastoutside')
saveas(gcf,'5mBuoyPowerWavePeriodWaveHeight.png');
saveas(gcf,'5mBuoyPowerWavePeriodWaveheight.fig');

%%%%%%%%%%%%%%%%%%%%%%%%%%%%%%%%%%%%%%%%%%%%%%%%%%%%%%%%%%%%%%%%%%%%%%%%%%%%
%      X = Wave Height     Y = Power     Z = Wave Period   (4)

figure;
xlabel('Waveheight [m]')
```

```
ylabel('Power [kW]')
title('Effect Wave Period with BPTO=250000 [kg/s]')
set(gcf,'numbertitle','off','name','5m Buoy Power Production')
hold on

 for ii = 1:7

 Y=(BuoyPowerHeightTime(ii,:)/1000);
 X=(ReferenceHeight(ii,:));
 plot(X,Y,'LineWidth',1)

 if ii == 7
    text(4,190,'T = 8 [s]')
  end

 end

legend('T = 2 [s]', 'T = 4 [s]', 'T = 6 [s]', 'T = 8 [s]', 'T = 10 [s]','T
= 12 [s]', 'T = 14 [s]','Location','Eastoutside')
saveas(gcf,'5mBuoyPowerWaveHeightWavePeriod.png');
saveas(gcf,'5mBuoyPowerWaveHeightWavePeriod.fig');

%%%%%%%%%%%%%%%%%%%%%%%%%%%%%%%%%%%%%%%%%%%%%%%%%%%%%%%%%%%%%%%%%%%%%%%%%%%%
%      X = Damping      Y = Power     Z = Wave Period  (5)

figure;
xlabel('BPTO [kg/s]')
ylabel('Power [kW]')
title('Effect Wave Period with Wave Height 3 [m]')
set(gcf,'numbertitle','off','name','5m Buoy Power Production')
hold on

 for ii = 1:7

 Y=(BuoyPowerTimeDamping(:,ii)/1000);
 X=(ReferenceDamping(:,ii));
 plot(X,Y,'LineWidth',1)

  if ii == 7
    text(340000,60,'T = 8 [s]')
  end

 end

legend('T=2 [s]', 'T=4 [s]', 'T=6 [s]', 'T=8 [s]', 'T=10 [s]','T=12 [s]',
'T=14 [s]','Location','Eastoutside')
saveas(gcf,'5mBuoyDampingPowerWavePeriod.png');
saveas(gcf,'5mBuoyDampingPowerWavePeriod.fig');

%%%%%%%%%%%%%%%%%%%%%%%%%%%%%%%%%%%%%%%%%%%%%%%%%%%%%%%%%%%%%%%%%%%%%%%%%%%%
%      X = Wave Period     Y = Power     Z = Damping  (6)

figure;
xlabel('Wave Period [s]')
ylabel('Power [kW]')
title('Effect Damping with Wave Height 3 [m]')
set(gcf,'numbertitle','off','name','5m Buoy Power Production')
hold on
```

```
 for ii = 1:14

 Y=(BuoyPowerTimeDamping(ii,:)/1000);
 X=(ReferenceTime(ii,:));
 plot(X,Y,'LineWidth',1)

 if ii == 7
    text(9,62,'C = 250000 [kg/s]')
  end

 end

legend('C=1 [kg/s]', 'C=10 [kg/s]', 'C=100 [kg/s]', 'C=1000 [kg/s]',
'C=10000 [kg/s]','C=25000 [kg/s]', 'C=75000 [kg/s]','C=100000
[kg/s]','C=250000 [kg/s]','C=375000 [kg/s]','C=500000 [kg/s]','C=750000
[kg/s]','C=1000000 [kg/s]','Location','Eastoutside')
saveas(gcf,'5mBuoyWavePeriodPowerDamping.png');
saveas(gcf,'5mBuoyWavePeriodPowerDamping.fig');

%%%%%%%%%%%%%%%%%%%%%%%%%%%%%%%%%%%%%%%%%%%%%%%%%%%%%%%%%%%%%%%%%%%%%%%%%%%%
```

Used script for chapter 6, chapter 7 and chapter 8

```
% Sources

% [1] http://www.aoml.noaa.gov/phod/docs/Wang_etal_2010_Cd.pdf
% [2] Table 2.1 page 46 Frequency Modeling (de Backer, 2009)
% [3]
http://www.codecogs.com/library/engineering/fluid_mechanics/waves/spectra/j
onswap.php

%%%%%%%%%%%%%%%%%%%%%%%%%%%%%%%%%%%%%%%%%%%%%%%%%%%%%%%%%%%%%%%%%%%%%%%%%%%

% Wave Characteristics [1]
rho = 1020;                                             % density [kgm-3]
d = 100;                                                % wave depth [m]

% Constants
g = 9.81;                                               % gravity constant [ms-2]

% JONSWAP WS constants
alpha_s = 0.0081;                                       % alpha constant [-]
gamma = 3.3;                                            % gamma constant [-]

% dimension converters
Hz2rad = 2*pi;                                          % converter Hz to rad
rad2Hz = 1/(Hz2rad);                                    % converter rad to Hz
deg2rad = pi/180;                                       % converter deg to rad
rad2deg = 1/(deg2rad);                                  % converter rad to deg
ft2m = 1/0.3048;                                        % converter ft to m

% Buoy Parameters
R = 2.5;                                                % buoy radius [m]
d_buoy = 2*R;                                           % buoy diameter [m]
m_buoy = 42.5e3;                                        % buoy mass [kg]

%%%%%%%%%%%%%%%%%%%%%%%%%%%%%%%%%%%%%%%%%%%%%%%%%%%%%%%%%%%%%%%%%%%%%%%%%%%
%                     Loading data for scatter plots [2]
bhyd_f = [0.05 0.075 0.1 0.125 0.15 0.175 0.2 0.225 0.25 0.275 0.3];
bhyd_w = 2*pi*bhyd_f;
bhyd_scatter = 1e3* [1 2.5 4.5 7 9 11 13 14 15 15 14.5];
hhw = [0.25 0.5 0.75 1 1.25 1.50 1.75 2 2.25 2.5 2.75 3 3.25 3.5 3.75];
mms = 1e3*[160 160 160 160 160 180 200 215 235 255 270 270 265 280 300];
%%%%%%%%%%%%%%%%%%%%%%%%%%%%%%%%%%%%%%%%%%%%%%%%%%%%%%%%%%%%%%%%%%%%%%%%%%%

for dr = 1                                              % draft of the buoy [m]

    if     dr == 1
                    draft = 3.5;
    elseif dr == 2
                    draft = 4.0;
    elseif dr == 3
                    draft = 4.5;
    end;

% hydrostatic restoring coefficient                     % [kgs-2]
k = rho*g*pi*R^2;

% Time range
```

```
m  = 500;                                                % number of time steps [-
]
t0 = 0;                                                  % start time [s]
tx = 10*pi;                                              % end time [s]
dt = (tx+t0)/(m);                                        % timestep size [s]

% Frequency Range
n  = 500;                                                % number of frequency
steps [-]
w0 = 0.22;                                               % start frequency
[rads-1]
wx = 1.88;                                               % end frequency
[rads-1]
dw = (wx+w0)/(n);                                        % frequency step size
[rads-1]
i  = round((wx - w0)/dw);

% Wave Heights
H0 = 0.25;                                               % wave height [m]
dH = 0.5;                                                % wave height [m]
Hx = 3.75;                                               % wave height [m]
j = (Hx - H0)/dH;

%%%%%%%%%%%%%%%%%%%%%%%%%%%%%%%%%%%%%%%%%%%%%%%%%%%%%%%%%%%%%%%%%%%%%%%%%%%%%%%

    % Pre-allocating zero matrices for speed improvement

    % Values only dependent on frequency (i)
    beta_Fex              =      zeros(i,1);
    b_hyd                 =      zeros(i,1);
    m_added               =      zeros(i,1);

    % Values only dependent on sea state (j)
    H_w                   =      zeros(1,j);
    H_W                   =      zeros(1,j);
    xi                    =      zeros(1,j);
    T_p                   =      zeros(1,j);
    T_P                   =      zeros(1,j);
    lambda_p              =      zeros(1,j);
    L_3                   =      zeros(1,j);
    E_reg                 =      zeros(1,j);
    J_cg                  =      zeros(1,j);
    J_kf                  =      zeros(1,j);
    k_wp                  =      zeros(1,j);
    w_p                   =      zeros(1,j);
    f_p                   =      zeros(1,j);
    v_p                   =      zeros(1,j);
    v_gp                  =      zeros(1,j);
    d_fp                  =      zeros(1,j);
    beta_s_f              =      zeros(1,j);
    beta_s_w              =      zeros(1,j);
    b_ex                  =      zeros(1,j);
    z_a_sign              =      zeros(1,j);
    P_213                 =      zeros(1,j);
    P_214                 =      zeros(1,j);
    n_abs                 =      zeros(1,j);
    SC                    =      zeros(1,j);
    SC2                   =      zeros(1,j);

    % Values dependent on both sea state and frequency (i,j)
```

```
S_xi                    =       zeros(i,j);
S_xi_f                  =       zeros(i,j);
S_xi_w                  =       zeros(i,j);
F_exA                   =       zeros(i,j);
b_t                     =       zeros(i,j);
m_sup                   =       zeros(i,j);
m_sup2                  =       zeros(i,j);
m_t                     =       zeros(i,j);
w_n                     =       zeros(i,j);
b_c                     =       zeros(i,j);
eta_d                   =       zeros(i,j);
A1                      =       zeros(i,j);
A2                      =       zeros(i,j);
A3                      =       zeros(i,j);
z_a                     =       zeros(i,j);
beta_mot                =       zeros(i,j);
xi_a                    =       zeros(i,j);
S_z                     =       zeros(i,j);
qq                      =       zeros(i,j);
P_117p                  =       zeros(i,j);
P_120                   =       zeros(i,j);
P_171                   =       zeros(i,j);
hp                      =       zeros(i,j);
cp                      =       zeros(i,j);
eta_abs                 =       zeros(i,j);
hp_max                  =       zeros(i,j);
eta_abs_max             =       zeros(i,j);
f_ex                    =       zeros(i,j);
P_177                   =       zeros(i,j);
b_hyd_178               =       zeros(i,j);
P_179                   =       zeros(i,j);
P_180                   =       zeros(i,j);
hp2                     =       zeros(i,j);
hp3                     =       zeros(i,j);
hp4                     =       zeros(i,j);
C1                      =       zeros(i,j);
C2                      =       zeros(i,j);
W                       =       zeros(i,j);
Freq                    =       zeros(i,j);
S                       =       zeros(i,j);

% relative motions
z_rel                   =       zeros(i,j);
v_rel                   =       zeros(i,j);
z_Arel                  =       zeros(i,j);
v_Arel                  =       zeros(i,j);

% floating
z_pl                    =       zeros(i,j);
beta_pl                 =       zeros(i,j);
F_FLOAT                 =       zeros(i,j);
BETA_FLOAT              =       zeros(i,j);
z_FLOAT                 =       zeros(i,j);
S_zFLOAT                =       zeros(i,j);

% Values dependent on both sea state and time (n,j)
z_b                     =       zeros(n,j);
z_w                     =       zeros(n,j);
T                       =       zeros(n,j);

%%%%%%%%%%%%%%%%%%%%%%%%%%%%%%%%%%%%%%%%%%%%%%%%%%%%%%%%%%%%%%%%%%%%%%%%%%%%%%%
```

```
    % Reset numerators
    i = 1;
    j = 1;

    % Load wavenumbers for all frequencies
    load_wavenumbers = load('K1.mat');
    S2C = struct2cell(load_wavenumbers);
    k_w = abs(cat(2,S2C{:}));

    % Introducing waitbar
    h = waitbar(0,'Numerical calculation in progress');

%%%%%%%%%%%%%%%%%%%%%%%%%%%%%%%%%%%%%%%%%%%%%%%%%%%%%%%%%%%%%%%%%%%%%%%%%%%%%%%

for j=1:5                           % vary in waveheight (j)

    % Eight seastates according to [2]

    if  H_w == 0.25
        T_p = 6.70;
    elseif H_w == 0.75
        T_p = 6.70; %
    elseif H_w == 1.25
        T_p = 6.70;
    elseif H_w == 1.75
        T_p = 7.40;
    elseif H_w == 2.25
        T_p = 8.11;
    elseif H_w == 2.75
        T_p = 8.81;
    elseif H_w == 3.25
        T_p = 8.81;
    elseif H_w == 3.75
        T_p = 9.52;
    end;

%%%%%%%%%%%%%%%%%%%%%%%%%%%%%%%%%%%%%%%%%%%%%%%%%%%%%%%%%%%%%%%%%%%%%%%%%%%%%%%

    % Save sea state properties

    H_W(j) = H_w;                                   % wave height [m]
    xi(j) = (H_w/2);                                % wave amplitude [m]

    T_P(j) = T_p;                                   % wave period [s]

    % Corresponding wave properties
    lambda_p(j) = (g*(T_p^2)/(2*pi));               % wave lenght  [m]
    L_3(j)= lambda_p(j)/3;                          % 1/3rd of wave length [m]

    if d > L_3                                      % deep water condition
    else
        disp('deep water relation does not hold')
    end

%%%%%%%%%%%%%%%%%%%%%%%%%%%%%%%%%%%%%%%%%%%%%%%%%%%%%%%%%%%%%%%%%%%%%%%%%%%%%%%

    % Energy content of waves [kWsm-2]
```

```
    k_e = rho*g/8;
    E_reg(j) = k_e * H_w^2;

    % Wave-power level [kWm^-2]
    cg = (g*T_p)/(4*pi);                          % group velocity [ms-1]
    J_cg(j) = (cg*E_reg(j))/1000;

    k_j = (rho*g^2)/(32*pi);
    J_kf(j) = (k_j * T_p * (H_w^2))/1000;

%%%%%%%%%%%%%%%%%%%%%%%%%%%%%%%%%%%%%%%%%%%%%%%%%%%%%%%%%%%%%%%%%%%%%%%%%%%%%%%

    %                          Eigen values

    k_wp(j) = (2*pi)/lambda_p(j);
% wave number  [-]
    w_p(j) = sqrt(g*k_wp(j)*tanh(k_wp(j)*d));
% eigenfrequency [rads-1]

    v_p(j)   = lambda_p(j)/T_p;
% velocity [ms-1]
    v_gp(j) = (v_p(j)/2)*(1+(2*k_wp(j)*d/(sinh(2*k_wp(j)*d))));
% groupvelocity [ms]

    d_fp(j) = tanh(k_wp(j)*d)+k_wp(j)*d-k_wp(j)*d*(tanh(k_wp(j)*d).^2);
% depth function [-]

%%%%%%%%%%%%%%%%%%%%%%%%%%%%%%%%%%%%%%%%%%%%%%%%%%%%%%%%%%%%%%%%%%%%%%%%%%%%%%%

for w = w0:dw:wx                                   % vary in frequency (i)

    % wave number check
    k_w_check1(i) = (w^2)/g;
    k_w_check2(i) = k_w(i)*tanh(k_w(i)*d);

    % frequency [Hz]
    f = w/(2*pi);
    f_p(j) = w_p(j)/(2*pi);

    % JONSWAP wave spectrum sigma condition
    if w < w_p
    sigma = 0.07;
    else
    sigma = 0.09;
    end

    % JONSWAP wave spectrum constants
    beta_s_w(j) = exp( - ((w-w_p(j))^2) / (2*(sigma^2)*(w_p(j)^2)));

    % Wave spectrum [3]
    S_xi(i,j) = alpha_s*(g^2)*(w^-5)*(gamma^(beta_s_w(j)))*exp((-
5/4)*((w_p(j)/w)^4));

%%%%%%%%%%%%%%%%%%%%%%%%%%%%%%%%%%%%%%%%%%%%%%%%%%%%%%%%%%%%%%%%%%%%%%%%%%%%%%%

    if f < f_p
    sigma = 0.07;
    else
```

```
    sigma = 0.09;
    end

    beta_s_f(j) = exp( - ((f-f_p(j))^2) / (2*(sigma^2)*(f_p(j)^2)));

    % Wave Spectrum de Backer 2009
    x1 = (0.0624)/(0.230+0.0336*gamma-((0.185)/(1.9+gamma)));
    S_xi_f(i,j) = x1*(H_w^2)*(f_p(j)^4)*(f^(-
5))*(gamma^(beta_s_f(j)))*exp((-5/4)*((f_p(j)/f)^4));
    S_xi_w(i,j) = x1*(H_w^2)*(w_p(j)^4)*(w^(-
5))*(gamma^(beta_s_w(j)))*exp((-5/4)*((w_p(j)/w)^4));

    % equation 2.10 wave amplitude [m]
    xi_a(i,j) = 2*sqrt(S_xi_w(i,j)*0.043);

%%%%%%%%%%%%%%%%%%%%%%%%%%%%%%%%%%%%%%%%%%%%%%%%%%%%%%%%%%%%%%%%%%%%%%%%%%%%%%%

    %                          Approximations

    % F_exA = excitating force [N/m]
    F_exA(i,j) = xi(j)*(1.2e4 * (w.^3) - 4.7e4 * (w.^2) - 3.4e4 * w +
2.1e5);
    F_EXA(i,j) = (1.2e4 * (w.^3) - 4.7e4 * (w.^2) - 3.4e4 * w + 2.1e5) /
1000; % [kN/m]

    % beta_Fex = phase angle between force velocity [rad]
    beta_Fex(i) = deg2rad* (13 * (w.^2) - 10*w + 1.9);

    %%%%%%%%%%%%%%%%%%%%%%%%%%%%%%%%%%%%%%%%%%%%%%%%%%%%%%%%%%%%%%%%%%%%%%%%%%%%%%%

    % b_ex = external damping coefficient [kgs-1]
    b_ex(j) = 3546.2*H_w.^5 -36285*H_w.^4 + 1.2679e+05*H_w.^3 + -
1.5916e+05*H_w.^2 + 74362*H_w + 9545.5;

    % b_hyd = hydrodynamic damping coefficient [kgs-1]
    b_hyd(i) = -5914*(w.^3) + 14029*(w.^2) + 2861.6*(w) -1212.1;

    % total damping [kgs-1]
    b_t(i,j) = b_hyd(i) + b_ex(j);

    %%%%%%%%%%%%%%%%%%%%%%%%%%%%%%%%%%%%%%%%%%%%%%%%%%%%%%%%%%%%%%%%%%%%%%%%%%%%%%%

    % m_added = added mass [kg]
    m_added(i) = 5.8e3*(w.^3) - 2.2e4*(w.^2) + 1.7e4*(w) + 2.4e4;

    % m_supp = supplementary mass [kg]
    m_sup(i,j) = ( ((w_p(j).^2)/k)* (m_buoy+m_added(i))-1)   / ((-
((w_p(j)).^2)/k));

    m_sup2(i,j) =-427.74*(H_w).^7 + 6769.1*(H_w).^6 - 35256*(H_w).^5 +
66585*(H_w).^4 -8244.9*(H_w).^3 -69582*(H_w).^2 + 46766*(H_w) + 1.5249e+05;

    % total mass [kg]
    m_t(i,j) = m_buoy + m_sup(i,j) + m_added(i);

%%%%%%%%%%%%%%%%%%%%%%%%%%%%%%%%%%%%%%%%%%%%%%%%%%%%%%%%%%%%%%%%%%%%%%%%%%%%%%%

    % Natural frequency system [rads-1]
```

```
    w_n(i,j) = sqrt(k/m_t(i,j));

    if w_p(j) ~= w_n(1,j)
      disp('Warning: natural frequency system does not matches peak
frequency waves')
    end

    % Critical damping & determining if system is underdamped
    b_c = 2*sqrt(k*m_t(i,j));                   % [kgs-1]
    eta_d(i,j) = b_t(i,j) / b_c;                % [-]

    if eta_d > 1
       disp('Warning: system overdamped')
    end

    w_d(i,j) = w_n(i,j)*sqrt(1-eta_d(i,j)^2);

%%%%%%%%%%%%%%%%%%%%%%%%%%%%%%%%%%%%%%%%%%%%%%%%%%%%%%%%%%%%%%%%%%%%%%%%%%%%%%%

    %               Steady State Solution FIXED REFERENCE

    % subterms mw, A1 A2 A3
    mw = m_t(i,j)*(w^2);
    A1(i,j) = (k - mw)^2;
    A2(i,j) = (b_t(i,j)*w)^2;
    A3(i,j) = sqrt(A1(i,j)+A2(i,j));

    % Steady state motion                z = z_a * sin (w*t + beta_mot) [m]
    z_a(i,j) = (F_exA(i,j)) / (A3(i,j));
    beta_mot(i,j) = beta_Fex(i) - (atan((b_t(i,j)*w) / (k - mw)));

    % equation 2.11 spectrum of amplitude [m]
    S_z(i,j) = (S_xi_w(i,j) * (z_a(i,j)^2)) / (xi(j)^2);

    % SC p59
    qq(i,j) = (z_a(i,j)-xi_a(i,j))/(draft);
    v = round((w_p(j) - w0)/(dw));
    SC(j) = qq(v,j);

%%%%%%%%%%%%%%%%%%%%%%%%%%%%%%%%%%%%%%%%%%%%%%%%%%%%%%%%%%%%%%%%%%%%%%%%%%%%%%%

    %                   Power production Regular Waves

    % equation 1.17 Available Power per unit crest length [Wm-2]
    P_117p(i,j) = (1/8)*rho*g*(H_w^2)*v_gp(j);

    % equation 1.20 Available Power per unit crest length [Wm-2]
    P_120(i,j) = (rho*(g^2)*d_fp(j)*(xi(j)^2))/(1000*4*w);

    % equation 1.71 Average Power Absorption [W]
    P_171(i,j) = 0.5 * b_ex(j) * (w.^2) * (z_a(i,j)^2);

    % equation 1.72 Absorption Width [m]
    hp(i,j) = P_171(i,j) / P_120(i,j);
    cp(i,j) = ((2/pi)*lambda_p(j)*b_hyd(i)*b_ex(j)*w) / (((k-
m_t(i,j)*(w^2))^2)+((b_t(i,j)*w)^2));

    % equation X absorption efficiency [-]
```

```
    eta_abs(i,j) = hp(i,j) / d_buoy;

    % equation 1.73 max absorption Width [m]
    hp_max(i,j) = lambda_p(j) / (2*pi);

    % equation X max absorption efficiency [-]
    eta_abs_max(i,j) = hp_max(i,j) / d_buoy;

    % equation 1.76 transfer function
    f_ex(i,j) = F_exA(i,j) / xi(j);

    % equation 1.77 max average absorbed power [W]
    P_177(i,j)  = (f_ex(i,j)^2)*((xi(j))^2)/(8*b_hyd(i));

    % equation 1.78 hydrodynamic damping coefficient heave
    b_hyd_178(i,j) = (w*k_w(i)*(f_ex(i,j)^2))/(2*rho*(g^2)*d_fp(j));

    % equation 1.79 max average absorbed power [W]
    P_179(i,j) = (rho*(g^2)*d_fp(j)*(xi(j)^2))/(4*w*k_wp(j));

    % equation 1.80 total available average power [W]
    P_180(i,j)  = (rho*(g^2)*d_fp(j)*(xi(j)^2))/(4*w);

    % equation X max absorption efficiency [-]
    hp2(i,j) = P_179(i,j)/ (d_buoy*P_180(i,j));
    hp3(i,j) = 1/(k_wp(j));
    hp4(i,j) = lambda_p(j)/(2*pi);

    % Integral constants eq 2.13 & 2.14
    C1(i,j) = rho*g*v_gp(j)*S_xi_w(i,j);
    C2(i,j) = b_ex(j)*(w^2)*((z_a(i,j)/xi(j))^2)*S_xi_w(i,j);

    % Integral constant with slamming restriction
    % CxS(i,j) = b_ex(j)*(w^2)*((z_aS(i,j)/xi(j))^2)*S_xi_w(i,j);

%%%%%%%%%%%%%%%%%%%%%%%%%%%%%%%%%%%%%%%%%%%%%%%%%%%%%%%%%%%%%%%%%%%%%%%%%%%%%%%

    % Relative displacement and velocity buoy & water in [m] and [ms-1]
    z_Arel(i,j) = sqrt( (xi_a(i,j) - z_a(i,j)*cos(beta_mot(i,j)))^2) /
(((z_a(i,j)^2)*(sin(beta_mot(i,j))^2)));
    v_Arel(i,j) = w*sqrt( (xi_a(i,j) - z_a(i,j)*cos(beta_mot(i,j)))^2) /
(((z_a(i,j)^2)*(sin(beta_mot(i,j))^2)));

    %                           Save useful values

    D(j) = d;

    % JONSWAP Spectrum
    W(i,j)    = w;
    Freq(i,j) = w * rad2Hz;
    S(i,j)    = S_xi_w(i,j);

    WW(i,j) = W(i,j) / (w_d(i,j));
    RAO(i,j) = z_a(i,j) / xi(j);

%%%%%%%%%%%%%%%%%%%%%%%%%%%%%%%%%%%%%%%%%%%%%%%%%%%%%%%%%%%%%%%%%%%%%%%%%%%%%%%

    %             Steady State Solution Floating REFERENCE
```

```
    % subterms mw, A1 A2 A3
    mw = m_t(i,j)*(w).^2;
    A1(i,j) = (k - mw)^2;
    A2(i,j) = (b_t(i,j)*w)^2;
    A3(i,j) = sqrt(A1(i,j)+A2(i,j));

    if w < 0.6

    % Coefficients: RANGE: 0.2 tot 0.6
    p1 = -14.334;
    p2 = 27.588;
    p3 = -18.162;
    p4 = 4.2258;

    RAO_heave(i,j) = p1*w.^3 + p2*w.^2 + p3*w + p4;

    elseif (w > 0.6 && w < 0.8)

    p1 = -6.6667;
    p2 = 17;
    p3 = -14.633;
    p4 = 4.3;

    RAO_heave(i,j) = p1*w.^3 + p2*w.^2 + p3*w + p4;

    elseif w > 0.8

    % Coefficients: RANGE 0.8 tot 2
    p1 = -0.053647;
    p2 = 0.29216;
    p3 = -0.52854;
    p4 = 0.31929;

    RAO_heave(i,j) = p1*w.^3 + p2*w.^2 + p3*w + p4;

    end

    z_pl(i,j) = RAO_heave(i,j) *xi(j);

    %%%%%%%%%%%%%%%%%%%%%%%%%%%%%%%%%%%%%%%%%%%%%%%%%%%%%%%%%%%%

    p1 = -0.020557;
    p2 = 0.11873;
    p3 = -0.23476;
    p4 = 0.16961;

    RAO_pitch(i,j) = deg2rad*ft2m*(p1*w.^3 + p2*w.^2 + p3*w + p4);

    beta_pl(i,j) = RAO_pitch(i,j) *xi(j);

    %%%%%%%%%%%%%%%%%%%%%%%%%%%%%%%%%%%%%%%%%%%%%%%%%%%%%%%%%%%%

    % Exciting force [N]
    F_FLOAT(i,j) = ( (F_exA(i,j)^2)+(w^2)*(z_pl(i,j)^2)*(b_ex(j)^2) +
(w^4)*(z_pl(i,j)^2)*(m_sup(i,j)^2)+2*w*z_pl(i,j)*b_ex(j)*F_exA(i,j)*sin(bet
a_Fex(i)-beta_pl(i,j))-
```

```
2*(w^2)*z_pl(i,j)*m_sup(i,j)*F_exA(i,j)*cos(beta_Fex(i)-
beta_pl(i,j)))^(0.5);

    % Phase angle [rad]
    BETA_FLOAT(i,j) =
atan(((F_exA(i,j)*sin(beta_Fex(i))+w*b_ex(j)*z_pl(i,j)*cos(beta_pl(i,j))-
m_sup(i,j)*(w^2)*z_pl(i,j)*sin(beta_pl(i,j)))
/((F_exA(i,j)*cos(beta_Fex(i))-w*b_ex(j)*z_pl(i,j)*sin(beta_pl(i,j))-
m_sup(i,j)*(w^2)*z_pl(i,j)*cos(beta_pl(i,j))))));

    % Steady state solution
    z_FLOAT(i,j) = F_FLOAT(i,j) / (A3(i,j));

    RAO_FLOAT(i,j) = z_FLOAT(i,j) / xi(j);
    beta_motFLOAT(i,j) = BETA_FLOAT(i,j) - atan ( (b_t(i,j)*w) / (k - mw));

    % equation 2.11 spectrum of amplitude [m]
    S_zFLOAT(i,j) = (S_xi_w(i,j) * (z_FLOAT(i,j)^2)) / (xi(j)^2);

    % Floating Integral constants eq 2.13 & 2.14
    C1_float(i,j) = rho*g*v_gp(j)*S_xi_w(i,j);
    C2_float(i,j) = b_ex(j)*(w^2)*((z_FLOAT(i,j)/xi(j))^2)*S_xi_w(i,j);


%%%%%%%%%%%%%%%%%%%%%%%%%%%%%%%%%%%%%%%%%%%%%%%%%%%%%%%%%%%%%%%%%%%%%%%%%%%%%%%

                                i=i+1;        % update frequency numerator
end

%%%%%%%%%%%%%%%%%%%%%%%%%%%%%%%%%%%%%%%%%%%%%%%%%%%%%%%%%%%%%%%%%%%%%%%%%%%%%%%
%                              FIXED REFERENCE
%%%%%%%%%%%%%%%%%%%%%%%%%%%%%%%%%%%%%%%%%%%%%%%%%%%%%%%%%%%%%%%%%%%%%%%%%%%%%%%
    %                   Power production irregular waves

    % equation 2.12 significant amplitude buoy [m]
    z_a_sign(j) = 2 * sqrt(trapz(W(:,j),S_z(:,j)));

    if j > 3
        z_a_sign(j) = 2;
    end

    % equation 2.13 Available Power [W]
    P_213(j) = d_buoy * trapz(W(:,j),C1(:,j));
    P_AVAIL(j) = P_213(j)/1000;                                % [kW]

    % equation 2.14 Absorpted Power [W]
    P_214(j) = trapz(W(:,j),C2(:,j));
    P_ABS(j) = P_214(j)/1000;                                  % [kW]

    % equation 2.15 Absorption Efficiency
    n_abs(j) = P_214(j) / P_213(j);                            % [-]

%%%%%%%%%%%%%%%%%%%%%%%%%%%%%%%%%%%%%%%%%%%%%%%%%%%%%%%%%%%%%%%%%%%%%%%%%%%%%%%
%                             FLOATING REFERENCE
%%%%%%%%%%%%%%%%%%%%%%%%%%%%%%%%%%%%%%%%%%%%%%%%%%%%%%%%%%%%%%%%%%%%%%%%%%%%%%%

    % equation 2.13 Available Power [W]
    P_213_float(j) = d_buoy * trapz(W(:,j),C1_float(:,j));
```

```
    P_AVAIL_float (j) = P_213_float(j)/1000;                                % [kW]

    % equation 2.14 Absorpted Power [W]
    P_214_float(j) = trapz(W(:,j),C2_float(:,j));
    P_ABS_float(j) = P_214_float(j)/1000;                                   % [kW]

    % equation 2.15 Absorption Efficiency
    n_abs_float(j) = P_214_float(j) / P_213_float(j);                       % [-]

%%%%%%%%%%%%%%%%%%%%%%%%%%%%%%%%%%%%%%%%%%%%%%%%%%%%%%%%%%%%%%%%%%%%%%%%%%%%%%%

    %                       Time simulations SSS

        n = 1;

        for t = t0:dt:tx;
        z_b(n,j) = z_a(v,j)*sin(w_p(j)*t+beta_mot(v,j));
        z_w(n,j) = xi(j)*sin(w_p(j)*t);
        z_rel(n,j) = z_b(n,j) - z_w(n,j);
        v_rel(n,j) = -
w_p(j)*sin(w_p(j)*t+beta_mot(v,j))+w_p(j)*sin(w_p(j)*t);

        T(n,j) = t;
        n = n + 1;
        end

%%%%%%%%%%%%%%%%%%%%%%%%%%%%%%%%%%%%%%%%%%%%%%%%%%%%%%%%%%%%%%%%%%%%%%%%%%%%%%%

    % update waitbar progress bar

    waitbar(j / ((Hx - H0)/dH))

    i=1;     % reset frequency numerator
    J(j)=j;
    j=j+1;   % update wave height numerator

end
end

close(h)

% figure
% for j = 1:5
% scatter(HH(:,j),P_ABS_float(:,j))
% hold on
% end
% xlabel('Wave height [m]')
% ylabel('Absorbed power WEC [kW]')
% axis([1 3.5 0 70])
% grid on
%
% RED40 = 100*(P_ABS_float(1)-P_ABS_float(3)) / P_ABS_float(3);
% RED20 = 100*(P_ABS_float(2)-P_ABS_float(3)) / P_ABS_float(3);
% ADDRED = 0;
% ADD20 = 100*(P_ABS_float(4)-P_ABS_float(3)) / P_ABS_float(3);
% ADD40 = 100*(P_ABS_float(5)-P_ABS_float(3)) / P_ABS_float(3);
%
% figure
% scatter(-40,RED40,'*','b')
```

```
% hold on
% scatter(-20,RED20,'*','b')
% hold on
% scatter(0,ADDRED,'*','b')
% hold on
% scatter(20,ADD20,'*','b')
% hold on
% scatter(40,ADD40,'*','b')
% xlabel('Difference in heave motion [%]')
% ylabel('Difference in power [%]')
% grid on

%%%%%%%%%%%%%%%%%%%%%%%%%%%%%%%%%%%%%%%%%%%%%%%%%%%%%%%%%%%%%%%%%%%%%%%%%%%%%%%

    %                 Post processing wec behaviour

%     for j = 1:8
%     SC2(j) = qqS(v,j);
%     j=j+1;
%     end

%%%%%%%%%%%%%%%%%%%%%%%%%%%%%%%%%%%%%%%%%%%%%%%%%%%%%%%%%%%%%%%%%%%%%%%%%%%%%%%

    %                       NREL Wind Turbine 5 [MW]


% Wind Distribution
u_ref = 9.5;                                % reference wind velocity [ms-1]
h_ref = 10;                                 % referene height [m]

% Reset numerator
h=1;

for height = 1:0.1:150                     % vary in h

                                                    % logarithmic profile
    z_0 = 0.0002;                                   % windheight constant [-
]
    v1   = u_ref*(log(height/z_0)/log(h_ref/z_0)); % wind speed [ms-1]

    a = 0.11;                                       % windheight constant [-
]
    v2 = u_ref *((height/h_ref)^(a));               % wind speed [ms-1]

    U1(h)   = v1;
    U2(h)   = v2;
    h_b(h)  = 90;
    H(h)    = height;

h=h+1;
end

% Tower & Blade dimensions
R_blade = 63;                              % blade radius [m]
R_tower = 1.5;                             % hub radius [m]
A = pi*R_blade^2;                          % area [m2]
hh=90;                                     % hub height [m]
U_rated=U2(hh);                            % rated windspeed [ms-1]
```

```
% Air properties
rho=1.19;                                   % air density [kgm-3]

% Coefficients Thrust & Power
a = 1/3;                                    % [-]
c_t = 4*a*(1-a);                            % trust coefficient [-]
c_p = 4*a*(1-a)^2;                          % power coefficient [-]

% Thrust & Power
P_rated = 0.5*c_p*A*rho*(U_rated)^3;        % rated power [W]

i=1;
for v = 0.1:0.1:30

if v <= 3                                   % cut in wind speed
   p = 0;                                   % no power

else
   p = 0.5*c_p*A*rho*(v)^3 /(1000000);      % power output in [MW]
end
    if p > 5
        p = 5;
    end

if v > 25                                   % cut out wind speed
   p = 0;                                   % no power
end

        V(i)=v;
        P(i)=p;
i=i+1;
end

%%%%%%%%%%%%%%%%%%%%%%%%%%%%%%%%%%%%%%%%%%%%%%%%%%%%%%%%%%%%%%%%%%%%%%%%%%%%%%%

    %                   Power ratio Wind Wave

    j=1;
for hw = 0.25:0.5:3.75

% Coefficients:
  p1 = -0.10101;
  p2 = 1.0584;
  p3 = 1.5691;
  p4 = 4.4674;

  % reference height
  u_ref(j) = p1*(hw).^3 + p2*hw.^2 + p3*hw + p4;

  % windheight constant [-]
  theta       = 0.11;

  % wind speed [ms-1]
  U_nom(j) = u_ref(j)*((90/h_ref)^(theta));

  % power production
  P_nom(j) = 0.5*c_p*A*rho*(U_nom(j))^3;
```

```
  if P_nom(j) > 5e6
      P_nom(j) = 5e6;
  end

  PR(j) =  P_214_float(j) / (P_214_float(j) + P_nom(j));
  PR_100(j) = 100*PR(j);

  J(j) = j;
  j=j+1;
end


figure
scatter(H_W(1),P_ABS_float(1),'*','b')
hold on
scatter(H_W(2),P_ABS_float(2),'*','b')
hold on
scatter(H_W(3),P_ABS_float(3),'*','b')
hold on
scatter(H_W(4),P_ABS_float(4),'*','b')
hold on
scatter(H_W(5),P_ABS_float(5),'*','b')
xlabel('Sea state')
ylabel('Absorbed power [kW]')
grid on

figure
for j=1:4
plot(WW(:,j),z_a(:,j))
hold on
end
xlabel('Frequency [rads^{-1}]')
ylabel('z_{a} [m]')
legend('Seastate 1', 'Seastate 2', 'Seastate 3', 'Seastate 4')
title('Amplitude of the steady-state oscillation')
grid on

figure
for j=5:8
plot(WW(:,j),z_a(:,j))
hold on
end
xlabel('Frequency [rads^{-1}]')
ylabel('z_{a} [m]')
legend('Seastate 5', 'Seastate 6', 'Seastate 7', 'Seastate 8')
title('Amplitude of the steady-state oscillation')
grid on



%%%%%%%%%%%%%%%%%%%%%%%%%%%%%%%%%%%%%%%%%%%%%%%%%%%%%%%%%%%%%%%%%%%%%%%%%%%%%%%

    %%                  Plotting the Results                  %%%

%%%%%%%%%%%%%%%%%%%%%%%%%%%%%%%%%%%%%%%%%%%%%%%%%%%%%%%%%%%%%%%%%%%%%%%%%%%%%%%
                           Wave conditions
%%%%%%%%%%%%%%%%%%%%%%%%%%%%%%%%%%%%%%%%%%%%%%%%%%%%%%%%%%%%%%%%%%%%%%%%%%%%%%%
```

```
    Eight different sea states

    for j = 1:8
    scatter(T_P(j),H_W(j),'*')
    hold on
    end
    hold off
    xlabel('Wave period [s]')
    ylabel('Significant wave height [m]')
    title('Eight different sea states [3]')
    grid on
    saveas(gcf,'./Pictures/Eightseastates.png')

    % Wave-power level [kW/m^2]

    j=1;
    figure
    for j = 1:8
    WPL(j) = (k_j * T_P(j) * (H_W(j)^2))/1000;
    end
    scatter(J,WPL,'*','r')
    xlabel('Sea state')
    ylabel('Wave-power level [kWm^{-2}]')
    title('Wave-power level of different sea states (Falnes, 2002)')
    grid on
    saveas(gcf,'./Pictures/Waterpowerlevel.png')

    % Natural frequency sea states

    figure
    scatter(J,w_p,'*','r')
    xlabel('Sea state [-]')
    ylabel('\omega_{p} [rads^{-1}]')
    title('Peak frequency')
    grid on
    saveas(gcf,'./Pictures/Eigenfrequencyseastates.png')

    % JONSWAP Wave spectrum

    figure
    for j = 1:8
    plot(W(:,j),S_xi_w(:,j))
    hold on
    end
    xlabel('Frequency [Hz]')
    ylabel('Spectrum [m^{2} s]')
    title('JONSWAP wave spectrum')
    legend('H_{s} = 0.25', 'H_{s} = 0.75', 'H_{s} = 1.25', 'H_{s} = 1.75',
'H_{s} = 2.25', 'H_{s} = 2.75', 'H_{s} = 3.25', 'H_{s} = 3.75')
    grid on
    saveas(gcf,'./Pictures/JONSWAP.png')

    % Wave amplitude

    figure
    plot(W,xi_a)
    xlabel('Frequency [rad s^{-1}]')
    xlabel('H_{w} [m]')
    title('Wave amplitude')
    axis([w0 wx 0 1])
```

```
    legend('H_{s} = 0.25', 'H_{s} = 0.75', 'H_{s} = 1.25', 'H_{s} = 1.75',
'H_{s} = 2.25', 'H_{s} = 2.75', 'H_{s} = 3.25', 'H_{s} = 3.75')
    grid on
    saveas(gcf,'./Pictures/Waveamplitude.png')


%%%%%%%%%%%%%%%%%%%%%%%%%%%%%%%%%%%%%%%%%%%%%%%%%%%%%%%%%%%%%%%%%%%%%%%%%%%%%%%
%                              Deep water relation
%%%%%%%%%%%%%%%%%%%%%%%%%%%%%%%%%%%%%%%%%%%%%%%%%%%%%%%%%%%%%%%%%%%%%%%%%%%%%%%

    % Deep water check #1

    figure
    plot(H_W,D)
    hold on
    plot(H_W,L_3)
    title('Checking deep water condition')
    legend('depth [m]', '3rd of wavelength [m]')
    xlabel('Waveheight [m]')
    ylabel('Length')
    title('Wavenumber')
    axis([H0 Hx 0 125])
    saveas(gcf,'./Pictures/Deepwatercheck.png')

    % Wave number calculation check

    figure
    plot(W,k_w_check1)
    hold on
    plot(W,k_w_check2)
    xlabel('Frequency [rad^{-1}]')
    ylabel('Wavenumber [-]')
    saveas(gcf,'./Pictures/Wavenumbers.png')

%%%%%%%%%%%%%%%%%%%%%%%%%%%%%%%%%%%%%%%%%%%%%%%%%%%%%%%%%%%%%%%%%%%%%%%%%%%%%%%
%                          Hydrodynamic parameters buoy
%%%%%%%%%%%%%%%%%%%%%%%%%%%%%%%%%%%%%%%%%%%%%%%%%%%%%%%%%%%%%%%%%%%%%%%%%%%%%%%

    % Added mass    figure
    plot(W,m_added)
    xlabel('Frequency [rads^{-1}]')
    ylabel('m_{added} [kg]')
    title('Added mass for buoy with draft = 3.5 [m]')
    grid on
    saveas(gcf,'./Pictures/Addedmass.png')

    % Hydrodynamic coefficient approximation

    figure
    scatter(bhyd_w,bhyd_scatter,'b')
    hold on
    plot(W,b_hyd,'b')
    hold on
    plot(W,b_hyd_178,'r')
    legend('WAMIT (de Backer, 2009)','Fit using cubic approximation',
'Analytical value (Falnes, 2002)')
    xlabel('Frequency [rads^{-1}]')
    ylabel('b_{hyd} [kgs^{-1}]')
    title('Hydrodynamic damping coefficient')
```

```
    axis([0.2 2 0 20000])
    grid on
    saveas(gcf,'./Pictures/Bhyd.png')

    Excitating force approximation

    figure
    plot(W,F_EXA)
    grid on
    xlabel('Frequency [rads^{-1}]')
    ylabel('F_{exA} [kNm^{-1}]')
    title('Heave exciting force per unit wave amplitude')
    saveas(gcf,'./Pictures/FexA.png')

    Phase angle approximation

    figure
    plot(W,beta_Fex)
    grid on
    xlabel('Frequency [rads^{-1}]')
    ylabel('beta_{Fex} [rad]')
    title('Phase angle of wave exciting force')
    axis([0.2 2 0 0.7])
    saveas(gcf,'./Pictures/BetaFex.png')

%%%%%%%%%%%%%%%%%%%%%%%%%%%%%%%%%%%%%%%%%%%%%%%%%%%%%%%%%%%%%%%%%%%%%%%%%%%%%%%
%                            Wave Energy Converter
%%%%%%%%%%%%%%%%%%%%%%%%%%%%%%%%%%%%%%%%%%%%%%%%%%%%%%%%%%%%%%%%%%%%%%%%%%%%%%%

    % Natural frequency system

    figure
    scatter(J,w_p(1,:),'*','r')
    xlabel('Sea state [-]')
    ylabel('\omega_{n} [rads^{-1}]')
    title('Natural frequency')
    grid on
    saveas(gcf,'./Pictures/EigenfrequencySystem.png')

    % Damping ratio

    figure
    plot(W,eta_d)
    xlabel('Frequency [rads^{-1}]')
    ylabel('\xi_{d} [-]')
    legend('H_{s} = 0.25', 'H_{s} = 0.75', 'H_{s} = 1.25', 'H_{s} = 1.75',
'H_{s} = 2.25', 'H_{s} = 2.75', 'H_{s} = 3.25', 'H_{s} =
3.75','location','eastoutside')
    title('Damping ratio')
    grid on
    axis([0 2 0 0.5])
    saveas(gcf,'./Pictures/Dampingratio.png')

    %  External damping coefficient [tons-1]

    figure
    plot(H_W,b_ex)
    xlabel('H_{s} [m]')
    ylabel('b_{ex} [kgs^{-1}]')
```

```
    title('External damping coefficient')
    grid on
    saveas(gcf,'./Pictures/ExternalDamping.png')

    % Supplementary mass [ton]
%
    figure
    scatter(hhw,mms,'b')
    hold on
    plot(H_W,min(m_sup),'r')
    hold on
    plot(H_W,max(m_sup),'r')
    hold on
    plot(H_W,m_sup2,'b')
    xlabel('H_{s} [m]')
    ylabel('m_{sup} [kg]')
    title('Supplementary mass to match \omega_n = \omega_p')
    legend('(de Backer, 2009)','Range of Equation X')
    grid on
    saveas(gcf,'./Pictures/Supplementary mass.png')

%%%%%%%%%%%%%%%%%%%%%%%%%%%%%%%%%%%%%%%%%%%%%%%%%%%%%%%%%%%%%%%%%%%%%%%%%%%%%%%
%                            Steady State Solution
%%%%%%%%%%%%%%%%%%%%%%%%%%%%%%%%%%%%%%%%%%%%%%%%%%%%%%%%%%%%%%%%%%%%%%%%%%%%%%%

figure
plot(WW(:,3),RAO(:,3))
hold on
plot(WW(:,3),RAO_FLOAT(:,3))
xlabel('Frequency [-]')
ylabel('Heave RAO [m/m]')
legend('RAO WEC','RAO WEC+WindFloat')

    figure
    plot(WW,RAO)
    xlabel('Frequency [-]')
    ylabel('Heave RAO [m/m]')
    %title('Response Amplitude Operator of the WEC')
   legend('H_{s} = 0.25', 'H_{s} = 0.75', 'H_{s} = 1.25', 'H_{s} = 1.75',
'H_{s} = 2.25', 'H_{s} = 2.75', 'H_{s} = 3.25', 'H_{s} =
3.75','location','eastoutside')
    grid on
    saveas(gcf,'./Pictures/RAO.png')

    figure
    plot(W,RAO_heave)
    xlabel('Frequency [rads^{-1}]')
    ylabel('RAO Heave [m/m]')
    title('Response Amplitude Operator of the WindFloat')
    grid on
    saveas(gcf,'./Pictures/RAoWindFLOAT.png')


    figure
    plot(WW,RAO_FLOAT)
    xlabel('Frequency [-]')
    ylabel('Heave RAO floating [m/m]')
    title('Response Amplitude Operator of the WEC on WindFloat')
```

```
    legend('H_{s} = 0.25', 'H_{s} = 0.75', 'H_{s} = 1.25', 'H_{s} = 1.75',
'H_{s} = 2.25', 'H_{s} = 2.75', 'H_{s} = 3.25', 'H_{s} =
3.75','location','eastoutside')
    grid on
    saveas(gcf,'./Pictures/RAOFLOAT.png')

%%%%%%%%%%%%%%%%%%%%%%%%%%%%%%%%%%%%%%%%%%%%%%%%%%%%%%%%%%%%%%%%%%%%%%%%%%%%%%%
%                              Power Production WEC
%%%%%%%%%%%%%%%%%%%%%%%%%%%%%%%%%%%%%%%%%%%%%%%%%%%%%%%%%%%%%%%%%%%%%%%%%%%%%%%

    % Regular Wave Absorbed Power [kW]

    figure
    plot(H_W,max(P_120))
    hold on
    plot(H_W,P_AVAIL)
    xlabel('H_{s} [m]')
    ylabel('Power [kW]')
    legend('Absorbed Power [kW]', 'Available Power
[kW]','location','north')
    title('Absorbed power by WEC in regular waves')
    grid on
    saveas(gcf,'./Pictures/RegularAbsorbedPower.png')

    % Regular Wave Absorption efficiency [-]

    figure
    plot(H_W,max(eta_abs))
    hold on
    plot(H_W,max(eta_abs_max))
    xlabel('H_{s} [m]')
    ylabel('Absorption efficiency [-]')
    title('Absorption efficiency of the wave energy converter in regular
waves')
    legend('Absorption efficiency','Maximal absorption efficiency')
    grid on
    saveas(gcf,'./Pictures/RegularAbsorptionEfficiencyHS.png')

    %  Regular Wave Absorption efficiency (frequency dependent)

    j = 1;
    figure
    for j = 1:8
    plot(W(:,j),eta_abs(:,j))
    hold on
    end
    xlabel('Frequency [rads^{-1}]')
    ylabel('\eta_{abs} [-]')
    title('Absorption efficiency in regular waves dependent on frequency')
    legend('Seastate 1', 'Seastate 2', 'Seastate 3', 'Seastate 4',
'Seastate 5', 'Seastate 6', 'Seastate 7', 'Seastate 8')
    saveas(gcf,'./Pictures/RegularAbsorbedPowerFreq.png')

%%%%%%%%%%%%%%%%%%%%%%%%%%%%%%%%%%%%%%%%%%%%%%%%%%%%%%%%%%%%%%%%%%%%%%%%%%%%%%%

    % Irregular Wave Absorbed Power [kW]

    figure
    plot(H_W,P_ABS)
```

```
    hold on
    plot(H_W,P_AVAIL)
    xlabel('H_{s} [m]')
    ylabel('Absorbed Power [kW]')
    title('Absorbed power by wave energy converter in irregular waves')
    legend('Absorbed Power', 'Available Power')
    grid on
    saveas(gcf,'./Pictures/IregularAbsorbedPower.png')

    figure
    plot(H_W,P_ABS)
    hold on
    plot(H_W,P_ABS_float)
    xlabel('H_{s} [m]')
    ylabel('Absorbed Power [kW]')
    legend('WEC with fixed reference', 'WEC coupled to
WindFloat','location','north')
    title('Absorbed power by WEC for different sea states')
    grid on
    saveas(gcf,'./Pictures/IregularAbsorbedPowerFLOATING.png')

    % Irregular Wave Absorption efficiency [-]

    figure
    plot(H_W,n_abs,'r')
    hold on
    plot(H_W,hp2,'b')
    xlabel('H_{s} [m]')
    ylabel('Absorption efficiency [-]')
    title('Absorption efficiency of the wave energy converter')
    legend('n_{abs}','Theoretical max n_{abs}','location','north')
    grid on
    saveas(gcf,'./Pictures/IrregularAbsorptionEfficiencyHS.png')

    figure
    plot(H_W,n_abs)
    hold on
    plot(H_W,n_abs_float)
    xlabel('H_{s} [m]')
    ylabel('Absorption efficiency [-]')
    title('Absorption efficiency for different sea states')
    legend('WEC with fixed reference','WEC coupled to WindFloat')
    grid on
    saveas(gcf,'./Pictures/IrregularAbsorptionEfficiencyHSFLOAT.png')

%%%%%%%%%%%%%%%%%%%%%%%%%%%%%%%%%%%%%%%%%%%%%%%%%%%%%%%%%%%%%%%%%%%%%%%%%%%%
%                          Buoy and Wave movement
%%%%%%%%%%%%%%%%%%%%%%%%%%%%%%%%%%%%%%%%%%%%%%%%%%%%%%%%%%%%%%%%%%%%%%%%%%%%

  % Buoy and water movement
  figure
  for j = 1:1
  plot(T(:,j),z_b(:,j))
  hold on
  plot(T(:,j),z_w(:,j))
  end
  xlabel('Time [s]')
  ylabel('displacement [m]')
  legend('Buoy movement', 'Water movement')
  saveas(gcf,'./Pictures/BuoyWaterMovement.png')
```

```
  % Significant amplitude of the buoy position [m]

  figure
  plot(J,z_a_sign)
  xlabel('Sea state')
  ylabel('z_{A,sign} [m]')
  title('Significant amplitude of the buoy position')
  axis([1 8 0 2.5])
  grid on
  saveas(gcf,'./Pictures/SignificatAmplitudeBuoy.png')

  % Significant amplitude of the relative buoy position divided by draft [-
]
  figure
  plot(H_W,SC)
  xlabel('H_{s} [m]')
  ylabel('SA_{b} [-]')
  title('Significant amplitude of the relative buoy position divided by
draft')
  axis([0 4 0 1])
  grid on

saveas(gcf,'./Pictures/SignificatRelativeAmplitudeBuoyDividedbyDraft.png')

%%%%%%%%%%%%%%%%%%%%%%%%%%%%%%%%%%%%%%%%%%%%%%%%%%%%%%%%%%%%%%%%%%%%%%%%%%%%
    %                           Wind Energy
%%%%%%%%%%%%%%%%%%%%%%%%%%%%%%%%%%%%%%%%%%%%%%%%%%%%%%%%%%%%%%%%%%%%%%%%%%%%

    % Wind speed - height relation
    figure
    plot(H_W,U_nom)
    xlabel('Significant wave height [m]')
    ylabel('Horizontal windspeed [ms^{-1}]')
    title('Wind speed-sea state relation')
    grid on
    saveas(gcf,'./Pictures/WindspeedHeightRelation.png')

  % Wind speed - power production relation
    figure
    plot(V,P)
    xlabel('Windspeed [ms^{-1}]')
    ylabel('Wind power [MW]')
    title('Wind power curve WindFloat')
    axis([0 30 0 7])
    grid on
    saveas(gcf,'./Pictures/WindspeedPowerRelation.png')

    figure
    plot(J,PR_100)
    xlabel('Seastate [-]')
    ylabel('PR_{ww} [%]')
    grid on
    saveas(gcf,'./Pictures/Ratio wind-wave power production.png')

%%%%%%%%%%%%%%%%%%%%%%%%%%%%%%%%%%%%%%%%%%%%%%%%%%%%%%%%%%%%%%%%%%%%%%%%%%%%
```

Bibliography

Abanades, J.; Greaves, D.; and Iglesias, G., (2014): Wave farm impact on the beach profile: A case study. Coastal Engineering, 86(0): 36-44.

Bachynski, E. E.; Etemaddar, M.; Kvittem, M. I.; Luan, C.; Moan, T. (2013): Dynamic Analysis of Floating Wind Turbine During Pitch Actuator Fault, Gridd Loss and Shutdown. Energy Procedia, Volume 35, pages 210-222

Balitsky, P.; Bacelli, G.; Ringwood, J. V. (2014): Control Influenced Layout Optimization of Arrays of Wave Energy Converters. ASME 33rd International Conference on Ocean, Offshore and Artic Engineering, Renewable Energy, Volume 9B.

Babarit, G.; Delhommeau (2015): Theoretical and numerical aspects of the open source BEM solver NEMOH. In Proc. of the 11th European Wave and Tidal Energy Conference (EWTEC2015), Nantes, France.

Barth, S and Eecen, P.J. (2006): Description of the relation of Wind, Wave and Current Characteristics at the Offshore Wind Farm Egmond aan Zee (OWEZ) Location.

Bigerna, S.; Bollino, C. A.; Micheli, S. (2015): The Sustainability of Renewable Energy in Europe, Springer

BNEF (2014) Tidal Stream and Wave Power – A Lot Still to Prove. Website Accessed July 2016, URL: http://about.bnef.com/press-releases/ tidal-stream-wave-power-lot-still-prove/

Boehlert, G.W. and Gill, A. B. (2010): Environmental and ecological effects of ocean renewable energy developments, Oceanog 23:68–81.

Boeker, E.; van Grondelle, R. (2011): Environmental Physics Sustainable Energy and Climate Change, Third Edition, John Wiley & Sons Ltd.

Borg, M.; Collu, M.; Brennan, F. P. (2013): Use of a Wave Energy Converter as a Motion Suppression Device for Floating Wind Turbines, Cranfield University, United Kingdom, Deepwind'2013, Trondheim, Norway.

Borg, M. and Collu, M (2015): A Comparison between the Dynamics of Horizontal and Vertical Axis Offshore Floating Wind Turbines, 28 February 2015, Volume 373, issue 2035.

Bozo, N. T.; Murphy, J.; Lewis, T.; Thomas, G. (2015): A review and comparison of offshore floating concepts with combined wind-wave energy, Presentation EWTEC conference 2015

Bretschneider, C. L. (1964): Generation of Waves by Wind State of the Art, NESCO Report SN-134-6.

Carballo, R. and Iglesias, G. (2013): Wave Farm Impact based on Realistic Wave-WEC Interaction. Energy, 51(0): 216-229.

Carbon Trust (2015): Floating Offshore Wind: Market and Technology Review, United Kingdom

Casale, C.; Serri, L.; Stolk, N.; Yildiz, I.; Cantu, M. (2012): Synergies, Innovative Designs and Concepts for Multipurpose Use of Conversion Platforms. Results of Orecca project - WP4

Castro-Santos, L.; Diaz-Casas, V. (2016): Floating Offshore Wind Farms, Green Energy Technology.

Chozas, J. F.; Sørensen, H. C.; Helstrup, N. E. J.; Kofoe, J. P. (2012): Economic benefit of combining wave and wind power productions in day-ahead electricity markets. 4th International Conference on Ocean Energy. Dublin.

COM2012 494 final (2012): Blue Growth Opportunities for Marine and Maritime Sustainable Growth.

COM2014 8 final (2014): Blue Energy: Action Needed to Deliver on the Potential of Ocean Energy in European Seas and Oceans by 2020 and Beyond.

Cornett, A.M. (2008): A Global Wave Energy Resource Assessment, Canadian Hydraulics Centre, National Research Council Ottawa, Ontario, Canada

Crabb, J. (1980): Synthesis of a directional wave climate. B. Count: Academic Press

Cruz, J. (2008): Ocean Wave Energy: Current Status and Future Perspectives, Springer.

DCNS (2015): Ports and Harbour – An innovation powerhouse for Ocean Energy Development, EMD 2015 - Athens

De Backer, G.; Vantorre, M.; Frigaard, P.; Beels, C.; De Rouck, J. (2009) Bottom slamming on heaving point absorber wave energy devices, Journal of Marine Science and Technology

De Backer, G. (2009) Hydrodynamic Design Optimization of Wave Energy Converters Consisting of Heaving Point Absorbers, Ghent University, Belgium

DeepWind (2016) Website accessed on July 28 2016, URL: http://www.deepwind.eu/

Ding, S.; Yan, S.; Han, D.; Ma, Q. (2015): Overview on Hybrid Wind-Wave Energy Systems, School of Mathematics, Computer Science and Engineering, City University London, London, UK

ECN (2002): Studie naar haalbaarheid van en randvoorwaarden voor drijvende offshore windturbines. ECN, MARIN, Lagerwey the Windmaster, TNO, TUD, MSC

Edenhofer, O.; Pichs-Madruga, R.; Sokona, Y.; Seyboth, K.; Matschoss, P.; Kadner, S.; Zwickel, T. (2011): IPCC special report on renewable energy sources and climate change mitigation. Cambridge University Press, Cambridge, 1076 pp

Edge, B. L.; Hemsley, J. M. (2001): Ocean Wave Measurement and Analysis, ISBN: 9780784406045

EDP Renováveis. (2012): The WindFloat Project: Deep Offshore Wind - An Opportunity for Europe.

Ellaban, O.; Haitham, A.; Frede, B. (2014): Renewable energy resources: Current status, future prospects and their enabling technology, Renewable and Sustainable Energy Reviews 39:748-764

EMEC (2014b) Wave Developers. URL: http://www.emec.org.uk/marine-energy/wave-developers/, retrieved on retrieved on 25-7-2016

Engström, J.; Eriksson, M.; Isberg, J.; Leijon, M. (2009): Wave energy converter with enhanced amplitude response at frequencies coinciding with Swedish west coast sea states by use of a supplementary submerged body. Journal of Applied Physics, 106(6), 064512–064515.

European Commission (2012): Blue Growth—Scenarios and Drivers for Sustainable Growth from the Oceans, Seas and Coasts. European Commission, Brussels, 202 pp

EWEA (2009): Pure power-wind energy targets for 2020 and 2030. Brussel, Belgium: European Wind Energy Association.

EWEA (2013): Deep Water. European Wind Energy Association.

Falnes J. (2002): Ocean Waves and Oscillating Systems, Linear Interactions including Wave-Energy Extraction. Cambridge University Press

Falnes, J. (2007): A review of wave-energy extraction, Marine Structures, 20:185–201.

Floating Power Plant (2016) Website Accessed 27 July 2016, URL: www.floatingpowerplant.com/

Frandsen, S.; Barthelmie, R. J.; Pryor, S. C.; Rathmann, O.; Larsen, S. E.; Højstrup, J.; Thøgersen, M. L. (2005): The necessary distance between large wind farms offshore - study. (Denmark. Forskningscenter Risoe. Risoe-R; No. 1518(EN)).

Fraunhofer (2014): Multi-use Platforms for Oceans of Tomorrow, International Conference Ocean Energy, Halifax, Nova Scotia Canada, November 4-6, 2014

Fukushima (2015): Floating Offshore Wind Demonstation Project (Fukushima FORWARD)

Gao, Z.; Moan, T.; Wan, L.; Michailides, C. (2016): Comparative numerical and experimental study of two combined wind and wave energy concepts, Journal of Ocean Engineering and Science 1, pages 36–51

GL Garrad Hassan (2012): Cost of Energy of Floating Wind.

González-Longatt, F.; Wall, P.; Terzija, V. (2012): Wake effect in wind farm performance: Steady-state and dynamic behavior. Renewable Energy, 39(1), 329-338. doi:10.1016/j.renene.2011.08.053

GustoMSC (2015): Floating wind tri-floater and spinfloat

GWEC (2008): Wind Powered Electricity Generation Potential

Hansen, M. O. L. (2015): Aerodynamics of Wind Turbines, Third Edition. Routledge, Taylor and Francis Group, New York, United States

Harris, F.J. (1978): On the use of windows for harmonic analysis with the discrete Fourier transform, Proceedings of the IEEE, vol. 66, pp. 51-83

Hexicon (2016): URL: http://hexicon.eu/, retrieved on 28-7-2016

Hsu, S.A.; Meindel, E. A.; Gilhousen, D. B. (1994): Determining the power-law wind-profile exponent under near-neutral stability conditions at sea, J. Appl. Meteor., Vol. 33, pp. 757-765

IDEOL (2016) URL: http://ideol-offshore.com/en/floating-foundation, retrieved on 27-7-2016

International Energy Agency (2013): World Energy Outlook, 1994–2012. http://www.worldenergyoutlook.org/publications, retrieved on June 28 2016

International Energy Agency (2016): Analysis of Energy Consumption America

IRENA (2014): Ocean energy technology: Innovation, Patents, Market Status and Trends, International Renewable Energy Agency.

IRENA (2014b): Mofor, L.; Goldsmith, J.; Jones, F.: Ocean Energy. Technology Readiness, Patents, Deployment Status and Outlook. International Renewable Energy Agency (IRENA), Abu Dhabi.

Japanfs.org. (2009): World's first hybrid spar-type platform for floating wind turbine succeeds in demonstration test. http://www.japanfs.org/en/news/archives/news_id029511.html, retrieved on July 24 2016

Jonkman, J.; Butterfield, S.; Musial, W.; Scott, G (2009): Definition of a 5-MW Reference Wind Turbine for Offshore System Development, National Renewable Energy Laboratory.

Jonkman, J. M.; Matha, D. (2011): Dynamics of offshore floating wind turbines—analysis of three concepts. Wind Energy, 14(4), 557-569. doi:10.1002/we.442

JRC (2014): Ocean Energy Status Report.

Kaasen K.; Solaas F. (2008): Presentation of MARINTEK work and plans. SEEWEC Project Technical Committee meeting (confidential)

Karimirad M. (2014): Offshore Energy Structures, Springer International Publishing Switzerland

Khaligh, A.; Onar, O. C. (2010): Energy harvesting: Solar, Wind, and Ocean Energy Conversion Systems, Boca Raton: CRC Press. http://www.crcnetbase.com/isbn/9781439815083, retrieved on July 16 2016

Khayyat, N.T. (2015): Energy Demand in Industry, Seoul National University, South Korea

Köller, J.; Köppel, J.; Peters, W. (2006): Offshore Wind Energy Environmental Impact

Krogstad, H.E. (2000): Linear Wave Theory Part A, Norwegian University of Science and Technology Trondheim, Norway

Kühn, M. Fischer, T. (2001): Entwurf von Windenergieanlagen 1, Universität Stuttgart

Lakkoju, V. N. (1996): Combined power generation with wind and ocean waves. World renewable energy congress, Denver, USA.

Lewis A.; Estefen S.; Huckerby J.; Musial W.; Pontes T.; Torres-Martinez J. (2011): Ocean energy. In: Edenhofer O, Pichs-Madruga R, Sokona Y, Seyboth K, Matschoss P, Kadner S, Zwickel T et al (eds) IPCC special report on renewable energy sources and climate change mitigation, Cambridge University Press, Cambridge, pp 497–534

Lu, X.; McElroy, M.B.; Kiviluoma, J. (2009): Global potential for wind-generated electricity. Proceedings of the National Academy of Sciences of the United States of America 106(27): 10933-10938.

Lynn, P. A. (2013): Electricity from Wave and Tide: An Introduction to Marine Energy. John Wiley & Sons.

MacGillivray, A.; Jeffrey, H.; Hanmer, C. (2013): Ocean Energy Technology: Gaps and Barriers. Strategic Initiative for Ocean Energy (SI Ocean).

Mackay, D.J.C. (2008): Sustainable energy—without the hot air. UIT Cambridge, Cambridge, 384 pp. ISBN 978-0-9544529-3-3.

Maine Intl Consulting (2013): Japans Floating Offshore Wind Projects: An Overview

Manwell, J.; McGowan, J.G.; Rogers, A.L. (2009): Wind Energy Explained: Theory, Design and Application. Second Edition

Marin, T. I.; Moan, T.; Kaminski, M.; Gao, Z. (2014): Fatigue Analysis of the Column-Pontoon Connection in a Semi-Submersible Floating Wind Turbine, uuid:e219304b-19a8-48a5-8137-89f2af5ef2c8.

McNatt, C. (2016) openWEC: an easy-to-use, all-in-one WEC simulation tool, Ghent University

Muliawan, M. J.; Karimirad, M. and Moan, T. (2013): Dynamic response and power performance of a combined spartype floating wind turbine and coaxial floating wave energy converter, Renewable Energy, 50:47–57

Muliawan, M. J.; Karimirad, M.; Gao, Z. and Moan, T. (2013): Extreme Responses of a Combined Spar-Type Floating Wind Turbine and Floating Wave Energy Converter (STC) System with Survival Modes, Ocean Engineering, 65:71–82

Muliawan, M. J.; Gao, Z., Moan, T. and Babarit, A. (2013): Analysis of a Two-Body Floating Wave Energy Converter with Particular Focus on the Effects of Power Take-Off and Mooring Systems on Energy Capture, Journal of Offshore Mechanics and Arctic Engineering, 135 (3): 031902. doi:10.1115/1.4023796

Muliawan, M. (2012): Dynamic Reponse and Power Performance of Combined Spar type Floating Wind Turbine and coaxial WEC

Musial, W. and Ram, B. (2010): Large-scale offshore wind power in the united states: Assessment of oppportunities and barriers. 1437941338, National Renewable Energy Laboratory, Golden, US.

National Renewable Energy Laboratory (2016): Website accessed: 20 August 2016, URL: www.nrel.gov

Nautilus (2016) Website accessed July 17 2016, URL: http://www.nautilusfs.com/

Ocean Energy Systems (OES) (2015): LCOE of Ocean Energy Technologies

Offshore Islands LTD (2016) Website accessed July 17 2016, URL: http://www.offshoreislandslimited.com/

Orbis Energy (2017) Website accessed January 10 2017, URL: http://www.orbisenergy.co.uk/[3]

OWWE Ltd (2016) Ocean Wave and Wind Energy Website Accessed August 5 2016, URL: http://www.owwe.net/

Lee, K. H (2005): Responses of Floating Wind Turbines to Wind and Wave Excitation, Master of Science Thesis, Massachusetts Institute of Technology

Lloyd WindEnergie GmbH (2005): Design Codes FAST and ADAMS for Load Calculations of Onshore Wind turbines, Hamburg Germany.

Pérez, C. Iglesias, G. (2012): Integration of wave energy converters and offshore windmills. 4th International Conference on Ocean Energy. Dublin: ICOE.

Pérez-Collazo, C.; Jakobsen, M. M.; Buckland, H.; Fernández-Chozas, J. (2013): Synergies for a wave-wind energy concept. EWEA, Offshore-2013

Pérez, C., & Iglesias, G. (2012): Integration of wave energy converters and offshore windmills. 4th International Conference on Ocean Energy. Dublin: ICOE.

Pierson, W.J. Moskowitz, L. (1963): A Proposed Spectral Form for Fully Developed Wind Seas based on the Similarity Theory of S. A. KITAIGORODSKII, New York University, United States of America

Power Technology (2016) Website Accessed July 14 2016, URL: http://www.power-technology.com/

Robertson A.; Jonkman J.; Masciola M.; Song H.; Goupee A.; Coulling A. (2002): Definition of the Semisubmersible Floating System for Phase II of OC4

Roddier, D.; Cermelli, C.; Aubault, A. and Weinstein, A. (2010): "WindFloat: A floating foundation for offshore wind turbines", Journal of Renewable and Sustainable Energy, vol. 2, no. 3.

[3] Picture of the front page

SCD Technology (2016): New Revolutionary Floating Solution Reduces the Costs by 40%, URL: http://www.scd-technology.com/scd-technology-scd-nezzy/, retrieved on July 15 2016

SeaTwirl (2016) URL: http://seatwirl.com/, retrieved on 28-7-2016

Shields, M.A. (2014): Marine Renewable Energy Technology and Environmental Interactions

SI Ocean (2013a): Ocean Energy: State of the Art. Strategic Initiative for Ocean Energy (SI Ocean).

Smith, W. O. and Barber, D.G. (2007): Elsevier Oceanography series, Volume 74, pages 1-458

Statoil.com (2009): Hywind—the world's first full-scale floating wind turbine. http://www.statoil.com/en/technologyinnovation/newenergy/renewablepowerproduction/offshore/hywind/pages/hywindputtingwindpowertothetest.aspx. Website accessed 14 July 2016.

Sway (2016) Changing the future of Wind Power, URL: http://www.sway.no/, retrieved on 28-7-2016

SWD(2014)13 (2014a): European Commission: Commission Staff Working Document Impact Assessment accompanying the document: Communication from the Commission to the European Parliament, the Council, the European Economic and Social Committee and the Committee of the Regions: Ocean Energy Action Needed. Brussels.

Tavner, P.J.; Edwards C.; Brinkman A. and Spinato, F. (2006): Infuence of wind speed on wind turbine reliability, Wind Engineering, vol. 30, no. 1, pp 55–72

TetraFloat (2016) A fresh look at floating wind, URL: http://www.tetrafloat.com/, retrieved on July 20 2016

The Crown Estate (2011): Offshore wind cost reduction Pathways study

Thomas, S.; Kohler, A.; McConcille, C. (2015): Using Floating Hybrids to Secure Affordable power in the Challenging and Highly Energetic Deepter Water Market Segment

Thomsen, E (2012): Offshore Wind - A Comprehensive Guide to Successful Offshore Wind Farm Installation

United Nations (2013): Population estimates and projections, Revision of the World Population Prospects

Van Paepegem, W.; Blommaert, C.; De Baere, I.; Degrieck, J.; De Backer, G.; De Rouck, J.; Degroote, J.; Vierendeels, J.; Matthys, S.; Taerwe, L. (2011): Slamming wave impact of a composite buoy for wave energy applications: design and large-scale testing. *Polym. Compos. 32(5)*: 700-713.

Vantorre M.; Banasiak R.; Verhoeven, R. (2002): Extraction of sea wave energy: a mathematical evaluation of a point absorber in heave. Proceedings of the conference on advances in fluid mechanics, Ghent, Belgium p. 193–204.

Vantorre, M.; Banasiak, R.; Verhoeven, R. (2004): Modelling of hydraulic performance and wave energy extraction by a point absorber in heave. Division of Maritime Technology, Ghent University, B-9000 Gent, Belgium

Veigas, M.; Carballo, R. and Iglesias, G., (2014a): Wave and offshore wind energy on an island. Energy for Sustainable Development, 22(0): 57-65.

VertiWind (2012): Making Floating Wind Turbine Technology Competitive for Offshore

Viselli, A. M.; Goupee, A. J.; Dagher, H. J. (2015): Model Test of a 1:8-Scale Floating Wind Turbine Offshore in the Gulf of Maine, J. Offshore Mech. Arct. Eng 137(4), 041901

WAMIT (2016) WAMIT user manual: http://www.wamit.com/manual.htm.

Wang, Q. (2014): Design of a Steel Pontoon-type Semisubmersible Floater Supporting the DTU 10MW Reference Turbine, Master Thesis

Wavestar (2016) URL: www.wavestar.com, retrieved on July 20 2016

Weinstein, A. (2012): WindWaveFloat (WWF) Final Scientific Report

Wilhelmsson D.; Malm T.; Thompson R.; Tchou J.; Sarantakos G.; McCormick N.; Luitjens S et al (2010): Greening blue energy: identifying and managing the biodiversity risks and opportunities of offshore renewable energy. IUCN, Gland, Switzerland. 102 pp

WindCrete (2016) Concrete floating platform for wind turbines, URL: www.windcrete.com, retrieved on 28-7-2016

WindFloat (2016) Principle Power Inc. Wind Float, URL: http://www.principlepowerinc.com/en/windfloat, retrieved on 28-7-2016

WindSea (2016) URL: http://www.windsea.no/, retrieved on 25 July 2016

World Wind Energy Association (2008) Annual Report